2011

Bi-harmonic atomic force microscopy

Santosh R. Kodandarama

Recommended Citation

Kodandarama, Santosh R., "Bi-harmonic atomic force microscopy" (2011). *Masters Theses*. 7364. https://scholarsmine.mst.edu/masters_theses/7364

BI-HARMONIC ATOMIC FORCE MICROSCOPY

by

SANTOSH RAMAIAH KODANDARAMA

A THESIS

Presented to the Faculty of the Graduate School of the

MISSOURI UNIVERSITY OF SCIENCE AND TECHNOLOGY

In Partial Fulfillment of the Requirements for the Degree

MASTER OF SCIENCE IN MECHANICAL ENGINEERING

2011

Approved by

Douglas A Bristow, Advisor
Robert G. Landers
Daniel S. Stutts
Jagannathan Sarangapani

ABSTRACT

In tapping mode atomic force microscopy, surface features are measured indirectly via the amplitude of the tapping cantilever. A change in surface profile is detectable only if it results in an amplitude change that is significant enough to be measured by the optics. Previous works have focused on improving sensitivity through the system's Q-factor, either by changing physical cantilever properties or using feedback control, but those approaches undesirably slow down the dynamic response. In this work we take a novel approach to sensitivity amplification by reshaping the tapping trajectory. By shaping the trajectory so that the probe spends a greater portion of each period close to the sample, where nonlinear forces is strongest, and the amplitude sensitivity can be altered. A trajectory using two harmonics is considered and standard feed forward control techniques are employed to generate the desired cantilever drive signal. Simulation and experimental results are included and benchmarked against previous literature using standard methods. The results demonstrate that measurement sensitivity can be improved by a significant amount.

ACKNOWLEDGMENTS

First and foremost, I would like to thank my advisor, Professor Douglas Bristow for the continuous support, patience and guidance throughout the past two and half years. His guidance and enthusiasm helped me in all the time of research and writing of this thesis. It is an honor to be a part of his first research team. I appreciate all his contribution, ideas and funding to make my Masters experience productive and stimulating.

I would like to thank Professor Daniel Stutts, Robert Landers and Jagannathan Sarangapani for agreeing to be on my thesis committee. Also, my special thanks to Professor Daniel Stutts for his immense help with the experiments. I would also like to thank Material Research Center for the funding and the support. Also, I thank Eric Bohannan for his help in the imaging and handling of the atomic force microscope. I thank my fellow labmates in the Precision Control Lab, especially Patrick White, Muthukumaran Loganathan and Qing Liu for their support and encouragement.

Last but not the least; I would like to thank my family members for supporting me throughout my life.

TABLE OF CONTENTS

APPENDICIES

LIST OF ILLUSTRATIONS

LIST OF TABLES

1. INTRODUCTION

Research at the atomic level is done to provide a fundamental understanding of the phenomena and materials at the nanoscale and to create and use structures, devices and systems that have novel properties and functions. Nanotechnology includes manipulation under control of nanoscale structures and their integration. The atomic force microscope is a measuring and fabrication tool that is facilitating the nanotechnology revolution. Scanning probe microscope is a general term used when a sharp tip is used to scan over the surface and measure some property of the surface. The atomic force microscope is one type.

1.1. ATOMIC FORCE MICROSCOPE

The Atomic Force Microscope (AFM) is a high resolution microscope invented by Binnig et al. [1] in 1986 to overcome the drawbacks of a scanning tunneling microscope [2], which can only image conducting and semiconducting samples. The AFM can measure the surface topography on a scale from angstroms to 100 microns. The lower limit is a thousand times better than the optical diffraction limit. It is a type of scanning probe microscope which consists of a cantilever with a sharp tip at its end and this tip is scanned over the surface. The radius of the tip is in the order of nanometers. When this tip is brought into proximity of the sample, forces between the tip and the sample lead to a deflection of the cantilever. The forces between the tip and the sample may include mechanical contact force, van der Waals force, capillary force, chemical bonding, electrostatic force, magnetic force, Casimir force and salvation force. The deflection of the cantilever is measured, which provides the topography of the surface.

Usually the measurement is obtained by a laser beam that is reflected from the top of the cantilever and onto a photo diode. In this way, the deflection is transduced as a voltage. The tip sample distance is maintained by a feedback loop such that there is constant force between the tip and sample to prevent tip breakage or sample damage. This laser beam deflection system was introduced by Meyer and Amer [3]. In this method the cantilevers are micro-fabricated from silicon or silicon nitride. A simple diagram of an AFM laser deflection system is shown in Figure 1.1. The AFM can be operated in different modes depending on the application.

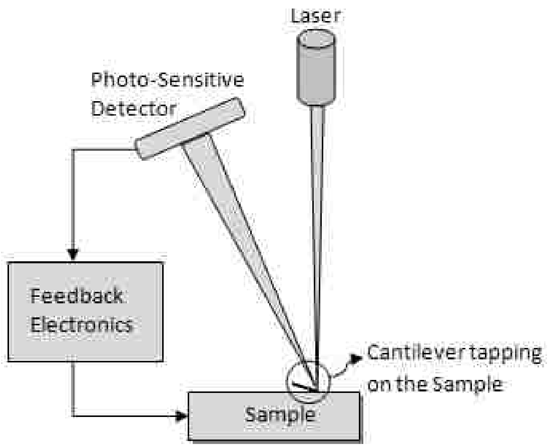

Figure 1.1. Simple AFM Diagram

1.2. MODES OF OPERATION

1.2.1. Contact Mode. In this mode the cantilever's tip is in contact with the sample always, as shown in Figure 1.2. The cantilever bends and corrects itself in response to the changes in the sample topography. The sample topography can be obtained by either having the scanner at a constant distance from the tip where the cantilever's deflection is used as feedback, or by maintaining a constant force between the sample and the tip, keeping the cantilever deflection constant and using the scanner's motion as feedback. Constant height mode [4], [5] is used when high scan speeds are necessary to get images of changing surfaces and Constant force mode is used for imaging flat samples where the cantilever deflections are small. The cantilever tips used for such a mode have low stiffness. In constant height mode, the variation of the cantilever deflection can be used directly to generate the topographic data as the height of the scanner is fixed during scanning. In constant force mode, the deflection is used as feedback for a circuit that moves the scanner adjusting to the sample topography. The total force applied to the sample is constant.

Figure 1.2. Contact Mode AFM

1.2.2. Non-Contact Mode. Contact mode can damage soft samples and result in tip wear because the tip is always in contact with the sample. Non-contact mode is a method where the tip is not in contact with the sample, but rather it is around 50 Angstroms from the sample. At that distance, attractive Van der Waal's forces can be detected and used to generate an image. The forces are very small when compared to the contact mode, hence the cantilever is made to oscillate near its resonance frequency. Detection and image generation occur as follows. A change in the sample topography results in a change in the Van der Waals forces on the cantilever. This, in turn, results in a change in amplitude and resonant frequency of the cantilever, either of which can be used to detect the change in sample topography and generate the image. To maintain a constant offset of around 50 Angstrom, feedback control is used [6].

1.2.3. Tapping Mode. In this mode the AFM tip is made to oscillate near the resonance frequency of the cantilever [6]. The tip is brought close to the sample surface so that it taps the surface and then lifts off, as shown in the Figure 1.3. Tapping prevents the tip from breaking, prevents the sample from being scratched and the lateral forces are eliminated. This also helps to avoid friction, adhesion and other forces which were otherwise problematic in contact mode. The amplitude of the oscillating tip reduces as the cantilever approaches the sample. The change in amplitude is used as a feedback variable. The piezo tube controlling the sample height moves to compensate for the change in amplitude thereby trying to keep constant amplitude of oscillation. The amount of change necessary to maintain the constant amplitude is used to generate the surface topography image.

The frequency of oscillation of the cantilever is usually very high which reduces the tip sample adhesion. This mode can be used to image samples in air or fluid medium. However in fluids, the resonant frequency of the cantilever dampens, hence the entire fluid cell is oscillated.

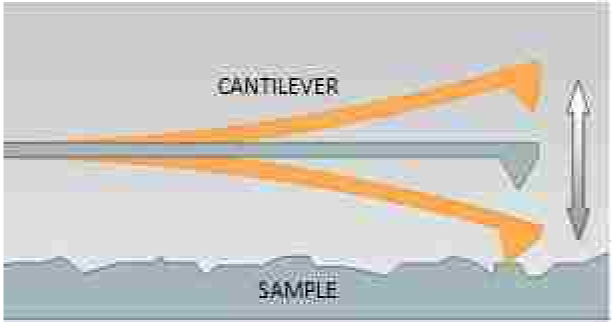

Figure 1.3. Tapping Mode

1.3. RESEARCH OBJECTIVE

Many advances are made to the experimental techniques and theoretical basis of AFMs towards the goal of making it more quantitative and easy to use. Technological innovation in the hard-disk drives, semiconductor industries and biological systems require critical nanoscale and smaller measurements. The extreme miniaturization in leading-edge designs motivates the need for precise measurements meaning higher sensitivity and faster detection of smaller variations by the feedback controller. Toward this end, the objective of this thesis is to enhance the measurement sensitivity in AFMs. Tapping mode AFMs is the focus of this thesis as it is the most prevalent when compared the non-contact AFM.

Using the basic principles of tapping mode AFM, a novel approach is developed in this thesis regarding a class of tapping mode trajectories that improves the imaging resolution. The remainder of the thesis is organized as follows. A literature review of sensing and actuation, cantilever modeling and control systems of an AFM is presented in section 2. In section 3, the tapping dynamics of an AFM cantilever with numerical analysis is presented along with experimental validation. AFM input shaping and the Bi-Harmonic AFM which increases the measurement sensitivity is described along with numerical analysis and experimental results in section 4. Conclusions are given in section 5.

2. ATOMIC FORCE MICROSCOPY: LITERATURE REVIEW

The atomic force microscope is specialized instrument for biological, material science and nanoscience applications. Its design should be simple to help scientists develop custom equipment specific to application. The functional diagram of atomic force microscope in tapping mode is shown in Figure 2.1. We can isolate six primary subsystems in a typical tapping mode AFM instrument: XYZ scanner, cantilever, feedback loop, imaging, tapping generation and sensing.

1. Cantilever – Tapping dynamics of a cantilever are critical in the functionality of an AFM. The vibrating micro cantilever with a nanoscale tip that interacts with the sample possesses several distinct modes and the interaction is non-linear. Due to this, cantilevers vibrate in interesting and unanticipated ways.
2. XYZ Scanner – The most common form of actuation of the sample is by using a piezo tube. The piezo tubes used in AFMs have generally X-Y-Z electrical configurations. When voltage is applied to the conductive areas of the tube, piezo movement along that axis is observed as shown in Figure 2.2.
3. Imaging – The control signal is used to generate the topographical image of the sample at the atomic level which is the main scope of the AFM. Analysis of chemical composition and structure of various blends, co-polymers, crystallines and fibres are based on visualization of this topographic data.

4. Feedback Control – The feedback loop regulates amplitude to keep the offset between the sample and tip constant. A phase-lock loop is used to convert high frequency tapping (100 of KHz) into low frequency amplitude (10s of KHz). The presence of this feedback is the main difference between the AFMs and stylus based instruments such as record players and profilometers. The faster the feedback loop can correct the deviations of the cantilever deflection, the faster the AFM can acquire images.
5. Tapping generation – A piezoelectric material is etched on the base of the cantilever. A signal is applied on this PZT to oscillate the cantilever. This drive signal is the main focus of this thesis.
6. Sensing - Although many methods of sensing the deflection and surface features are known, the optical lever arrangement is commonly used. In this method, a laser beam is reflected off the back of the cantilever and the spot is focused on a photodiode as shown in Figure 1.1. The cantilever is deflected by the irregularities in the sample and the spot on the detector moves. One disadvantage of this method is that the optical detection system is very noisy. But this is the simplest and most accurate way to sense the sample features.

In the following section, we review variations to the AFM instrument that have been investigated.

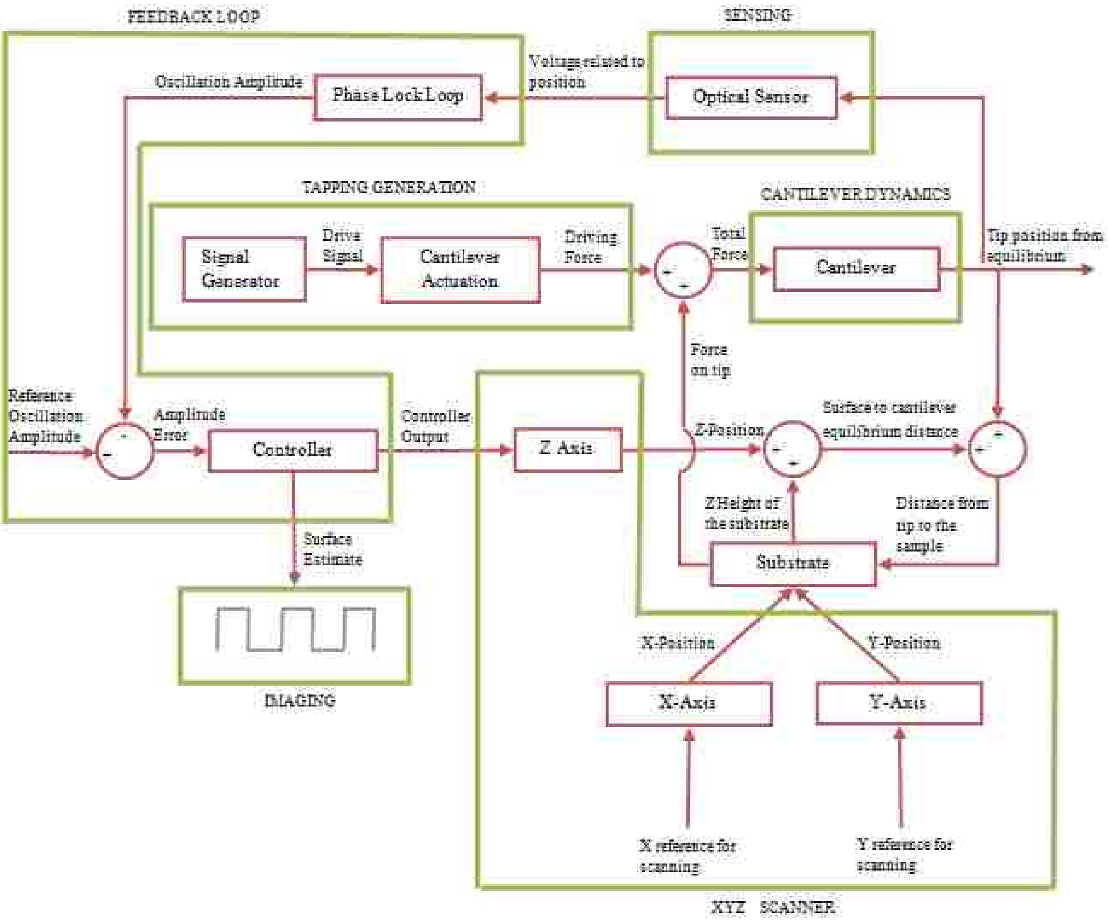

Figure 2.1. Functional diagram of a tapping mode atomic force microscope

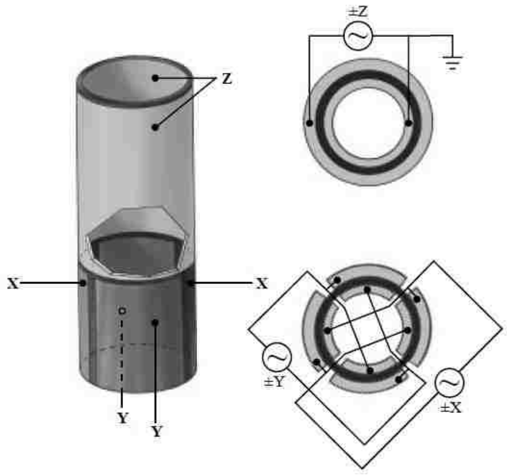

Figure 2.2. Cross Sectional view of a Piezo Tube [14]

2.1. SENSING AND ACTUATION TECHNIQUES IN AN AFM

2.1.1. Cantilever Sensing and Actuation. In one approach [6], sensing and tapping generation subsystems are integrated on the cantilever. The cantilever is coated with two piezoelectric films, PZT and ZnO which provide the means for sensing and actuation. Figure 2.3 shows a schematic of the voltage bridge circuit and amplifier used to monitor cantilever deflection.

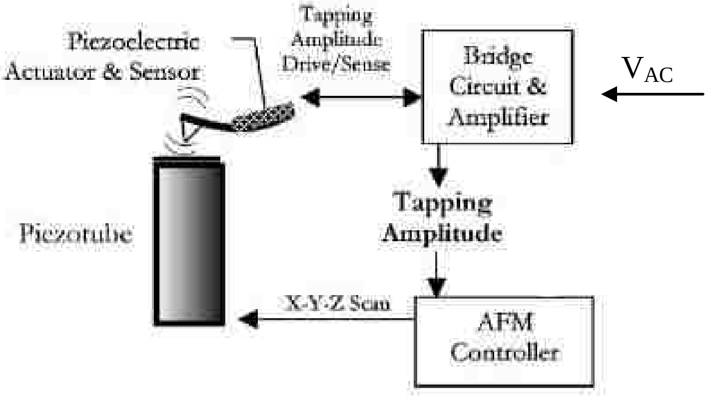

Figure 2.3. Integrated Sensing and Actuation using a bridge circuit [6]

Cantilevers with sensing and actuation capabilities were also tried in [12]. In this method, a piezo resistive material is coated on the cantilever which detects the bending of the cantilever by the sample as shown in Figure 2.4. The ZnO piezoelectric film provides the vertical motion of the cantilever.

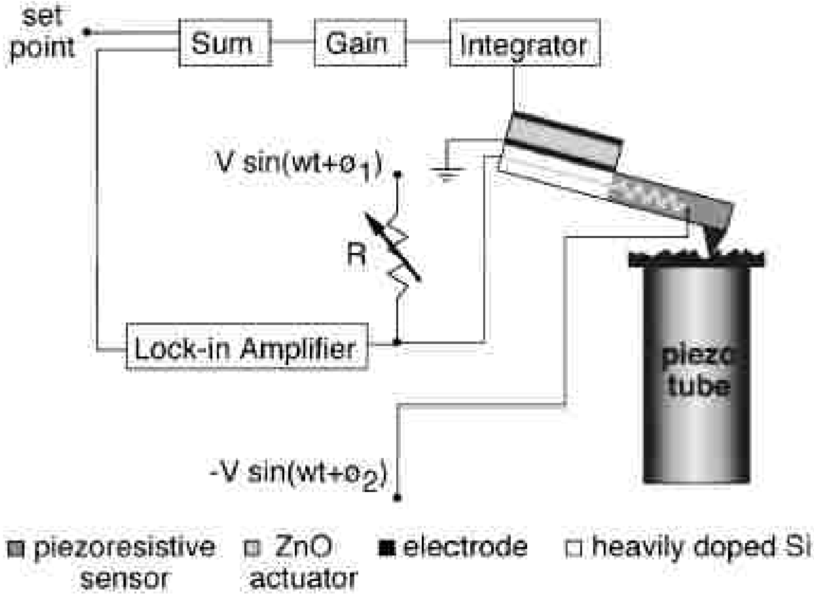

Figure 2.4. Integrated Sensing and Actuation [12]

In [8], feedback is introduced into the tapping generation subsystem so that the need for external oscillator is eliminated which represents the progress toward multiple probe AFMs, in general miniaturization of the SPMs. As shown in Figure 2.5, the piezoelectric actuator determines the frequency from the oscillator circuit which consists of an operational amplifier provided with positive feedback to sustain oscillation. Passive band pass filter elements along with the feedback allow the cantilever to oscillate near its resonant frequency. A piezo tube is employed to keep the tapping amplitude at a desired set-point. Also notable in the approach of [8] is that the sample does not move in the Z-direction, it remains fixed. Instead, all XYZ motion is generated by the cantilever. This approach is advantageous for very large samples, which may be difficult to actuate with the piezo-tube.

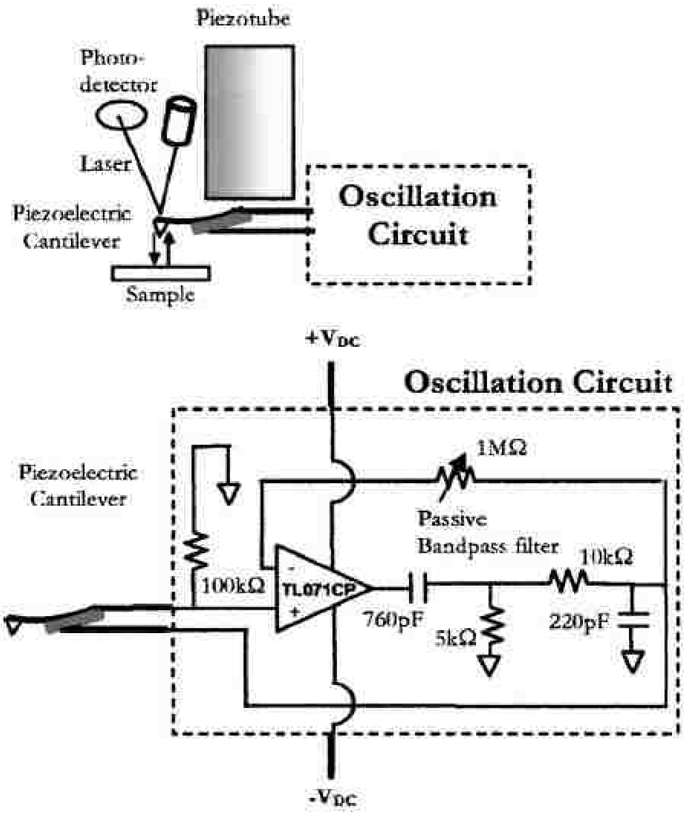

Figure 2.5. Self Oscillating Setup [8]

A number of alternatives to the piezoelectric actuator have been developed to provide tapping actuation. In [9], an insulated piezoelectric micro-actuator is employed by which magnetic methods of vibrating the cantilever can be avoided. There are no scattered spikes in the signal while tuning. Later, several other methods to actuate the cantilever were developed such as electrostatic actuation [7], acoustic radiation [10] and use of a tuning fork [11]. In electrostatic actuation, the probe structure is built over a gap on a transparent substrate with a metallic grating which serves as a fixed electrode is used. The Langevin acoustic radiation pressure principle (a measure of acoustic radiation pressure, equal to the difference between the mean pressure on an absorbing or reflecting wall and that in the same acoustic medium, at rest, behind the wall) is used in actuation by acoustic radiation where a propagating acoustic wave encounters an interface along its path in an unconfined medium. This acoustic transducer technology is used to exert force on AFM cantilevers. In [11], a U-shaped cantilever is symmetrically attached to a tuning fork such that each leg of the cantilever is fixed to one of the prongs of the tuning fork. When the tuning fork moves in the x-y direction, the cantilever is oscillated in the z direction as shown in Figure 2.6.

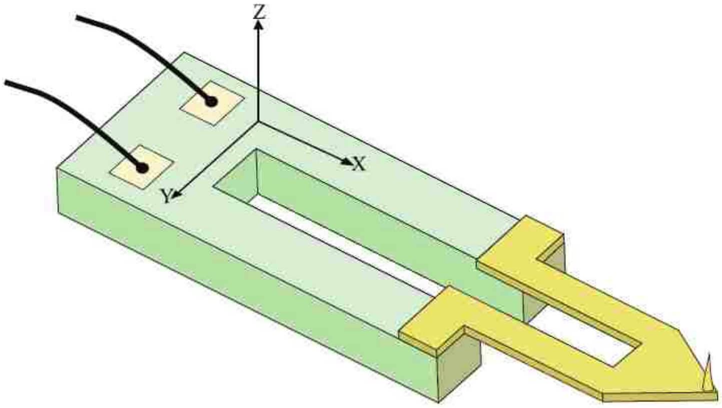

Figure 2.6. Tuning fork AFM probe [11]

2.1.2. Sample Actuation. The previous section discussed the various techniques developed for cantilever tapping actuation and sensing. Another important aspect in AFM instrumentation is the positioning of the sample. The XYZ scanner determines the speed at which the scanning can occur, the maximum sample size and the accuracy of the image.

In [13], a new mechanical scanner design that allows scanning speeds that are more than two orders of magnitude faster than current commercial AFM systems is described. The scanner combines individual actuators into a 3-D positioner with a high, lowest resonant frequency. In this design, the Z actuator is mounted on a center piece that is moved by the X and Y piezos as shown in the Figure 2.7.

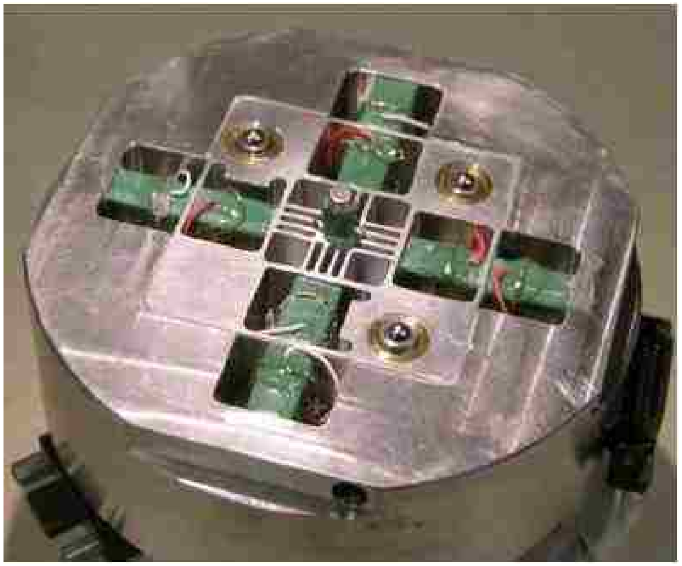

Figure 2.7. Photograph of high speed scanner showing the Z piezo in the center [13]

In another approach [15], stacked piezoelectric actuators are used whose first resonant frequency is 260 KHz. The y-piezo displaces the base 1 on which the Z and X scanners are mounted and the X piezo displaces base 2 on which Z scanner is mounted as shown in the Figure 2.8.

However, this scanner is not sufficient to minimize vibrations. As reported in [15], quick displacements of the Z piezo and simultaneous displacements of two piezo actuators cause impulsive forces leading to large vibrations.

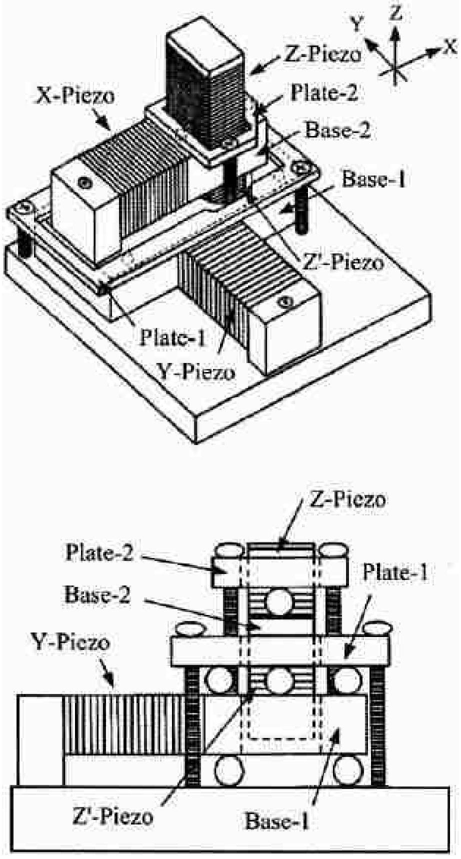

Figure 2.8. Two layered scanner assembly [15]

2.2. MATHEMATICAL MODELING OF AFM SYSTEMS

With the cantilever being the most critical part in the working of an AFM, a thorough analysis of its dynamics and control is important to enhance its performance. Several different mathematical models to describe the cantilever and its interaction forces with the sample have been developed in the literature and are explained here. The simplest linear model is developed in [17]; Burnham considers a model in which the cantilever is treated to be a lumped mass-spring-damper system. A dashpot is introduced to account for the damping between the base of the cantilever and the tip. The model is as shown in Figure 2.9. However, one must take into account the nonlinear long range attractive forces between the tip and the sample, nonlinear mechanical compliance in the contact region and the contact area as described in the survey by Jalili in [16]. Therefore, we focus on the development of several non-linear models.

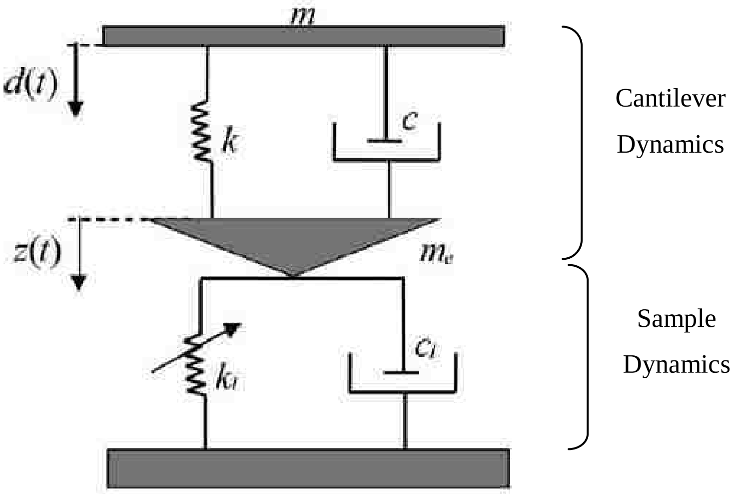

Figure 2.9. Lumped mass spring damper model for the AFM cantilever [17]

As in [17], it is common to model the cantilever as a lumped mass spring damper system with a non-linear force model for the tip-sample interaction. Thus, typical models take the form shown in Figure 2.10. The force is a lumped combination of all nonlinear forces acting on the tip from the sample. The force is treated only as a function of tip-sample distances. This model is explained in more detail in the following section.

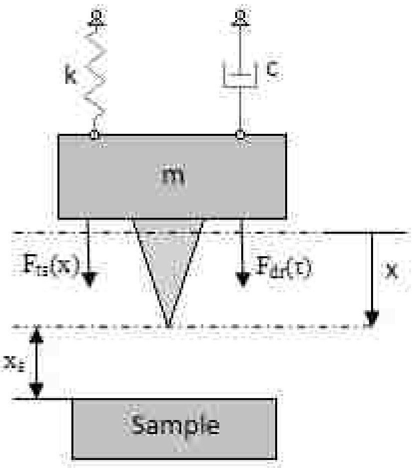

Figure 2.10. Simple cantilever model

Another linear model is considered in [20], where the cantilever is modeled using an electric circuit. In this method, the tip is treated as a forced oscillator and the sample as an elastic material with adhesive properties. The electrical circuit for the tip sample system is shown in Figure 2.11. The model is equivalent to a mechanical model where mass is replaced with inductors, springs with capacitors, dashpots with resistors and forces with voltages.

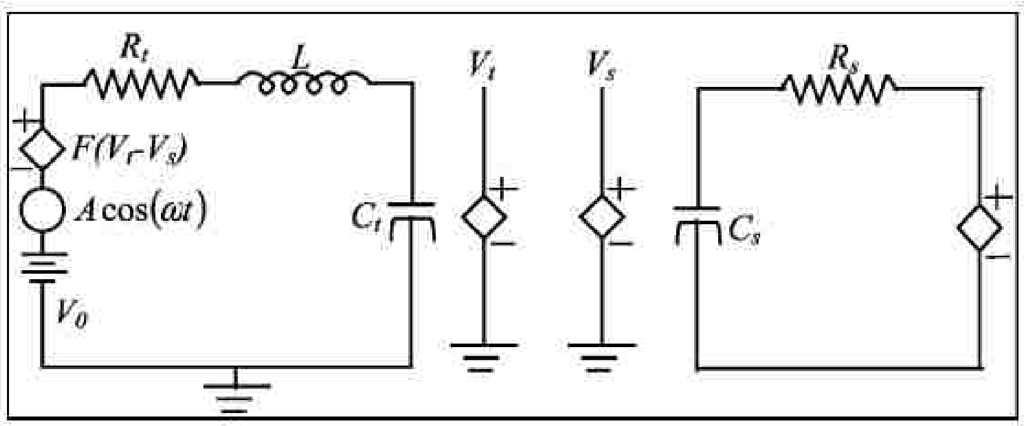

Figure 2.11. Equivalent electric circuit of a mechanical model of the tip and sample in an AFM [20]

Finally, an energy approach, which is very different from the above models, has been developed in [19]. In this approach, there is no need to solve the differential equation for the oscillating cantilever, and in turn, no need to find a tip sample interaction model. From the external drive signal, the power input is obtained which is equal to the sum of average energy dissipated by the cantilever due to movement and by tip sample interaction. A simple model as shown in Figure 2.12 is used which consists of a spring and two dampers.

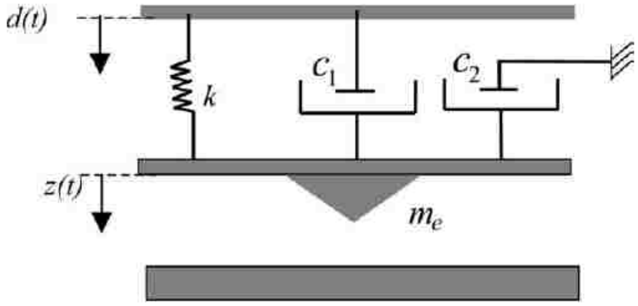

Figure 2.12. Model for dynamic AFM for Energy approach [19]

2.3. TIP SAMPLE INTERACTION FORCES

The atomic force microscope relies on the forces between the tip and the sample surface. These forces are critical for imaging and for accurately modeling the dynamics. In practice, the tip sample interaction forces are not measured directly, but calculated by measuring the deflection of the cantilever due to the surface irregularities and knowing the stiffness of the cantilever.

Figure 2.13 shows a typical plot for these forces.

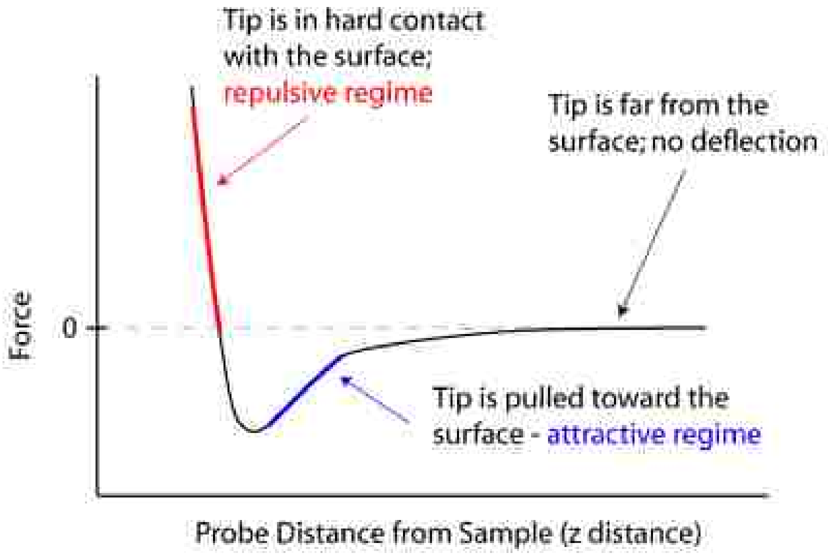

Figure 2.13. Interaction forces versus the tip sample distance [21]

The AFM probe undergoes different forces as it approaches towards the sample surface. The various forces are shown in Figure 2.14. These are described as follows.

- **Fluid Film Damping:** This phenomenon is exclusive to oscillating probes. A damping air film is developed when an oscillating probe is brought within 10 microns of the sample surface. This air film is squeezed each time the cantilever moves towards the sample and when the probe rebounds upward, vacuum is created. In extreme cases, this can lead to false engagement of the surface.

- **Electrostatic Forces:** The probe experiences electrostatic forces when it comes 0.1 to 1 micron close to a charged sample. These forces can be strong enough to interfere with imaging, but can be neutralized with a positive ion source.

- **Fluid Surface Tension:** This is usually seen between a wet sample and a dry tip. This force is attractive in nature and pulls down the tip and is strong enough to make an indent in some soft materials. This is seen at 10 to 200 nm above the surface and is dependent upon water vapor content.

- **Van Der Waals Force:** These forces are nothing but the sum of the attractive and repulsive forces that are exerted between the molecules. This is usually seen at a angstrom level above the surface.

- **Coulomb Forces:** When the tip and the sample make contact, the respective atoms encounter Coulomb forces. The electron shells from atoms of the tip repel the shells from the atoms of the sample surface. When pressure is exerted beyond this level, both materials may be damaged.

We will assume that we are imaging dry (non-biological), uncharged samples. Thus, we are primarily concerned with Van der Waals and Coulomb forces. Note the attractive and the strong repulsive regimes as the tip approaches the sample. Two models are primarily used for this purpose, the Lennard-Jones (LJ) and Derjaguin-Muller-Toporov (DMT). The non linear force is derived from the Lennard-Jones (LJ) potential for interaction between two molecules.

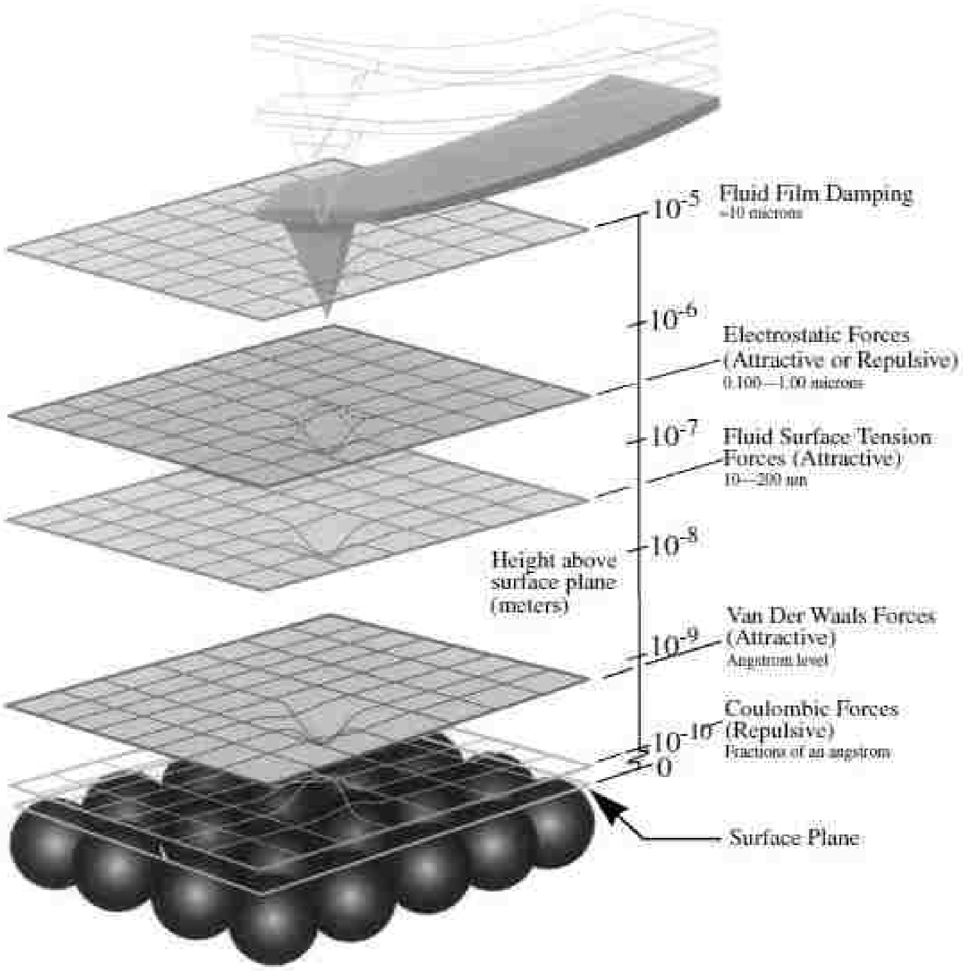

Figure 2.14. Sample Probe Boundary Layers [14]

In this model, the tip of the cantilever is modeled as a sphere held from a planar sample by a spring as shown in Figure 2.15. The ideal system is not conservative (both damped and forced) but in this model it is assumed that the damping and external forces are negligible. The LJ model includes short range repulsive interactions and Van der Waal's forces. The interaction is approximated by integrating the pairwise, intermolecular LJ potential through the volumes of sphere and sample half space [18]. The LJ interaction force at an instantaneous gap z is

$$P_{LJ}(Z) = \frac{A_1 R}{180 Z^8} - \frac{A_2 R}{6 Z^2} \tag{1}$$

where A_1 and A_2 are the Hamaker constants for the repulsive and attractive potentials respectively.

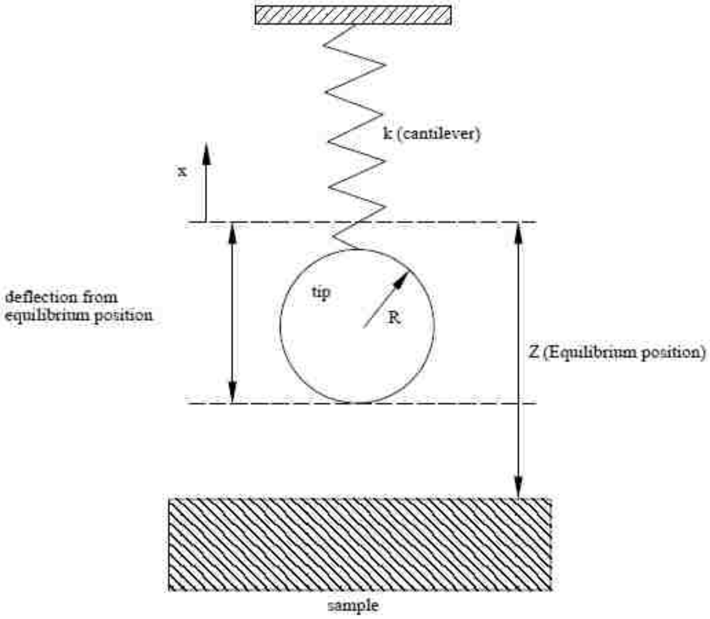

Figure 2.15. Tip-Sample Model using Lennard-Jones potential [18]

The DMT [22] model is named after Derjaguin, Muller and Toporov, which is a alternative model for adhesive contact. The DMT model is applied to systems which have tips with small curvature radius and high stiffness. The Van der Waals forces acting along the contact area perimeter results in an attractive force which weakens the elastic repulsion. DMT model is used for the numerical analysis in this thesis. The tip sample interaction force given by the DMT model is as follows.

$$F_{ts}(x)=\begin{cases}-\dfrac{HR}{6(x+x_s)^2},x+x_s\geq a_0\\ -\dfrac{HR}{6a_0^2}+\dfrac{4}{3}E\sqrt{R}(a_0-x-x_s)^{\frac{3}{2}},x+x_s<a_0\end{cases} \qquad (2)$$

where H is the Hamaker constant, R the tip radius, x_s the tip sample distance from the equilibrium position, a_0 is the interatomic distance, $E=\left[\left(1-v_t^{\,2}\right)/E_t+\left(1-v_s^{\,2}\right)/E_s\right]$ is the effective tip sample stiffness, v_s and v_t are the Poisson ratios for the sample and tip and E_t , E_s are the elastic moduli of the tip and the sample respectively.

2.4. CREEP, HYSTERESIS AND THERMAL DRIFT IN THE PIEZO SCANNER IN AN AFM

The AFM scanners are made from piezoelectric material, which expands and contracts proportionally to an applied voltage. Whether they elongate or contract depends upon the polarity of the voltage applied. Figure 2.16 illustrates the effect of applied voltage on piezoelectric materials.

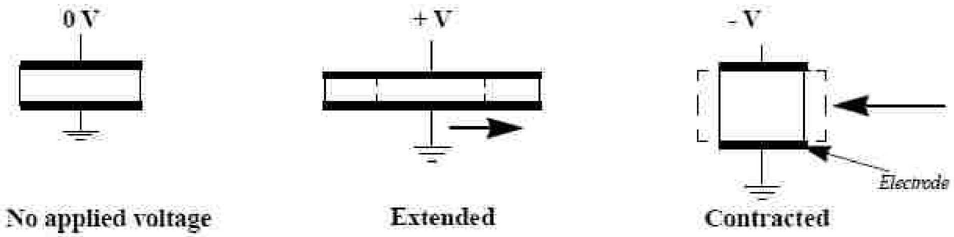

Figure 2.16. Piezoelectric tube when voltage is applied [14]

The scanner is constructed by integrating three independent piezo electrodes, one for each direction (X, Y and Z), into one single tube which can manipulate the samples and probes with extreme precision. Because of the differences in material properties and dimensions of each element in the piezoelectric tube, each scanner acts differently for the same voltage applied. In other words, for the same voltage, the piezo extension/retraction is not the same. Usually, for piezo scanners this response is expressed as resolution which is the ratio of piezo movement to piezo voltage. In other words, it is how far the piezo extends/contracts per volt. Figure 2.17 shows the forward and reverse scan directions depicting different behavior.

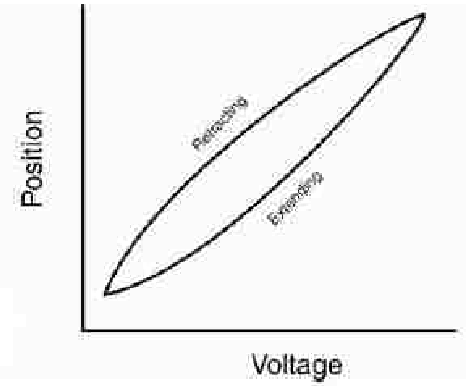

Figure 2.17. Hysteresis in AFM scanner [14]

This non-linear relationship is corrected during calibration by applying a non-linear voltage in real-time as shown in Figure 2.18 [23]. The hysteresis in an AFM scanner should not depend on the scan rate while imaging. The effect on imaging due to hysteresis is shown in Figure 2.19. The differences in spacing, size and shape of the pits between the two is demonstrated. Most of the scanners used in the field of force microscopy use this method [24].

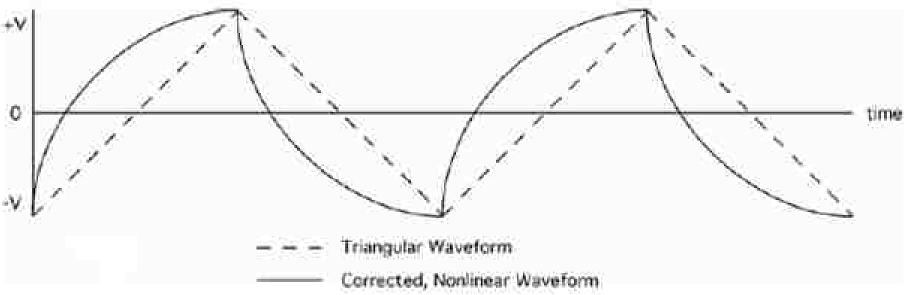

Figure 2.18. Waveform used to get linear scanner movements [14]

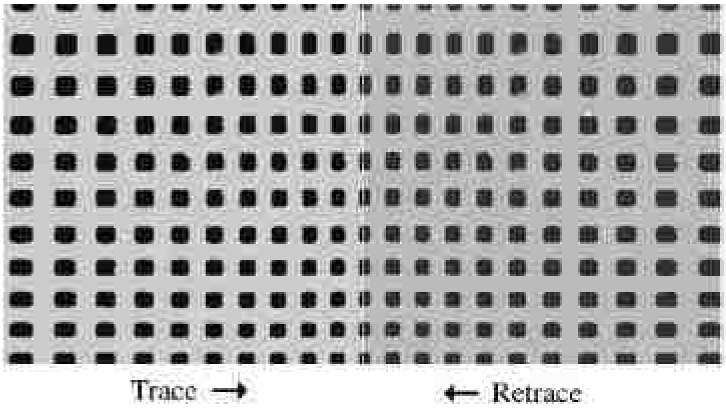

Figure 2.19. 100µm x 100µm scans in the trace and retrace directions of a two dimensional 10µm pitch grating without linearity correction [14]

Creep on the other hand is the drift of the piezo displacement after a DC offset voltage is applied to the piezo. When a large offset voltage is applied to the piezo, it initially moves the majority of the offset quickly and then slowly moves over the remainder. Creep appears as an elongation or stretching of features in the direction of the offset for a short period of time while imaging as shown in Figure 2.20. The creep can be reduced by offsetting beyond the desired point and then offsetting back to the desired point.

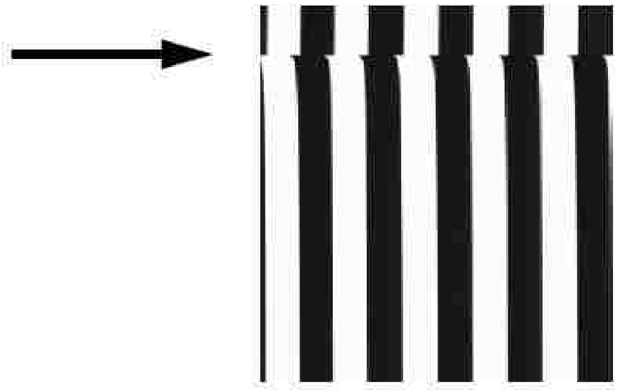

Figure 2.20. An Example of creep in a calibration grating [14]

Thermal drift in atomic force microscopy is one of the major hurdles in an AFM. Even small changes in temperature cause most of the AFM components to vary slightly in size due to thermal expansion and contraction, resulting in an unknown displacement between the tip and sample. Operating the AFM under homogeneous environmental conditions can reduce thermal drift but cannot completely eliminate it. Amounts ranging from 0.01 to 0.2 nm/s are evident even in highly temperature controlled conditions.

A simple way to reduce this hysteresis and creep is shown in [25]. By inserting a suitable capacitor in series with a scanner as shown in the Figure 2.21, the size of the hysteresis loop is reduced. The use of a capacitor is to reduce the sensitivity of the charge on the piezo to changes in the piezo's capacitance.

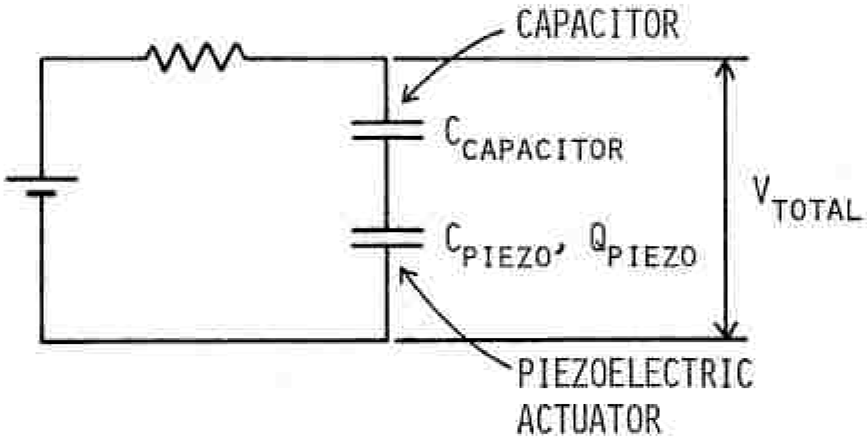

Figure 2.21. Simple Circuit to reduce Hysteresis [25]

Inserting the capacitor improves the linearity of the piezo actuator, but it greatly reduces the range of the actuator. An approach to increase the positioning bandwidth is to use an actuator with a fast dynamic response. The disadvantage of this approach is that the stiffening of the piezo actuator tends to limit its positioning range. A feedback based control method can also be used to improve the linearity [24], but for this purpose a very high resolution sensor should be used.

An integrated inversion based approach is presented in [26]. In this approach, the piezoactuator system is modeled as the cascade of hysteresis, creep and vibration sub-models as shown in Figure 2.22.

The hysteresis is modeled as an input non-linearity. This model is intended to compensate for hysteresis loss during long range applications and creep effects during positioning for a long period of time. Also, this method can be used where real-time compensation is required such as in nanofabrication.

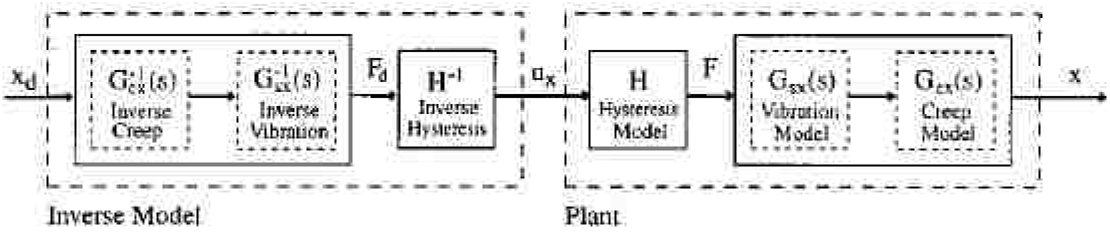

Figure 2.22. Inversion based approach for scan control [26]

3. TAPPING DYNAMICS: NUMERICAL ANALYSIS AND VALIDATION

As discussed in section 2, in a tapping mode atomic force microscope, the tip interacts with the sample intermittently via short and long range forces. These forces are highly non linear and the cantilever exhibits several modes which make the study of the vibrating cantilever important. The cantilever has multiple degrees of freedom, but a single degree of freedom approximation is sufficient to produce the dynamic richness observed in practice, including the existence of both high and low amplitude states.

3.1. CANTILEVER MODEL

As presented in the previous section, a simple lumped linear model is used to model the AFM cantilever. A spring-mass-damper system is commonly used to describe the cantilever dynamics as shown in Figure 3.1 [4, 5].

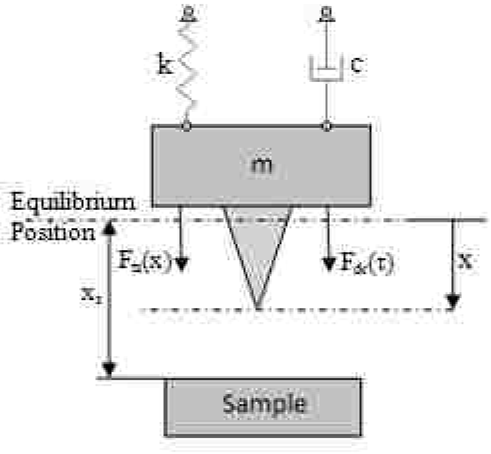

Figure 3.1. Cantilever Model

The dynamic equation of motion is given by:

$$m\ddot{x}+c\dot{x}+kx=F\left(x,t\right) \tag{3}$$

where m is the effective mass at the end, c is the equivalent damping, k is the stiffness, and x denotes the deflection of the tip from its unforced rest position. The term F(x,t) is the force acting on the tip which is given by,

$$F\left(x,t\right)=F_{dr}\left(t\right)+F_{ts}\left(x\right) \tag{4}$$

where, F_{dr} is the driving force and F_{ts} is the tip-sample interaction force. Generally, the driving force for the cantilever is sinusoidal in the form,

$$F_{dr}=A sin\left(\omega t\right) \tag{5}$$

'A' being the amplitude and ω being the frequency of the drive signal. In tapping mode, the cantilever is vibrated slightly above the resonant frequency. As discussed in the literature review, tip sample force can be modeled with LJ or DMT models.

Here, we follow the approach of [4] and use the DMT model for numerical analysis. Recall that the tip sample interaction force is given by

$$F_{ts}(x)=\begin{cases}-\dfrac{HR}{6(x+x_s)^2},x+x_s\geq a_0\\-\dfrac{HR}{6a_0^2}+\dfrac{4}{3}E\sqrt{R}(a_0-x-x_s)^{\frac{3}{2}},x+\end{cases} \tag{6}$$

where H is the Hamaker constant, R the tip radius, x_s the tip sample distance from the equilibrium position, a_0 is the interatomic distance, $E = \left[\left(1-v_t^2\right)/E_t + \left(1-v_s^2\right)/E_s\right]$ is the effective tip sample stiffness, v_s and v_t are the Poisson ratios for the sample and tip and E_t, E_s are the elastic moduli of the tip and the sample respectively. A plot of the DMT force is shown in Figure 3.2.

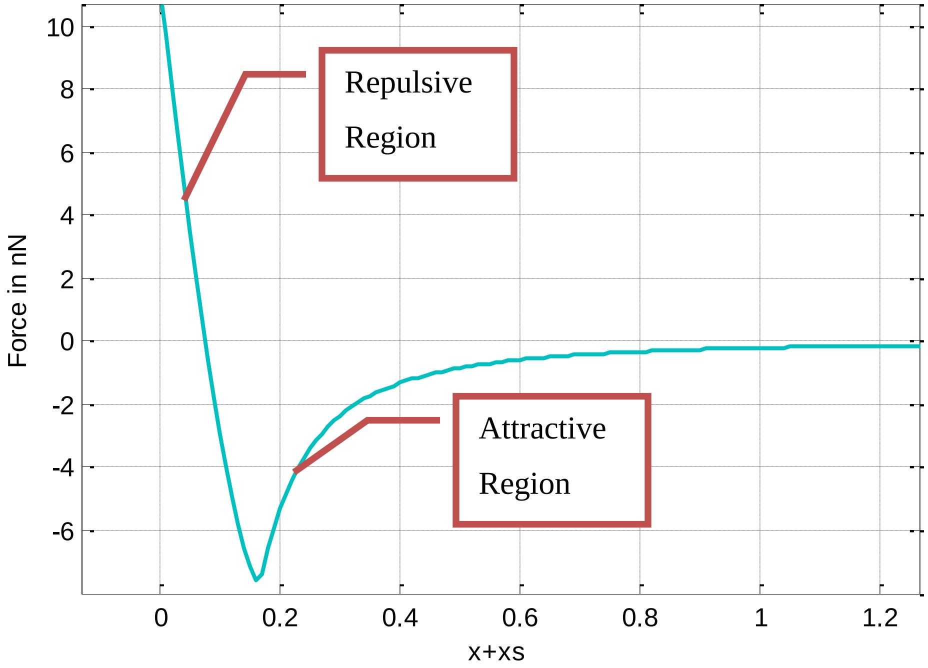

Figure 3.2. Force profile from the DMT model

Following the approach of [27], the equation of motion is normalized with respect to time. The normalization is shown in detail below.

Dividing (3) by *m*,

$$\ddot{x}(t)+\frac{c}{m}\dot{x}(t)+\frac{k}{m}x(t)=\frac{F(x,t)}{m} \tag{7}$$

Introducing the dimensionless time, $\tau=t\omega_0$,

$$\frac{dx}{dt}=\frac{dx}{d\tau}\omega_0, \tag{8}$$

$$\frac{d^2x}{dt^2}=\frac{d^2x}{d\tau^2}\omega_0^2, \tag{9}$$

where,

$$\omega_0=\sqrt{\frac{k}{m}} \tag{10}$$

Define Q as,

$$\frac{c}{m}=\frac{\omega_0}{Q}. \tag{11}$$

Substituting (8), (11) and (11) into (7), and dividing the entire equation by ω_0^2, we obtain,

$$\ddot{x}(\tau)+\frac{1}{Q}\dot{x}(\tau)+x(\tau)=\frac{F(x,\tau)}{k} \tag{12}$$

The normalized driving force is given by the following equation.

$$F_{dr} = A sin\left(\beta\tau\right) \tag{13}$$

where β is the normalized frequency, $\beta = \omega/\omega_0$. This driving force in equation (13) is referred to here as the single harmonic drive signal.

3.2. NUMERICAL ANALYSIS TAFM - AMPLITUDE RESPONSE AND SENSITIVITY

3.2.1. Amplitude Response. Amplitude response is the peak-to-peak steady state amplitude of the tip in response to the drive signal (13) and sample interaction (6). It is easier to understand the behavior of the system by examining the amplitude response. For a particular drive signal, the amplitude will also depend on the tip-sample distances. Firstly, it is important to know the trend in amplitude response when the tip is not hitting the sample, also called the free response. Secondly, the tip-sample distance is varied and the amplitude response is studied to see if it results in one or two stable equilibria.

3.2.2. Sensitivity. We define sensitivity as the ratio of change of cantilever oscillation amplitude to the change in tip sample distance. A large sensitivity means that the tapping amplitude has a large change for a small change in the height of the sample. Let Aβ(xs) be the amplitude response with frequency ratio β, and offset distance xs. Mathematically, the sensitivity is given by,

$$S\left(\beta,x_s\right) \triangleq \frac{d\left(A_\beta\left(x_s\right)/A_0\right)}{dx_s} \approx \frac{\left[A_\beta\left(x_s+h\right)-A_\beta\left(x_s\right)\right]/A_0}{h} \tag{14}$$

where h is the small change in the offset.

3.2.3. Simulation Setup. Numerical analysis is performed using the drive signal given in (13) in MATLAB to obtain the amplitude response. The parameters used are k=7.5 Nm-1, R=20 nm, Et=129 GPa, Es=70 GPa, vt=0.28, vs=0.17, Q=100, a0=0.166 nm, H=6.4X10-20J and A0=20 nm (free amplitude). A Simulink model is developed to solve the differential equation (12). The solver used in the simulations is ODE23s with a variable step time and the maximum being 0.001. The models are shown in Figure 3.3 and Figure 3.4.

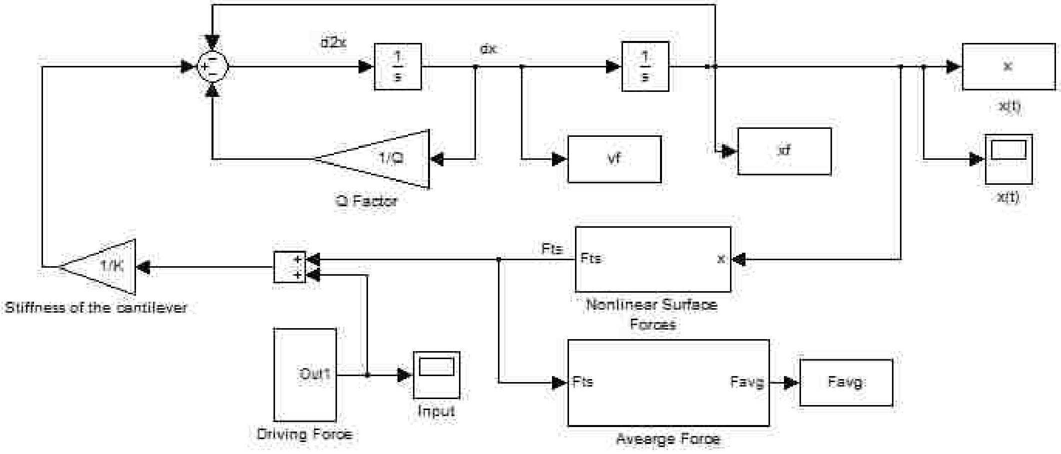

Figure 3.3. Simulink model is to solve (12)

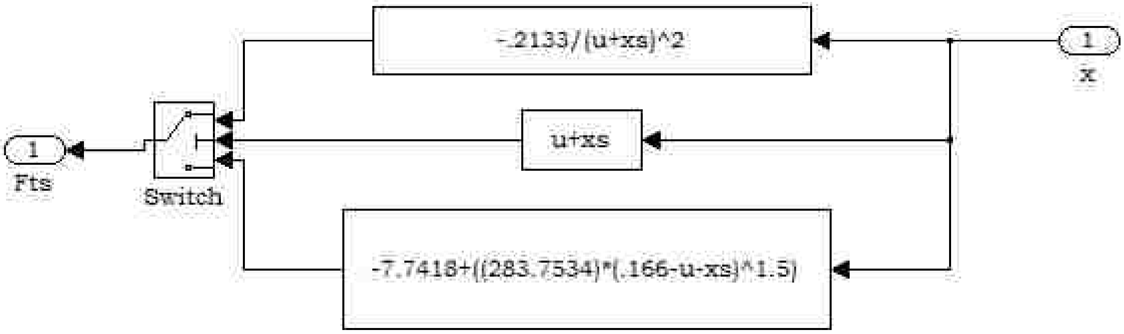

Figure 3.4. Non-linear surface forces

The time domain response of the amplitude versus the normalized time is shown in Figure 3.5. As seen in the figure, there is a long transient before the amplitude reaches a steady state. Ignoring the tip-sample forces, settling time is calculated as shown below.

$$T_s = \frac{4}{\xi \omega_n} = 8Q \tag{15}$$

From the simulations, the nonlinear forces do not appear to have much impact on the settling time, so we use this as a benchmark for the time to reach steady state in experiments. Because our Q-factor is 100, the settling time is 800 units of normalized time, τ.

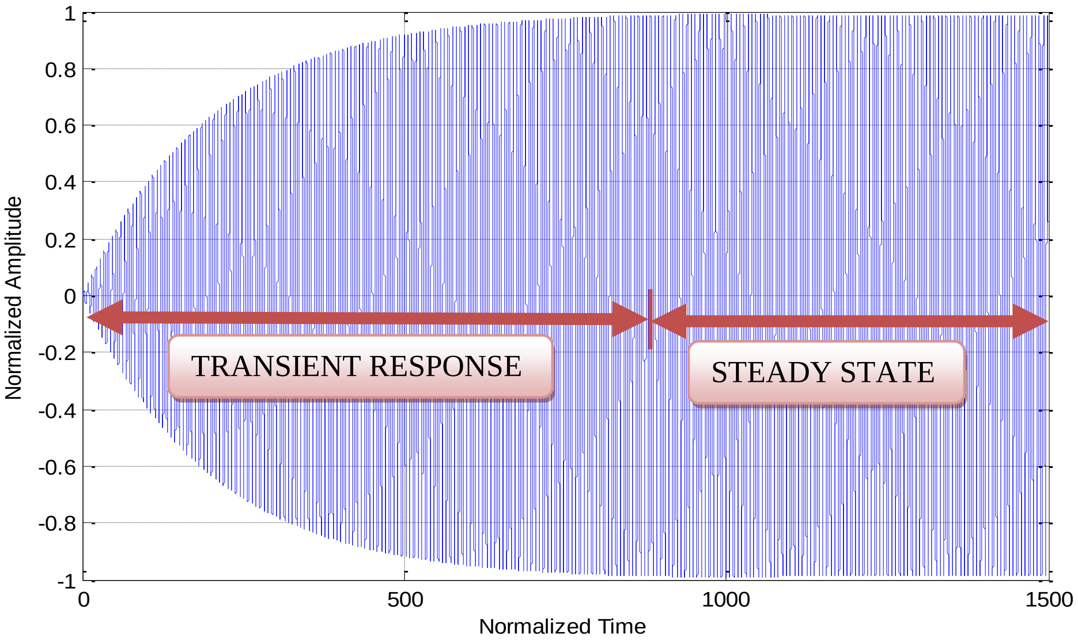

Figure 3.5. Time domain response at A_0=1 and β=1

A MATLAB code (Appendix B) is written to run the Simulink model while sweeping through a range of frequencies. In this program, the frequency switching happens as the amplitude of the cantilever reaches a steady state. The code is setup in such a way that the frequency switches to the next value if the amplitude between two consecutive periods is within a range of 0.001 units of the amplitude of the response. At that point, the peak to peak amplitude is recorded. The simulations are run on the MAE department cluster for several tip sample distances. The simulation takes approximately 10 hours to get the amplitude response when the normalized frequency is varied from 0.9 to 1.1 with a step size of 0.001 for one tip sample distance. The data is saved as a '.txt' file.

3.2.4. Simulation Results. The simulation results was consolidated and plotted for analyses. The dotted line in Figure 3.6 is the free response of the vibrating cantilever over the range of frequencies. The free response behaves such that the amplitude increases as the frequency is increased until the resonant frequency and then decreases with increase in frequency. The amplitude response changes when the tip is brought near to the surface. When the tip is at a distance of 0.4 (normalized with respect to the free amplitude) the amplitude response makes a forward and reverse sweep as shown in the Figure 3.6. The forward sweep on the tapping response begins similarly to the free response, with increasing amplitude as frequency increases, until the probe makes contact with the surface.

After contact, the amplitude growth is approximately linear and follows a high amplitude solution for frequencies well above the resonant frequency. At some higher frequency (not shown in Figure 3.6), the amplitude drops onto the low amplitude solution. Sweeping the frequency in the reverse direction (from high to low) follows the low amplitude solution, approximately tracing the free response. Sweeping past the resonant frequency results in another high amplitude solution for a small range of frequencies.

Figure 3.7 shows the amplitude response at several different tip sample distances. This plot matches the plot in [27] from which our model and model parameters are obtained. The tip sample distances are normalized with the amplitude of the response. The term “drop frequency” is the frequency where the amplitude in the forward sweep drops from the high amplitude state to the low amplitude state. In Figure 3.7, the drop frequency increases as the tip sample distance decreases. As shown in the following sections, the drop frequency is key parameter for maximizing measurement sensitivity.

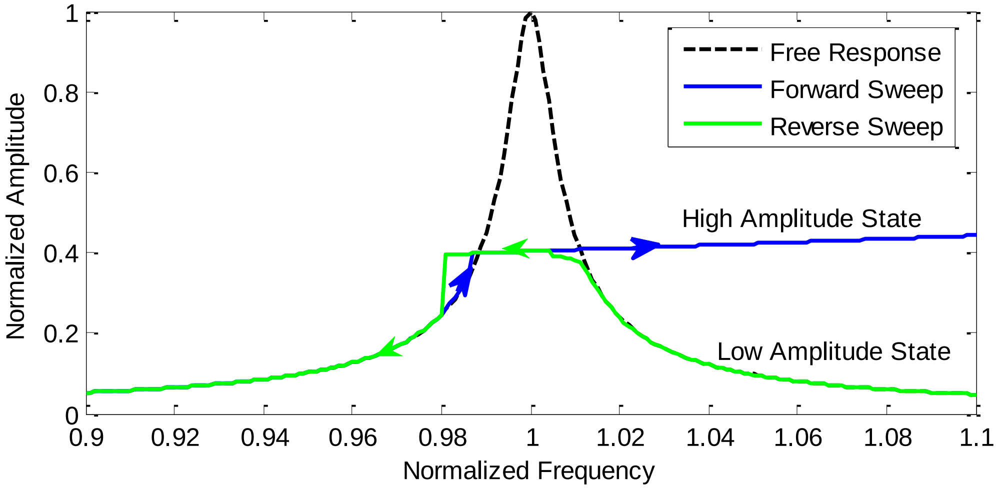

Figure 3.6. Amplitude response at a tip sample distance of x_s=0.4

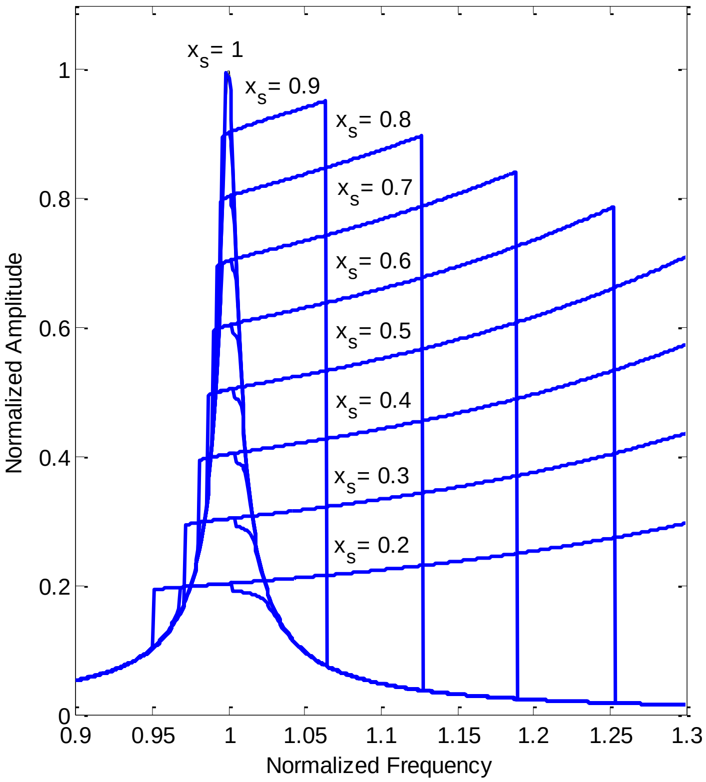

Figure 3.7. Amplitude response at different tip sample distances

3.3. TAPPING MODE AFM: EXPERIMENTS

In the following section, we setup an AFM to perform a series of experiments to validate the numerical results in section 3.2.

3.3.1. Experimental Setup. The experiments were conducted using the Digital Instruments (Veeco), Multimode scanning probe microscope shown in Figure 3.8. The cantilevers used are TESP from Veeco Instruments which have a resonant frequency in the range 250 KHz to 347 KHz.

The software used for the scanning probe microscope system is Nanoscope Version 5.12b. The experimental setup also includes Signal access module III from digital instruments, National Instruments - PXI system with 8110 Controller, 5421 function generator, 5122 oscilloscope and 6221 multifunction DAQ. A vibration and acoustic isolation chamber is used for reducing noise during imaging. The sample piezo is driven by a TREK 2205, DC high voltage amplifier with a gain factor of 50 (Maximum Voltage – 500V and Current - ±40mA).

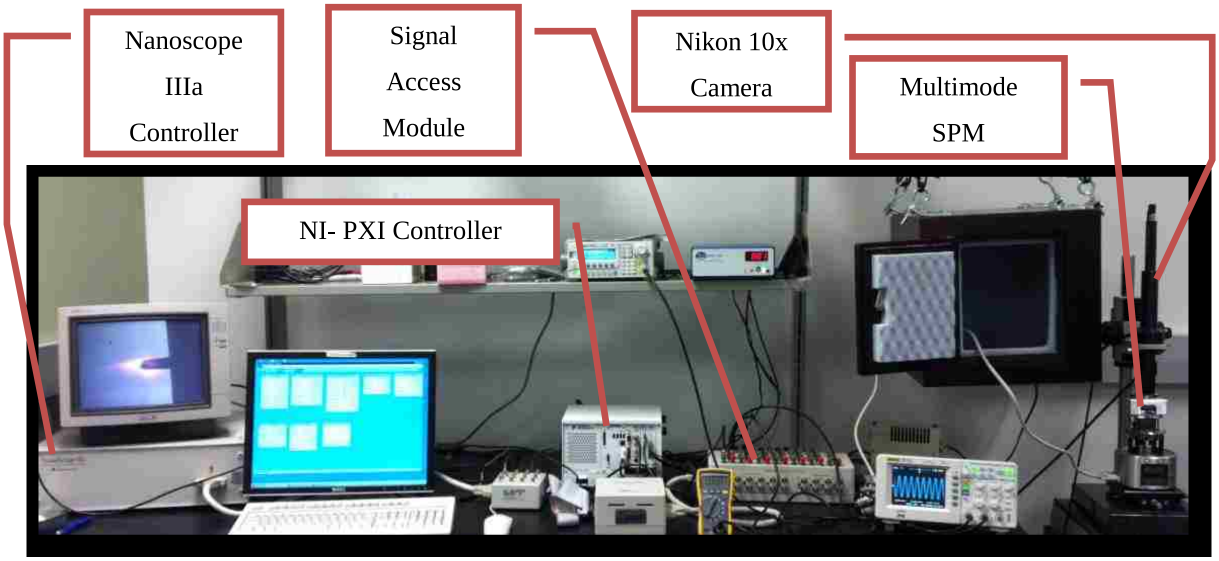

Figure 3.8. A photograph of the experimental setup in 205 Toomey Hall

Figure 3.9 shows a line diagram of all the connections for the experimental setup. To perform the experiments, it is necessary to intercept and replace certain signals between the Nanoscope IIIa controller and the AFM. This is achieved through the use of two signal access modules. The signal access module channels that are used are listed in Table 3.1.

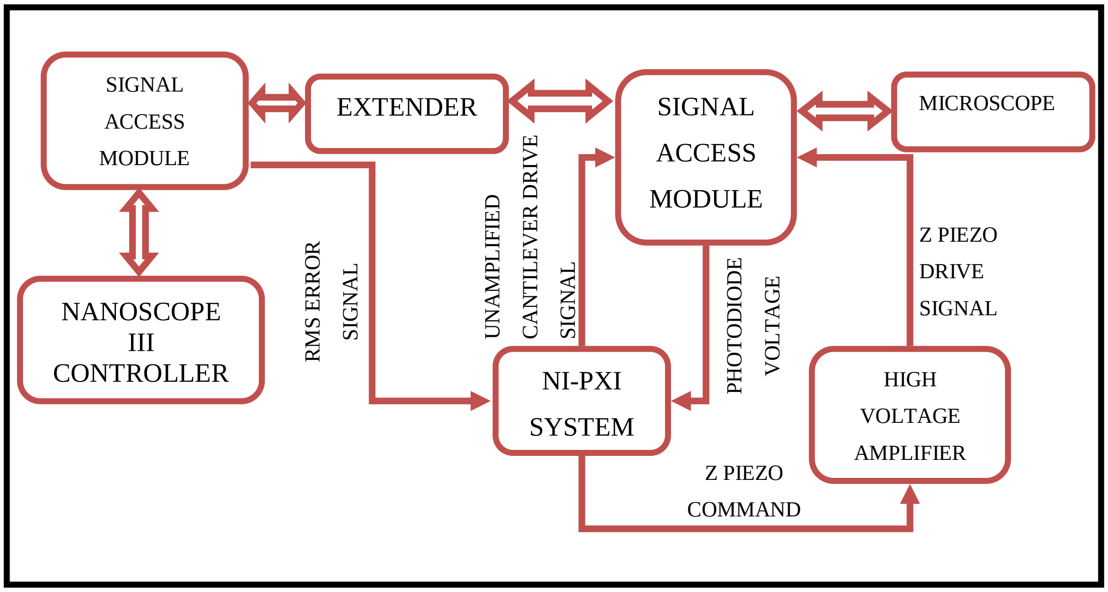

Figure 3.9. Functional Diagram of the experimental Setup

Table 3.1 Signal Access Module Channels

MODULE	**CHANNEL**	**FUNCTION**
II	**ANA 1 (Input)**	Drive Signal
II	**IN 0 (Output)**	Oscillation Amplitude of the Cantilever
II	**High Voltage Z (Input)**	Z-Piezo control
I	**OUTD0 (Output)**	RMS of the Error Signal

The NI-PXI system is used to capture and generate signals for the experiment. It is equipped with Windows Vista Professional and Labview 2009 (Service Pack 1). For our experiments, the PXI must generate two signals: the unamplified Z piezo drive signal, and the cantilever drive signal. The cantilever drive signal is generated on the 5421 function generator which can generate arbitrary functions with upto four million samples at a rate of 100 MHz. This is discussed further in 3.3.3.1.

The Labview programs also control the Z piezo drive signal of the AFM to compensate for thermal and electrical drift. The custom controller replaces the Digital Instruments Nanoscope IIIa controller and is necessary for the sensitivity experiments detailed in section 4.2.1. The PXI 6221 DAQ has a 16 bit resolution with a maximum voltage range of ±10V. The Z axis piezo voltage range is ±220V. The bit value of an analog-to-digital converter refers directly to its resolution. That refers to how finely it slices its full-scale measurement range. The resolution of the Z-piezo is the smallest distance that it can move, and is calculated by using the formula [28] given below.

$$Resolution = \frac{V_D * E}{V_s * 2^n} \tag{16}$$

where, V_s is the full-scale input voltage of the DAQ card, V_D is the voltage range used, E is the maximum Z-piezo extension and n is the bit resolution of the ADC

Therefore,

$$\begin{aligned} Resolution &= \frac{10 * 3.52e-6}{4.2 * 2^{16}} \\ &= 0.19\, nms \end{aligned} \tag{17}$$

The samples used for scanning are gold spluttered silicon, HS 20 MG and Tip check samples from Budget Sensors. Images of these samples are given in appendix D.

3.3.2. Cantilever Tuning and Force Curves. Finding the resonant frequency of the cantilever is referred to as cantilever tuning. This section describes steps required to find the resonant peak of the cantilever and adjust the oscillation voltage so the cantilever will vibrate at the desired amplitude. Input voltages spanning a range of frequencies are applied to the cantilever and the frequency which produces the largest response is selected. The tuning can be done automatically in the Nanoscope software by entering the start and end frequencies, or it can be tuned manually by sweeping across a frequency range. The ranges of frequencies to enter are mentioned on the cantilever case. Manual tuning is sometimes useful, for example, to offset the drive frequency above or below resonant frequency as is often done in magnetic force microscopy and electrostatic force microscopy. Detailed procedure is explained below for manually tuning the cantilever.

- Set the drive amplitude to a value near the center of the range of the resonance frequencies specified for the cantilever. For example, if the frequency range is specified as 240-420 KHz, select a drive frequency of 330 KHz.
- Change the drive amplitude in small steps because the cantilever may detach from the holder if the amplitude is too high and the amplitude setpoint is zero.
- If a peak in the frequency response plot does not appear then increase the drive amplitude and sweep width.
- If the peak still has not appeared, then increase the sweep width by first increasing the drive frequency and maximizing the sweep width.
- After identifying the maximum amplitude peak, center the peak on the frequency sweep plot as shown in the Figure 3.10. If the top of the resonance peak is off the plot, then increase the amplitude set point until it appears.

Figure 3.10. Frequency Sweep after tuning the cantilever (Screenshot from Nanoscope Software)

The amplitude obtained from the photodiode has the unit volts. To obtain the amplitude in nanometers, force calibration is necessary. The amplitude in nanometers is essential for our sensitivity calculations. Force calibration is a process of obtaining the force plot which is a graph of the piezo's extension versus the oscillating tip's amplitude. When performing the force plot in tapping mode AFM, the piezo moves to the center of the current XY scan and then turns off the scanning in those directions. A triangular waveform is applied to the Z electrode of the piezo tube which moves the tip up and down with respect to the sample. The piezo positions the sample just below the tip and then extends a known distance closer to the tip as shown in Figure 3.11. In this process, if the oscillating tip encounters the sample surface then the amplitude starts to decrease.

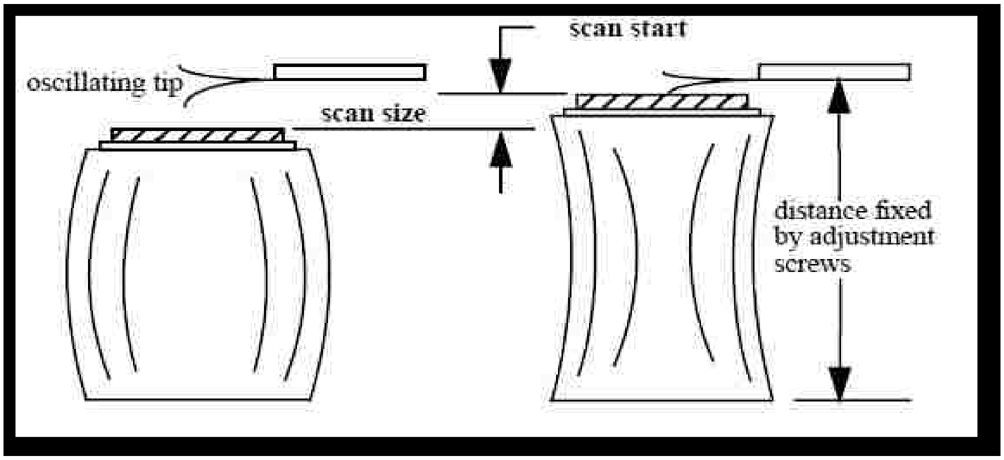

Figure 3.11. Piezo movement for obtaining the force plot [14]

When the tip touches the sample surface, the tip's motion is reduced resulting in a decrease in amplitude as shown in Figure 3.12. When the Z piezo is moved closer to the tip, the amplitude drops down to zero. The point from where the amplitude slopes down to where it becomes flat gives the free amplitude in nanometers.

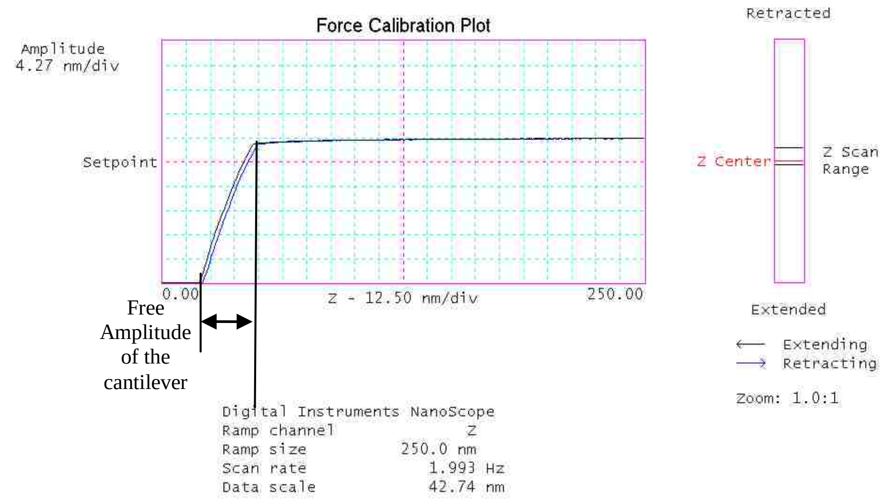

```
Digital Instruments NanoScope
Ramp channel              Z
Ramp size           250.0 nm
Scan rate              1.993 Hz
Data scale             42.74 nm
```

Figure 3.12. Amplitude and deflection versus the Z piezo position (Screenshot from the Nanoscope software)

3.3.3. Labview Programming. In this section, the LabVIEW programs for capturing and generating the various signals used in the experiments are discussed. As shown in Figure 3.13, there are 3 programs to perform the various tasks.

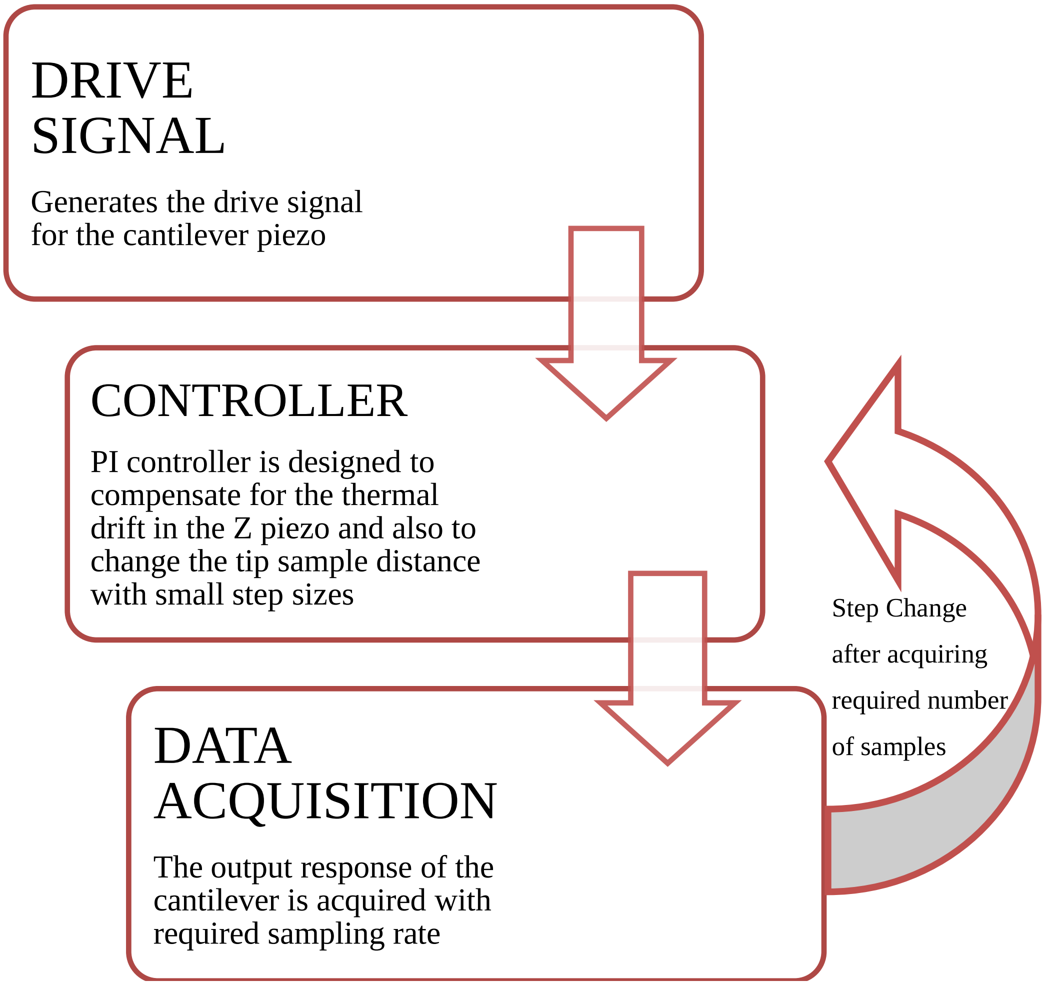

Figure 3.13. Software Organization

3.3.3.1 Driving signal. This program (Figure C.1 in the appendix) generates a driving signal for the cantilever using advanced waveform sequencing and triggering. The program generates dynamic waveforms using scripting which is a series of instructions that indicates how waveforms saved in the onboard memory should be sent.

Initially, two waveforms are uploaded on the card with an equal number of samples. The script is written for switching between signals using a trigger. When it gets the trigger, the second waveform is output, and the previous waveform is cleared from the memory. Hence, a new waveform can be uploaded in real-time. Bursting trigger mode is used, in which the signal generator on receiving the trigger completes the total number of cycles of the present waveform and then switches to the new waveform as shown in the Figure 3.14.

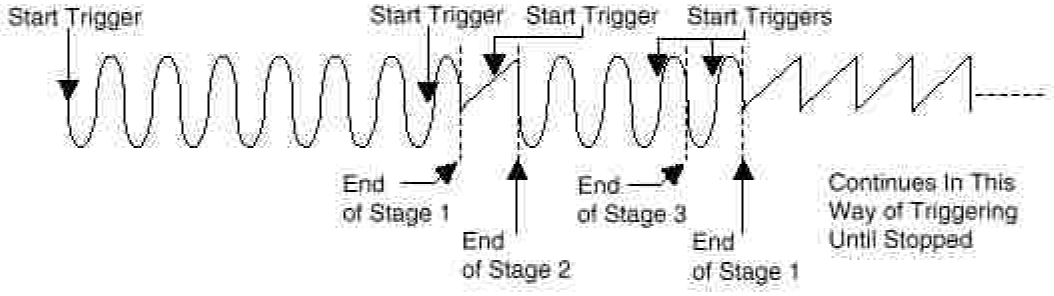

Figure 3.14. Burst Trigger Mode

A subprogram creates the arbitrary waveform required as an array of values and “Write Named Waveform” writes it on to the onboard memory. The block diagram of the program is attached in the appendix C. The “Write Named Waveform” accepts only values normalized between -1 to 1. Hence, the output array from the sub VI is normalized from 1 to – 1. Using the property node for the Write Waveform, the waveform is amplified back by the same factor that is used during normalization as shown in Figure 3.15.

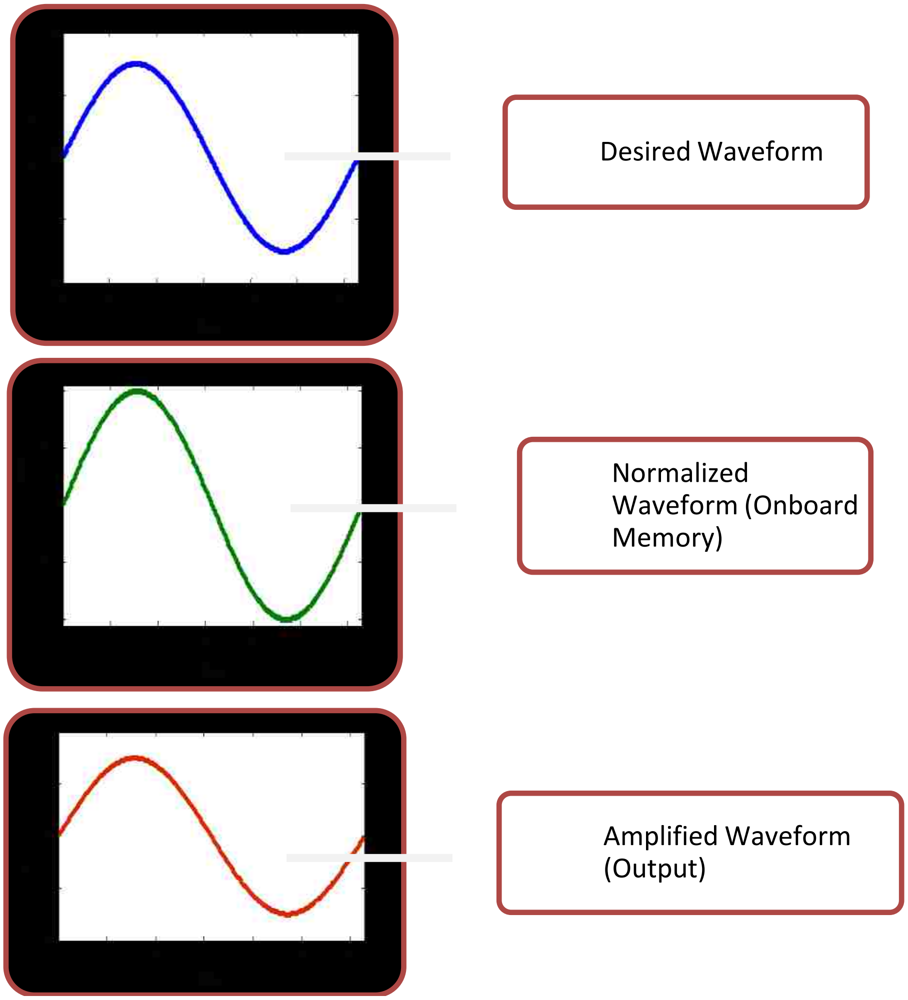

Figure 3.15. Waveform Array Sequence when writing onto the PXI card

For the experiments, it is necessary to sweep over a range of frequencies. The process of switching from one frequency to the next is critically important, as incorrect switching can create transients that change the dynamic mode of the cantilever from high to low. To achieve proper switching, it is necessary that each signal begin and end at the same phase. To achieve this, it is sometimes necessary to slightly change the signal frequency from the desired frequency. For our signals, assume that N=4,000,000 samples are used and the sample period is t_s=0.000001s. Then, the tapping signal is $f(nt_s)$ = A*sin(2π f_0nt_s) for n=0,1,…,(N-1). To end at the same phase as we begin, we need f_0Nt_s to be an integer. Therefore, the frequency f_0 must be selected as $f_0 = K/Nt_s$, where K is an integer. Thus, the frequency resolution of our system is $f_0 = 1/Nt_s$ = 25 Hz. After acquiring the response, frequency is changed, this is taken as a new waveform. This new waveform starts after finishing the previous waveform and hence we can say that there are no transients while switching. In this way, the frequency sweep of the cantilever is obtained.

3.3.3.2 Z piezo control. This program (Figure C.3 in the appendix) is a simple closed loop control system designed as shown in Figure 3.16 to compensate for the drift of the piezo tube in the AFM. In the program, the controller for the loop can be entered as a transfer function. For this purpose a discrete transfer function block is used with the parameter source being terminal. A continuous transfer function is implemented in the Math Script and converted to a discrete transfer function using zero-order hold for conversion. The reference value is the RMS error signal which has to be zero to overcome the drift. The feedback is the RMS error signal obtained from the signal access module. This feedback signal is read by the analog input channel of the multi acquisition DAQ card and compared with the reference input and then passed through the controller. The controller output is sent to the analog output of the DAQ card which is amplified before sending it to the piezo tube. A discrete low pass filter with a time constant of 2 seconds is used to filter the feedback signal preventing the piezo from oscillating rapidly. The entire program is in a timing loop whose period is 30 milliseconds. The time taken for execution of each iteration in the timing loop is determined the period is selected. A step value is added to the controller output to step the Z piezo using a shared variable whose value changes in all the VI where it is used. The block diagram of the program is attached in the appendix C.

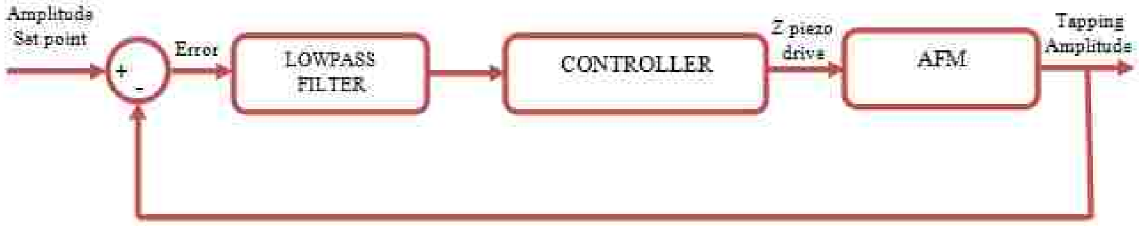

Figure 3.16. Z piezo control loop

3.3.3.3 Acquisition. This program (Figure C.4 in the appendix) acquires the waveform with the given sampling rate and the vertical range. Fetch VIs (a standard in-built function to acquire) are used which acquire data asynchronously, meaning they store data on the digitizer memory only when it is asked for. Also, the main advantage of using these is that one can initiate acquisition and also ask for a query when it is complete. Software reference trigger, a type of trigger is used, which initiates trigger upon identifying the resource. The maximum number of samples that can be acquired is 4x106 samples at the rate of 100 MHz.

The output waveform acquired is a 1D array which is converted to a spreadsheet string and a text file is created using ‘Write to text’ (Standard VI which saves an array of values into a text file). For our experiments, a sampling rate of 25 MHz and maximum number of samples is typically used.

3.3.4. Experimental Procedure. The following experiments use the gold spluttered silicon sample in air. The procedure followed for sweeping through frequencies and measuring amplitude in Multimode SPM.

1. Cantilever is tuned to obtain its resonance frequency.
2. Force calibration is done to obtain the amplitude conversion factor.
3. The resonant frequency is entered in the Labview "Drive Signal" program. This signal is sent to the ANA 1 input channel of the signal access module.
4. The 'High Voltage Z' switch on the signal access module is changed to 'Input' so the PXI system controls the Z piezo. Maximum voltage to the piezo is applied such that the piezo tube extends to its maximum.
5. Using the step motor menu in the nanoscope software, the sample is brought towards the cantilever in steps of 250 nms.
6. When the amplitude starts to decrease, the motor step size is reduced to 26 nm. When the amplitude becomes very low in comparison with the free amplitude, then the piezo tube is retracted.
7. The Labview "Controller Program" is started. This program tracks the sample and compensates for the drift of the piezo tube. The reference value of this control loop can be used to step the cantilever up and down.
8. After the response reaches steady state it is acquired. The frequency on the "Drive Signal" program is changed by a small step, for example, 0.1 KHz.
9. Step 8 is repeated for the desired range of frequencies.

3.3.5. Experimental Results. A sample of the acquired data is shown in Figure 3.17 and Figure 3.18. The cantilever resonant frequency is 294.9 KHz and the amplitude conversion factor is 15 nm/V. A drive amplitude of 0.025 V generates a free amplitude of 24 nm.

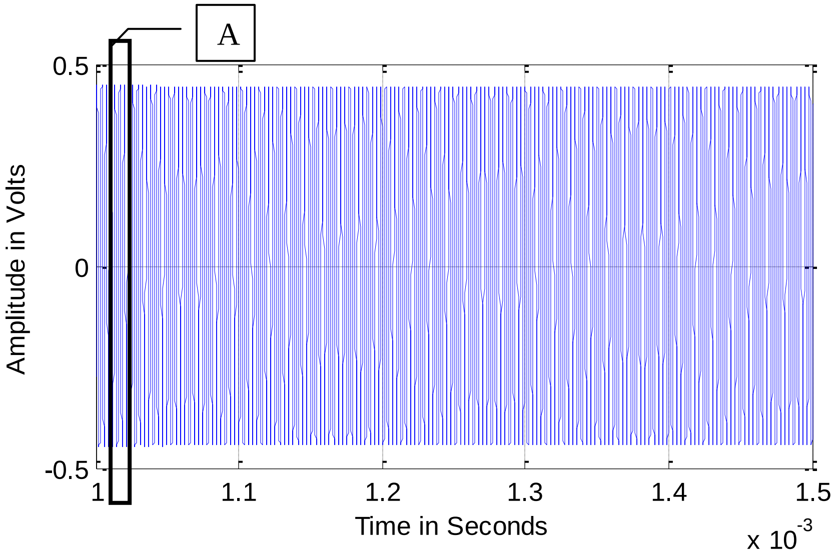

Figure 3.17. Time Domain Response in steady state where the amplitude is averaged

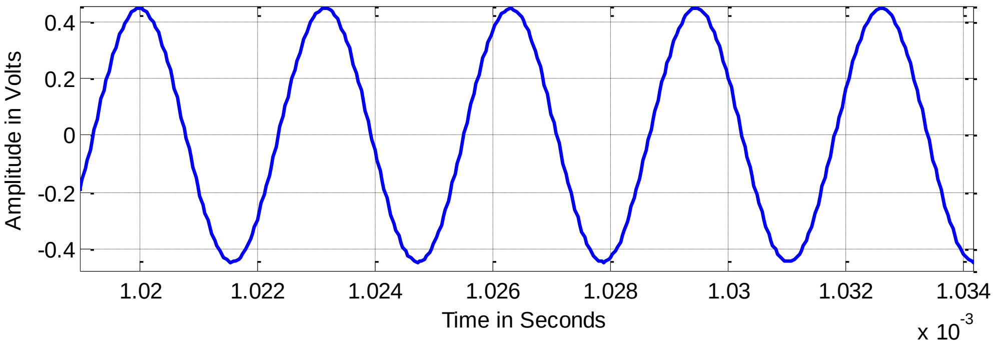

Figure 3.18. Expanded View of Section A from Figure 3.17

Each amplitude value is obtained by averaging the amplitude for 1000 cycles in the steady state. The compiled results are shown in Figure 3.19.

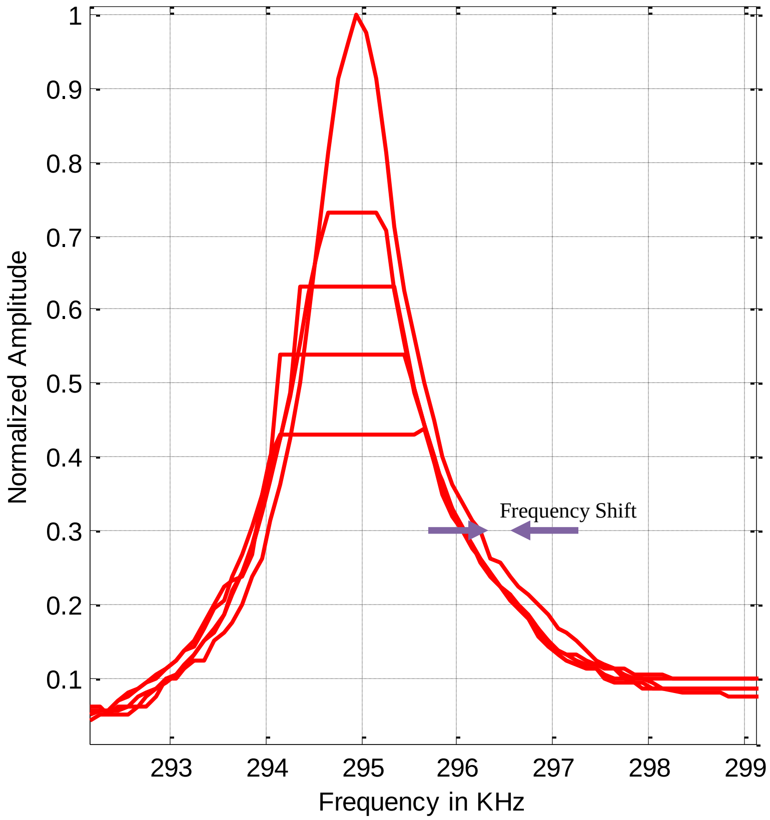

Figure 3.19. Experimental frequency response with free amplitude of 24 nm

In the frequency response, the resonant peak is clearly visible. The flat response of amplitude at different offset is evident. There is some discrepancy in amplitude response when compared with the simulation results. This is likely due to the errors in the force calibration. The primary difference between simulation and experiments is the high amplitude state which does not appear in experiments.

The lack of high amplitude state in experiments has been noted by other researchers [29], [30] and [31]. The existence of a high amplitude state in practice depends on a number of factors. Based on the interaction surface potential, the free amplitudes vary with every sample. The observed switching behavior influences image acquisition and that is the main reason to initiate study in this area (High amplitude state). The magnitude of the attractive forces decreases with decreasing tip size. In other words, the sharper the tip, the smaller the magnitude and lesser is the probability of switching [30]. The tip-sample distance also plays an important role in achieving the high amplitude state [31]. For very small separations the tip adheres onto the surface and for higher separations the low amplitude state dominates. In summary, the factors on which the high amplitude state results are dependent on are listed below.

- Sample Properties (Interaction surface properties)
- Free amplitude of the cantilever
- Tip sample distance
- Tip Radius

Considering these factors, the experiment is carried out for different cantilevers for different samples. For silicon-nitride cantilevers, it is observed that for small free amplitude (15-30 nm) the high amplitude state is not achieved. The system reaches the high amplitude state for the same sample with higher free amplitudes (150-250 nm). The tip radius of the cantilevers was 20 nm and the normalized tip sample distance for which the high amplitude state was observed is between 0.3 and 0.5.

In Figure 3.20, experimental amplitude response plot is shown whose free amplitude was 200 nanometers and the resonant frequency is 283.4 KHz. The high amplitude state is thus achieved and it can be said that the high amplitude range is larger with smaller tip-sample distances as in simulation.

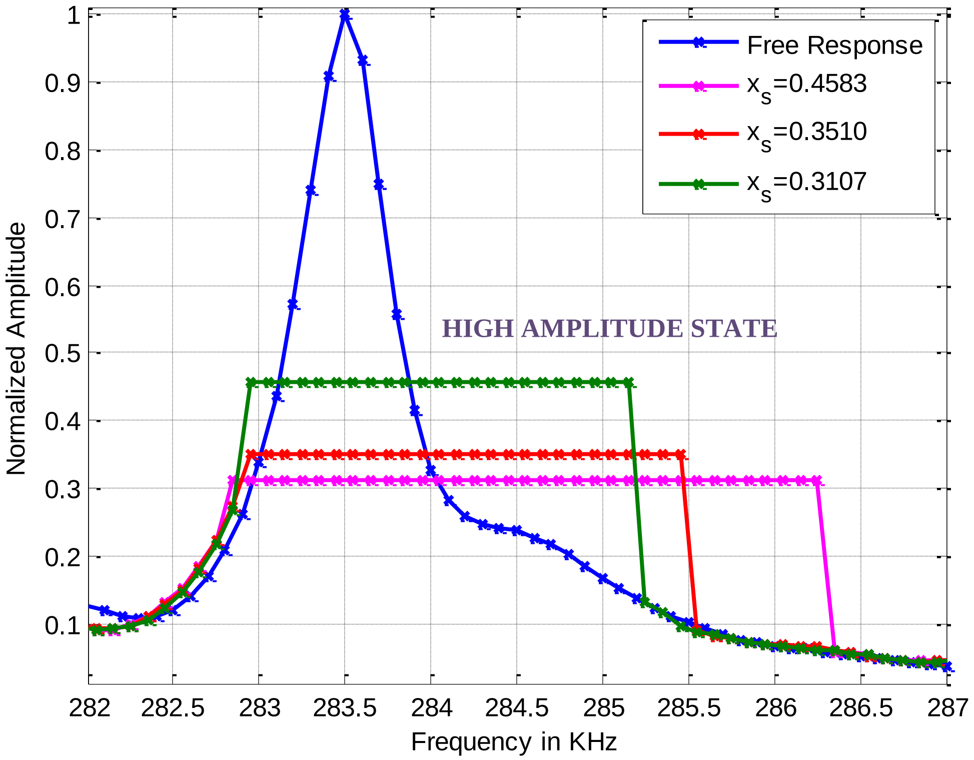

Figure 3.20. Amplitude response at different tip sample distances

When compared with the simulation, the high amplitude state is much smaller which is expected in the experiments. Nonetheless, these results validate that, at least for certain parameters, the high amplitude state exists and extends well beyond the resonant frequency.

4. ATOMIC FORCE MICROSCOPE INPUT SHAPING

In this section, a new technique to shape the drive signal to the piezo actuator on the cantilever is developed. Usually in tapping mode AFMs, the drive signal is sinusoidal as shown in the (13). The amplitude of the drive signal is adjusted to achieve the desired free amplitude of oscillation of the cantilever. The new drive signal developed here is used to increase the measurement sensitivity of the AFM.

4.1. BI-HARMONIC ATOMIC FORCE MICROSCOPE

In this method, a desired free response trajectory is specified and used to design the drive signal. It is believed that the free response trajectory is a more intuitive domain for designing higher order driving signals. The critical portion of the cantilever trajectory is the lowest point of the waveform where the probe strikes the sample surface. In Figure 4.1, the standard tapping mode atomic force microscope trajectory is shown in comparison with a ‘broad valley’ trajectory defined later. The broad valley trajectory will experience more of the nonlinear tip sample interaction forces as the probe spends a longer portion of the trajectory near the sample surface. The main purpose of this thesis is to show that the Bi-harmonic AFM has better measurement sensitivity when compared with the tapping mode AFM.

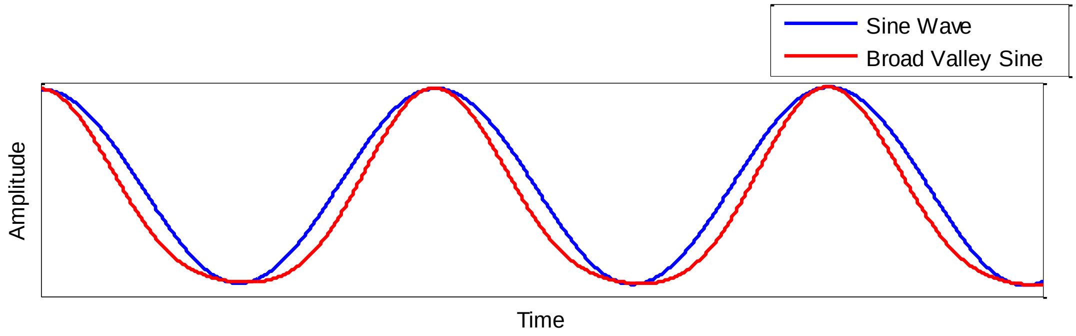

Figure 4.1. Sine wave trajectory and wide-valley sine wave trajectory

Design Procedure. Consider the desired broad-valley trajectory,

$$x_{desired}(\tau) = K\left[sin(\tau) + \gamma\, sin\left(2\tau - \frac{\pi}{2}\right)\right] \tag{18}$$

which generates a sinusoid with a broad valley like the one in Figure 4.1 for $0 \leq \gamma \leq 0.25$. Using the first and second time-derivative of $x_{desired}$, it is straightforward to show the following properties for $0 \leq \gamma < 1/4$:

P1. There is one local minimum of $x_{desired}$ per period, located at $\tau_{min} = -\frac{\pi}{2} + 2\pi i$, $i = 0, \pm1, \pm2, \cdots$

P2. There is one local maximum of $x_{desired}$ per period, located at $\tau_{max} = \frac{\pi}{2} + 2\pi i$, $i = 0, \pm1, \pm2, \cdots$

P3. The amplitude, $\frac{\left[x_{desired}(\tau_{max}) - x_{desired}(\tau_{min})\right]}{2} = K$.

P4. The second time-derivative at the minimum is,

$$\ddot{x}_{desired}\left(\tau_{min}\right) = K\left(1-4\gamma\right).$$

P3 shows that the amplitude of the desired trajectory does not scale with γ, while P4 shows that γ controls the width of the valley. Therefore, (18) provides a suitable model for a broad-valley oscillating trajectory with γ as a tuning parameter.

To generate the broad-valley trajectory, we note that (18) contains only two harmonics. Therefore, it is sufficient to consider a drive signal of two harmonics,

$$F_{dr} = A\left[sin\left(\tau+\phi_1\right)+B\,sin\left(2\tau+\phi_2\right)\right] \tag{19}$$

Then,

$$\begin{aligned} x_{desired}\left(\tau\right) = {} & A\left|G\left(j\right)\right| sin\left(\tau+\phi_1+\angle G\left(j\right)\right) \\ & +AB\left|G\left(2j\right)\right| sin\left(2\tau+\phi_2+\angle G\left(2j\right)\right) \end{aligned} \tag{20}$$

where,

$$G\left(j\omega\right) = \frac{Q/k}{Q\left(1-\omega^2\right)+j\omega} \tag{21}$$

is the Fourier Transform of (3), for large x_s.

Thus,

$$\left|G\left(j\right)\right| = Q/k$$

$$\angle G\left(j\right) = -90^\circ$$

For large Q,

$$\left|G\left(2j\right)\right| = \frac{Q}{k\sqrt{9Q^2+4}} \cong \frac{Q}{3K}$$

$$\angle G(2j) = -180^\circ + tan^{-1}\left(\tfrac{2}{3Q}\right) \approx -180^\circ .$$

From (18) and (20), we have,

$$A = K\frac{k}{Q},\ \phi_1 = 90^\circ,\ B = 3\gamma Q, \text{ and } \phi_2 = 90^\circ .$$

Following the same approach as is taken with the single sine wave driving signal, we add the frequency β as a tuning variable to (18). Therefore, the broad-valley driving signal is given by,

$$F_{dr} = A\left[cos(\beta\tau) + B\,cos(2\beta\tau)\right] \tag{22}$$

where A > 0 is proportional to the free-response amplitude, B > 0 is proportional to the valley width (and should not exceed 3Q/4), and β is the drive frequency. We refer to Equation (22) as a Bi-Harmonic drive signal and use "Bi-Harmonic Atomic Force Microscopy" to refer to the use of this drive signal in imaging. The above approach can be extended to generating a tunable drive signal for any desired periodic trajectory. Here, we limit our approach to two harmonics to keep the number of tuning variables small. It is straightforward to modify the above approach for generating free-response trajectories with a narrow valley. For narrow-valley trajectory, set $-1/4 < \gamma \leq 0$, which corresponds to $(-3Q/4) < B \leq 0$. A narrow valley response may be useful for increasing the force applied by the probe on the surface, such as during nano-indentation.

4.2. NUMERICAL ANALYSIS

Through numerical analysis it can be shown that the broad-valley bi-harmonic can increase the resolution of tapping mode AFM. Numerical simulations were performed in MATLAB using the cantilever model presented in the section 3. Section 4.2.1 analyses sensitivity at the resonant frequency, $\beta=1$. Section 4.2.2 analyses sensitivity for high β where high amplitude state is present.

4.2.1. Resonance Dynamics: Sensitivity. To measure the sensitivity, the tip-sample distance is kept constant for a certain period of time and then a step value is added or subtracted. One such example where the tip sample distance is changed from 0.8 to 0.7 is shown in the Figure 4.2. The change in amplitude when divided by the step value gives the sensitivity. Similarly, the tip sample distance is changed with a step size of 0.1, and for different B/Q values, the sensitivity values are recorded. The plot of sensitivity versus normalized tip sample distance is shown in Figure 4.3. For comparison, parameter 'B' is normalized by Q, as the Q-factor for each cantilever is different. The sensitivity is best when the normalized tip sample distance is in the range of 0.7 to 0.9.

The forward sweeps in Figure 4.3 are run in 0.1 increments of x_s. Note that B=0 is what is used in tapping mode AFMs today. For these systems, 1nm change in sample height will result in a 1nm change in amplitude response. However, with the bi-harmonic drive, sensitivity will increases with increasing β. That is, a 1nm change in sample height will result in a greater than 1nm change in the cantilever amplitude, effectively increasing the resolution.

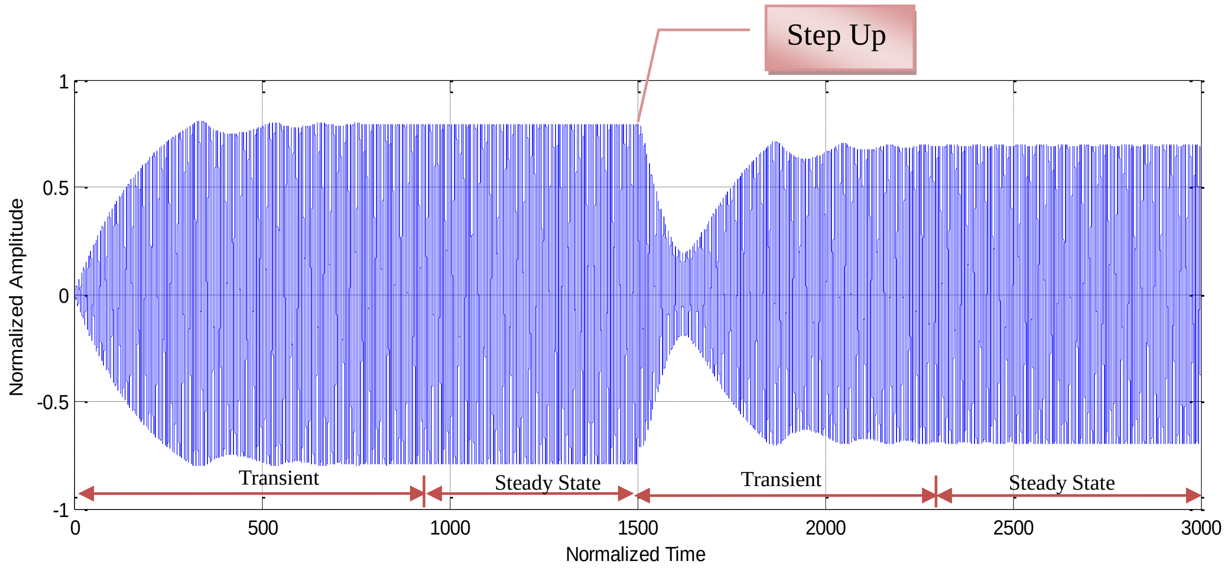

Figure 4.2. Time Domain Response at the resonant frequency (Simulation), Q=100, B=0 and β=1

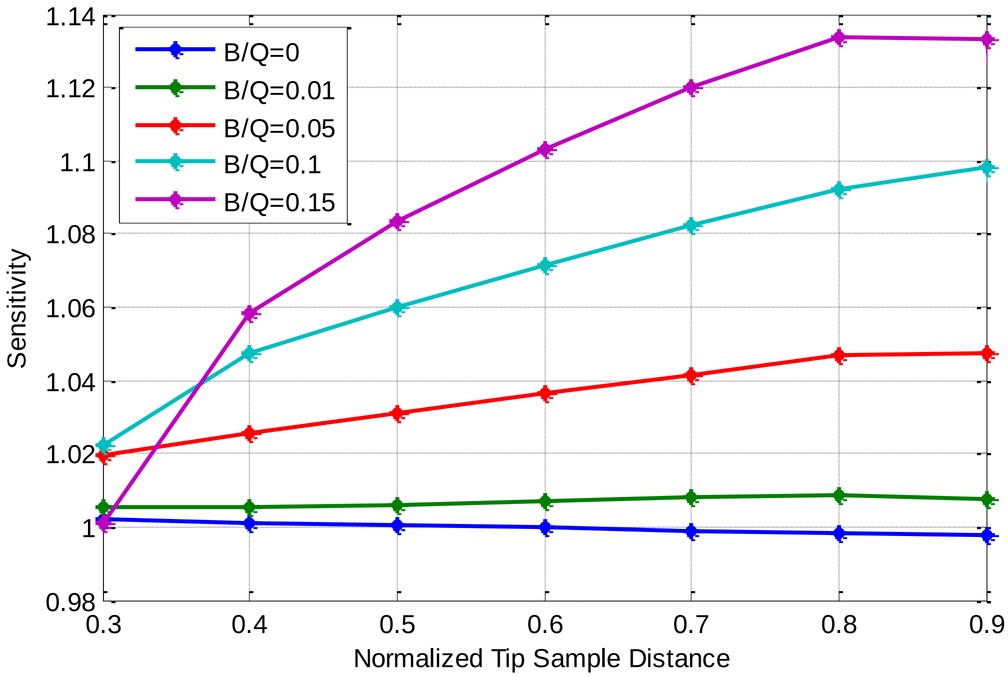

Figure 4.3. Sensitivity Plot (Q factor=100) at the drive frequency β=1

4.2.2. High Amplitude Dynamics. A frequency sweep of the bi-harmonic drive signal with different values of B is investigated. The amplitude response is shown in Figure 4.4 for the forward sweep of frequencies when xs = 0.5. Over low frequencies (up to β=1.7), the amplitude response of more than one bi-harmonic AFM closely match that of the tapping mode AFM (although sufficiently different to increase sensitivity as shown in the previous section). However, as the value of B increases, the cantilever stays in high amplitude mode over a larger frequency range. Furthermore, the amplitude grows at a rate faster than linear. While the single harmonic also demonstrates a similar growth rate, the high amplitude state is only achievable in single harmonic for a range that is approximately linear. It will be shown in the later part of this section that the growth rate is directly related to measurement sensitivity.

The trend shown in Figure 4.4 continues for different x_s offset values. In Figure 4.5, we show the amplitude response for a range of x_s with B=2. The frequency is swept from 0.9 to 1.6 (forward sweep) and then from 1.6 to 0.9 (reverse sweep). As was seen in Figure 4.5, the amplitude response of the bi-harmonic AFM is similar to the tapping mode AFM except that the high amplitude state is stable for a higher range of frequencies.

It is seen that the amplitude increases as the frequency increases and the amplitude drops at a particular frequency. The broad response has the drop at higher frequencies depending upon the tip sample distance. After a certain tip sample distance, the narrow response drops at higher frequencies when compared to the tapping mode AFM.

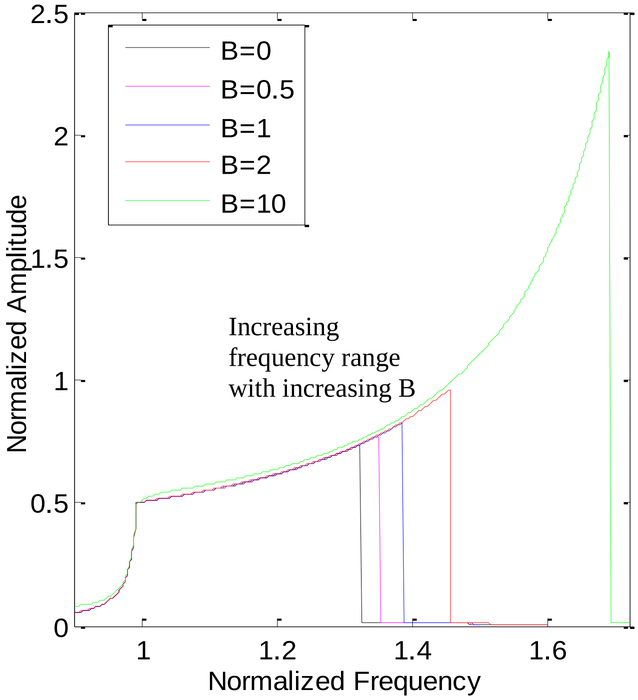

Figure 4.4. Amplitude response of the high amplitude mode for different values of B at $x_s = 0.5$

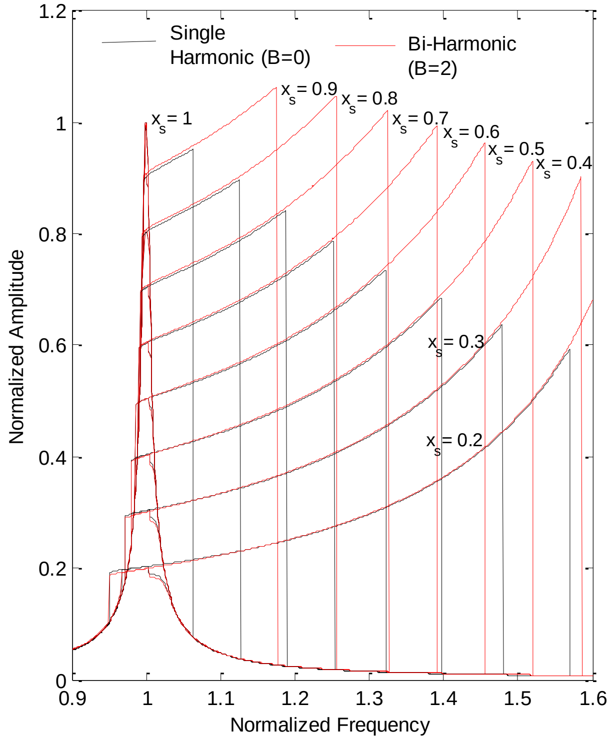

Figure 4.5. Normalized amplitude versus normalized frequency (β) for bi-harmonic and single harmonic drive signals. Bi-harmonic uses B=2.

The time-history of a cantilever with a single harmonic and a bi-harmonic drive as the cantilever crosses a step change in sample height is shown in Figure 4.6. The 0.75nm step occurs at τ=1000 in each plot. As can be seen, the response for the bi-harmonic (after transients have settled) changes by approximately twice that of the single harmonic (over 3nm peak-to-peak change as compared to 1.5nm peak-to-peak). Also notable is that the settling time remains unchanged (800 units of nondimensional time, or 2.7 ms).

This is because we have only changed the driving signal to the cantilever without altering the dynamics and differs fundamentally from high Q control methods [32] which use feedback to change the response at the expense of settling time. As discussed above, the measurement sensitivity for both single harmonic and bi-harmonic drive signals changes with offset height and frequency. The maximum sensitivity occurs when β is at its largest and x_s is smallest.

In Figure 4.7, maximum sensitivity for several choices of B and x_s is shown. For each data point the maximum β in high amplitude state is used. Clearly, the sensitivity increases with increasing B, or wider valley trajectories.

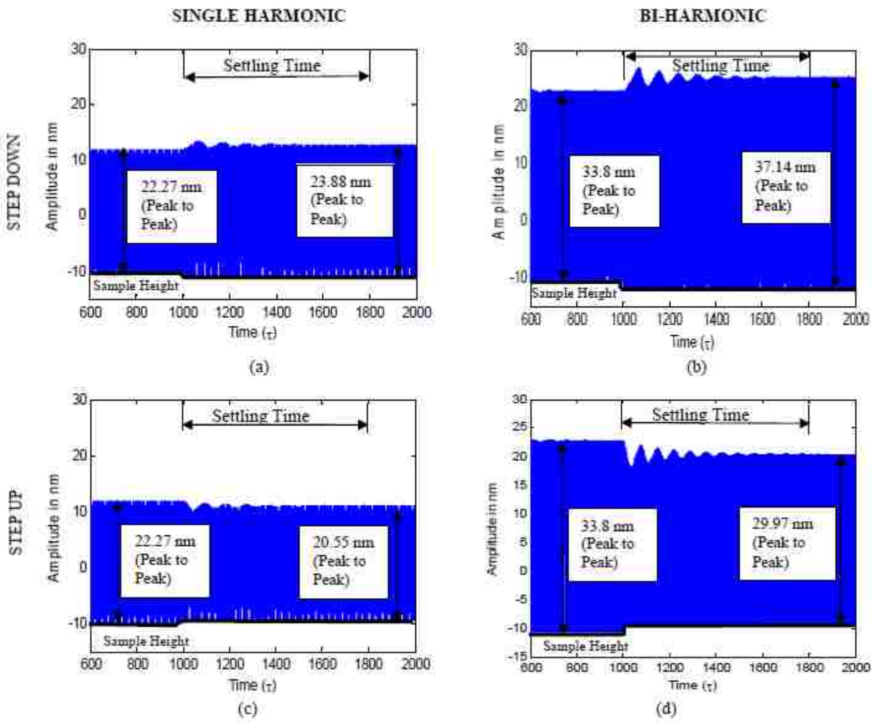

Figure 4.6. Time history plots showing the cantilever response to step changes in the sample height. Plots (a) and (c) show the response using a single harmonic drive signal with β=1.2. Plots (b) and (d) show the response using a bi-harmonic drive signalwith B=10 and β=1.5 (Simulation)

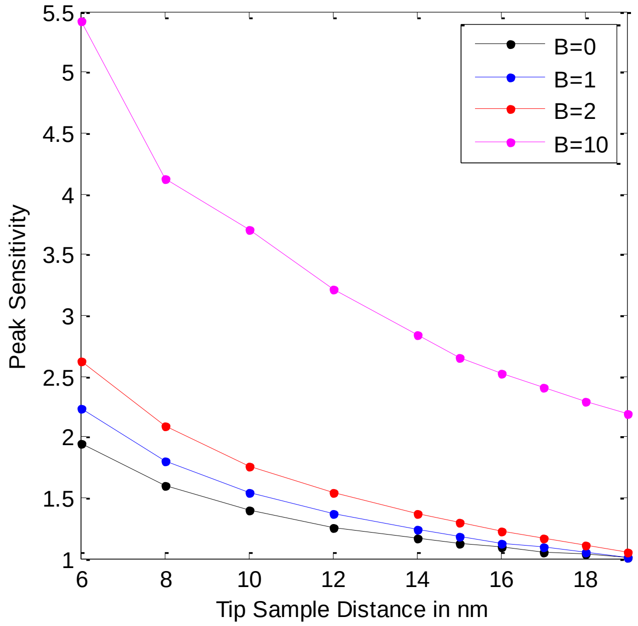

Figure 4.7. Peak sensitivity versus Tip sample distance

4.3. BI-HARMONIC EXPERIMENTS

4.3.1. Resonance Dynamics. In the following, the change in amplitude at different tip sample distances for tapping AFM and the Bi-Harmonic AFM are compared at resonant frequency. The steady state amplitude before and after the step are the values of interest to find the sensitivity change. To obtain these values, a MATLAB code (attached in the appendix B.2) is developed. The response obtained from the digitizer is too noisy to detect the small change in amplitude which is shown in Figure 4.8. Hence, the signal is filtered using the filter design and analysis toolbar in MATLAB. A band pass IIR Butterworth filter is designed to isolate the response at the tapping frequency. The magnitude response is shown in Figure 4.9 and the filtered response is shown in Figure 4.10.

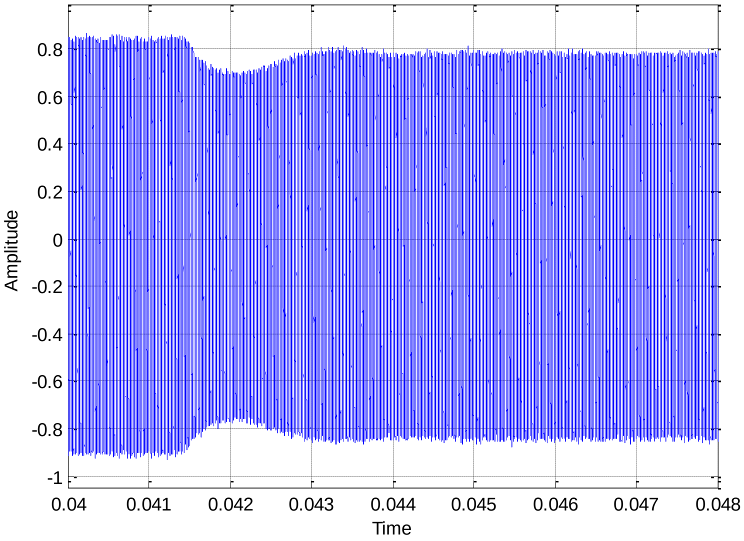

Figure 4.8. Unfiltered time domain response with a single harmonic drive signal depicting the amplitude change after the stepping

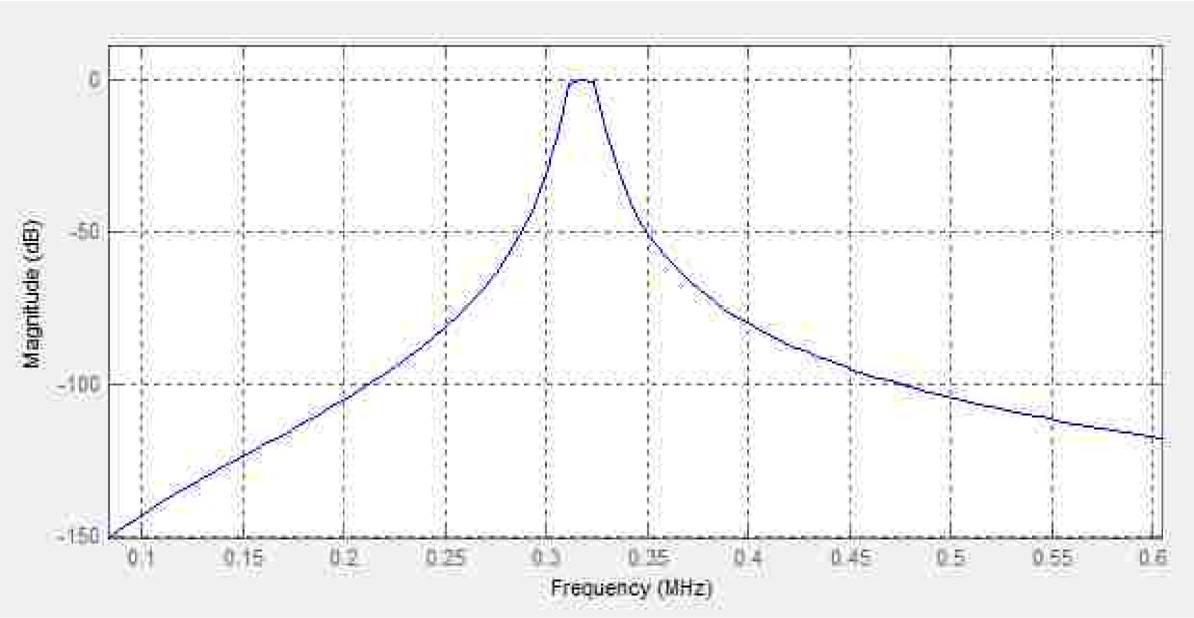

Figure 4.9. Magnitude Response of the filter

To calculate the steady state amplitude, we use 1000 cycles of the step. The start of the step is determined manually, as shown in Figure 4.10.

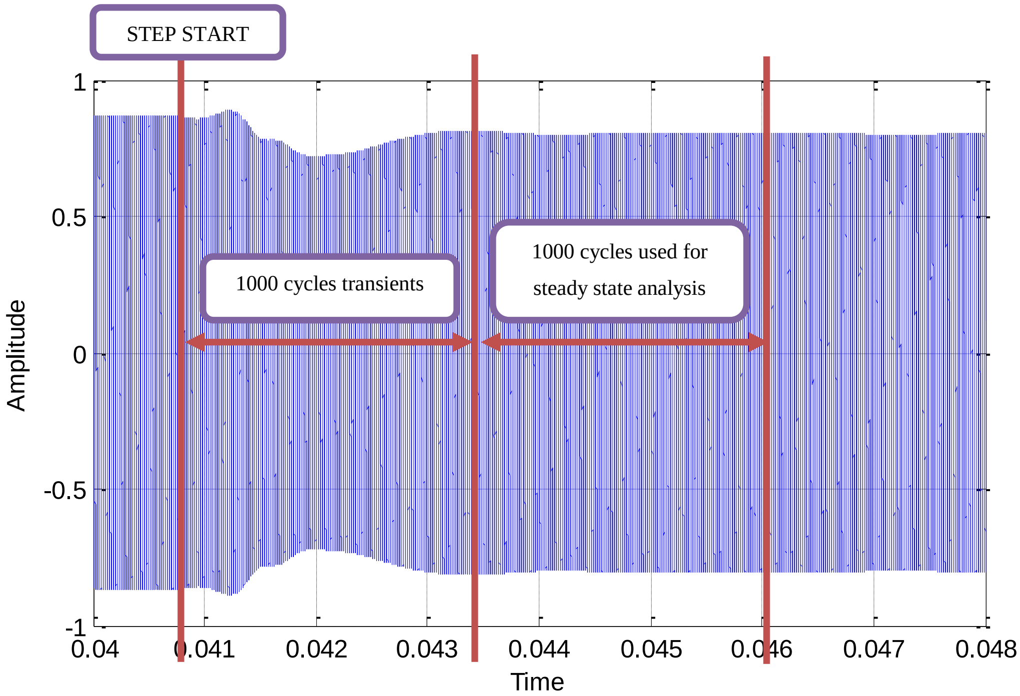

Figure 4.10. Filtered time domain response from Figure 4.8

The integral gain in the Z-piezo controller program is reduced so that the acquired response has more than 1000 cycles in the steady state after stepping. The experiment is repeated 15 times keeping all the variables constant. The values obtained are recorded. Similarly, for different B/Q values of the drive input signal, 15 iterations are carried out per B/Q value and these are also recorded as shown in the Table 4.1.

Table 4.1. Experimental amplitude values averaged over 1000 cycles in steady state before and after stepping.

B=0

Iteration	Before Stepping	After Stepping	Change in Amplitude
1	0.44564	0.42208	0.02356
2	0.44114	0.41609	0.02505
3	0.44232	0.41705	0.02527
4	0.44409	0.41786	0.02623
5	0.44132	0.41722	0.02410
6	0.44268	0.41803	0.02465
7	0.44239	0.41890	0.02349
8	0.44501	0.41650	0.02851
9	0.44188	0.41197	0.02991
10	0.44391	0.41564	0.02827
11	0.44274	0.42191	0.02083
12	0.44341	0.42269	0.02072
13	0.44274	0.42191	0.02083
14	0.44413	0.42073	0.02340
15	0.44258	0.41919	0.02339

Table 4.1. Experimental amplitude values averaged over 1000 cycles in steady state before and after stepping. (Contd..)

B=0.01

Iteration	Before Stepping	After Stepping	Change in Amplitude
1	0.44361	0.41946	0.02415
2	0.44343	0.42761	0.01582
3	0.44146	0.41888	0.02258
4	0.44201	0.42176	0.02025
5	0.44315	0.42453	0.01862
6	0.44231	0.41431	0.02800
7	0.44093	0.42179	0.01914
8	0.44288	0.42212	0.02076
9	0.44364	0.42799	0.01565
10	0.44681	0.41945	0.02736
11	0.44416	0.41539	0.02877
12	0.44354	0.41800	0.02554
13	0.44303	0.42126	0.02177
14	0.44001	0.41724	0.02277
15	0.44463	0.41697	0.02766

B=0.02

Iteration	Before Stepping	After Stepping	Change in Amplitude
1	0.44194	0.41744	0.02450
2	0.44263	0.41661	0.02602
3	0.44118	0.41514	0.02604
4	0.44140	0.41707	0.02433
5	0.44175	0.41881	0.02294
6	0.44307	0.41928	0.02379
7	0.44338	0.42089	0.02249
8	0.44189	0.42150	0.02039
9	0.44320	0.41635	0.02685
10	0.44225	0.42670	0.01555
11	0.44391	0.42573	0.01818
12	0.44334	0.42320	0.02014
13	0.44443	0.42200	0.02243
14	0.44375	0.41575	0.02800
15	0.44416	0.42265	0.02151

Table 4.1. Experimental amplitude values averaged over 1000 cycles in steady state before and after stepping. (Contd..)

B=0.03

Iteration	Before Stepping	After Stepping	Change in Amplitude
1	0.44323	0.42321	0.02002
2	0.44168	0.41990	0.02178
3	0.44373	0.42118	0.02255
4	0.44289	0.41916	0.02373
5	0.44506	0.41858	0.02648
6	0.44451	0.41968	0.02483
7	0.44336	0.42609	0.01727
8	0.44088	0.41649	0.02439
9	0.44545	0.42433	0.02112
10	0.44323	0.42591	0.01732
11	0.44137	0.42612	0.01525
12	0.44292	0.41945	0.02347
13	0.44102	0.42121	0.01981
14	0.44265	0.42080	0.02185
15	0.44292	0.41945	0.02347

B=0.04

Iteration	Before Stepping	After Stepping	Change in Amplitude
1	0.44167	0.42618	0.01549
2	0.44363	0.42409	0.01954
3	0.44106	0.42684	0.01422
4	0.44433	0.42270	0.02163
5	0.44383	0.42111	0.02272
6	0.44252	0.42535	0.01717
7	0.44233	0.42402	0.01831
8	0.44257	0.42233	0.02024
9	0.44155	0.41777	0.02378
10	0.44168	0.41844	0.02324
11	0.44426	0.42138	0.02288
12	0.44245	0.41970	0.02275
13	0.44251	0.42019	0.02232
14	0.44102	0.42128	0.01974
15	0.44279	0.42326	0.01953

Table 4.1. Experimental amplitude values averaged over 1000 cycles in steady state before and after stepping. (Contd..)

B=0.05

Iteration	Before Stepping	After Stepping	Change in Amplitude
1	0.44094	0.41566	0.02528
2	0.44003	0.41448	0.02555
3	0.44383	0.41681	0.02702
4	0.44265	0.41922	0.02343
5	0.44269	0.42143	0.02126
6	0.44234	0.42227	0.02007
7	0.44123	0.42246	0.01877
8	0.44196	0.42201	0.01995
9	0.44202	0.42373	0.01829
10	0.44313	0.42165	0.02148
11	0.44294	0.42220	0.02074
12	0.44358	0.42339	0.02019
13	0.44351	0.42137	0.02214
14	0.44402	0.41898	0.02504
15	0.44374	0.41521	0.02853

B=0.1

Iteration	Before Stepping	After Stepping	Change in Amplitude
1	0.44161	0.42515	0.01646
2	0.44296	0.41399	0.02897
3	0.44214	0.41277	0.02937
4	0.44051	0.40886	0.03165
5	0.43853	0.41628	0.02225
6	0.44230	0.42370	0.01860
7	0.44265	0.42020	0.02245
8	0.44279	0.42195	0.02084
9	0.44306	0.42162	0.02144
10	0.44321	0.41944	0.02377
11	0.44351	0.41800	0.02551
12	0.44309	0.41435	0.02874
13	0.44306	0.41646	0.02660
14	0.44396	0.41359	0.03037
15	0.44452	0.41958	0.02494

Table 4.1. Experimental amplitude values averaged over 1000 cycles in steady state before and after stepping. (Contd..)

B=0.15

Iteration	Before Stepping	After Stepping	Change in Amplitude
1	0.43995	0.42103	0.01892
2	0.43955	0.42276	0.01679
3	0.44088	0.41725	0.02363
4	0.44090	0.42340	0.01750
5	0.44110	0.42629	0.01481
6	0.44262	0.42361	0.01901
7	0.44029	0.41723	0.02306
8	0.43946	0.41368	0.02578
9	0.44262	0.41688	0.02574
10	0.44198	0.42164	0.02034
11	0.44011	0.42102	0.01909
12	0.43950	0.42014	0.01936
13	0.44136	0.41838	0.02298
14	0.44247	0.41795	0.02452
15	0.44049	0.41955	0.02094

The mean and the variance for each B/Q value are shown in Table 4.2.

Table 4.2. Mean and Variance of the change in amplitude for the experimental results shown in Table 4.1

B/Q	MEAN	VARIANCE
0	0.02023	0.0000086005
0.01	0.02083	0.0000111224
0.02	0.02155	0.0000098465
0.03	0.02251	0.0000097372
0.04	0.02258	0.0000184460
0.05	0.02287	0.0000113669
0.1	0.02454	0.0000077979
0.15	0.02479	0.0000202544

The results in Table 4.1 show a clear trend of increasing sensitivity with increasing B. To further validate these results, hypothesis testing is used.

Hypothesis testing, which is to know how if a result is unlikely to have occurred by chance, is carried out with the experimental results. The two sample t-test is used to obtain the probability with which the bi-harmonic sensitivity is more than the single harmonic. The probability values are shown in Table 4. and the sensitivity values are shown in Table 4..

Table 4.3. Probability that Bi-Harmonic is more sensitive than single harmonic

B/Q	PROBABILITY
0.01	0.92
0.02	0.92
0.03	0.99
0.04	0.99
0.05	0.99
0.15	0.99

From the hypothesis test results, it can be concluded that the bi-harmonic AFM gives a larger change in amplitude when compared with the tapping AFM. The mean of the change in amplitude is calculated for the 15 iterations and the percentage increase in sensitivity with the tapping AFM is calculated.

Table 4.4. Sensitivity when compared with the TAFM

B/Q	Percentage Increase in Sensitivity
0.01	2.9
0.05	13.1
0.1	21.3
0.15	22.5

4.3.2. High Amplitude State Dynamics. Following the steps explained in section 3.3.4, the free amplitude of the cantilever is set to 200 nm and is brought close to the sample till it comes in contact. The parameter ‘B’ in the drive signal is changed keeping the tip sample distance constant. The amplitude response for different bi-harmonic drive amplitudes when the tip sample distance is 0.3633 of the normalized amplitude is shown in Figure 4.11. Clearly, increasing the value of B has had the effect of increasing the frequency range of the high amplitude state, as observed in the simulations. However, we do not see an increasing slope in the amplitude in the experimental results that were seen in the simulation. This may be due to the relatively small values of B that were used. Because of saturation limits in this system, we cannot extend to higher values, so the positive sloping is seen in the simulations cannot, at present be validated.

Likewise, the rapid increase in sensitivity cannot be validated. It is important to note that B cannot be made arbitrarily large. In our system saturation occurs when voltage to the piezo on the cantilever exceeds ±10 V. Thus, the maximum ‘B’ that can be used in our system is given by,

$$B = \frac{10}{A} \tag{23}$$

To get free amplitude of around 200 nms as shown in Figure 4.11, ‘A’ should be 0.1 V. Therefore, maximum bi-harmonic drive amplitude that can be used is 100.

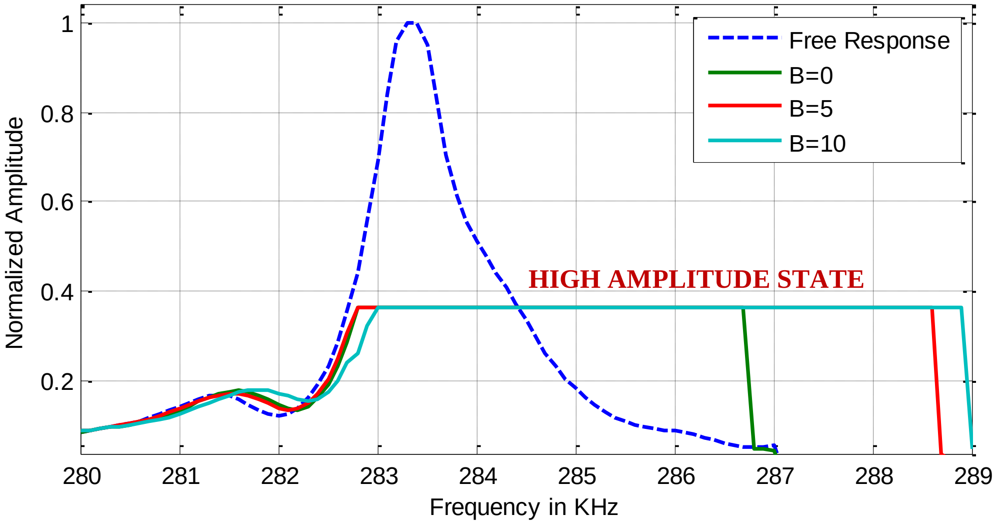

Figure 4.11. Experimental Amplitude Response when xs=0.3633 for different bi-harmonic drive amplitude

4.3.3. Bi-Harmonic AFM Imaging. From the bi-harmonic sensitivity results at resonance frequency, the resolution of the images with the bi-harmonic drive signal should be higher when compared to the single harmonic. The imaging is done using the following procedure.

1. The cantilever is tuned to determine the resonance frequency.
2. The ANA1 channel in the signal access module is switched to input and the bi-harmonic drive signal is generated from the output of the PXI FGEN card.

3. In the nanoscope software, the scan parameters like scan size, scan rate, number of samples and the offsets are entered. The cantilever is engaged.
4. After engage, the amplitude setpoint is varied until the Z piezo bar in the nanoscope software is centered.
5. The image is captured and after scanning the sample for the scan size mentioned, the 'B' value in the drive signal is changed. The next frame is again captured and the procedure is repeated for different bi-harmonic drive amplitudes.

The imaging is done at the same spot each time for different bi-harmonic drive amplitudes. In one trial, a silicon sample with a thin film wear resistant film is imaged for a scan size of 1µm. The sample does not have any regular shapes. The bi-harmonic AFM images in comparison with the TAFM are shown in Figure 4.12, Figure 4.13, Figure 4.14. The sharpness of image indicates the clarity of detail. We expect higher measurement sensitivity to appear as improved sharpness of the image. It can be seen from the images that the sharpness of the image increases as the value of B/Q increases. In general, the sharpness of the image describes how quickly the image information transitions at an edge. The resolution of the image is the ability of distinguish closely spaced elements in detail as shown in the images. As the value B/Q is increased, the features are more prominent.

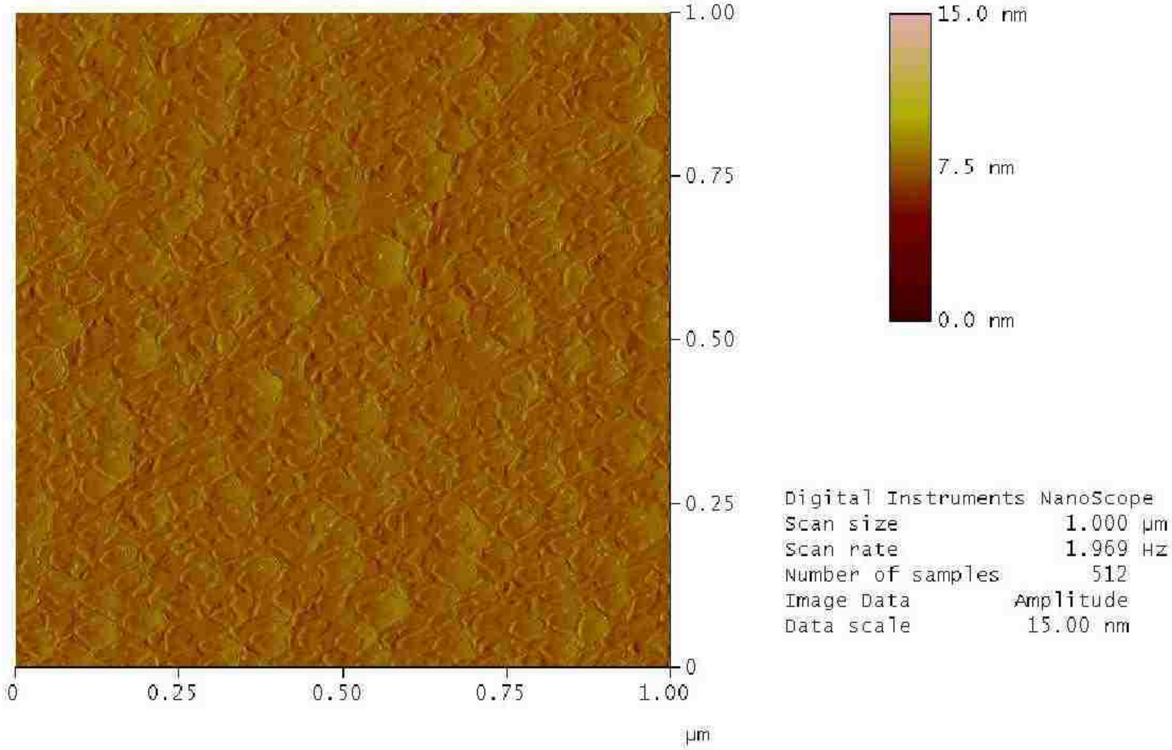

```
Digital Instruments NanoScope
Scan size                1.000 µm
Scan rate                1.969 Hz
Number of samples          512
Image Data             Amplitude
Data scale             15.00 nm
```

Figure 4.12. Silicon sample with thin film wear resistant coating when B/Q=0

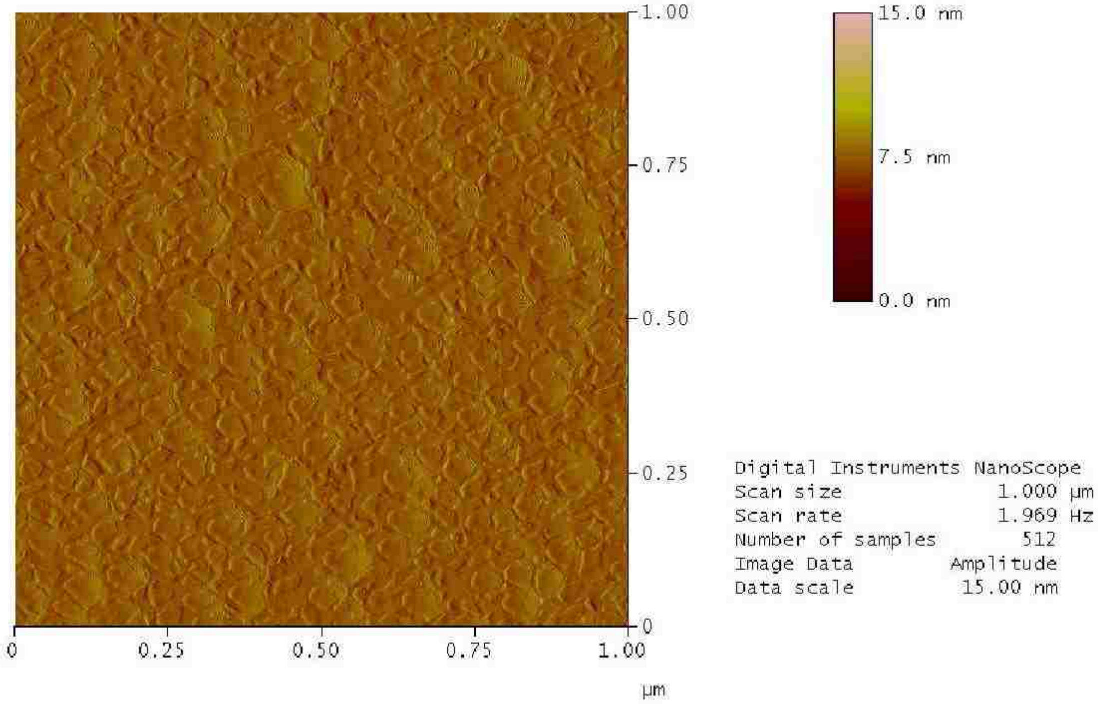

```
Digital Instruments NanoScope
Scan size                1.000 µm
Scan rate                1.969 Hz
Number of samples          512
Image Data             Amplitude
Data scale             15.00 nm
```

Figure 4.13. Silicon sample with thin film wear resistant coating when B/Q=0.05

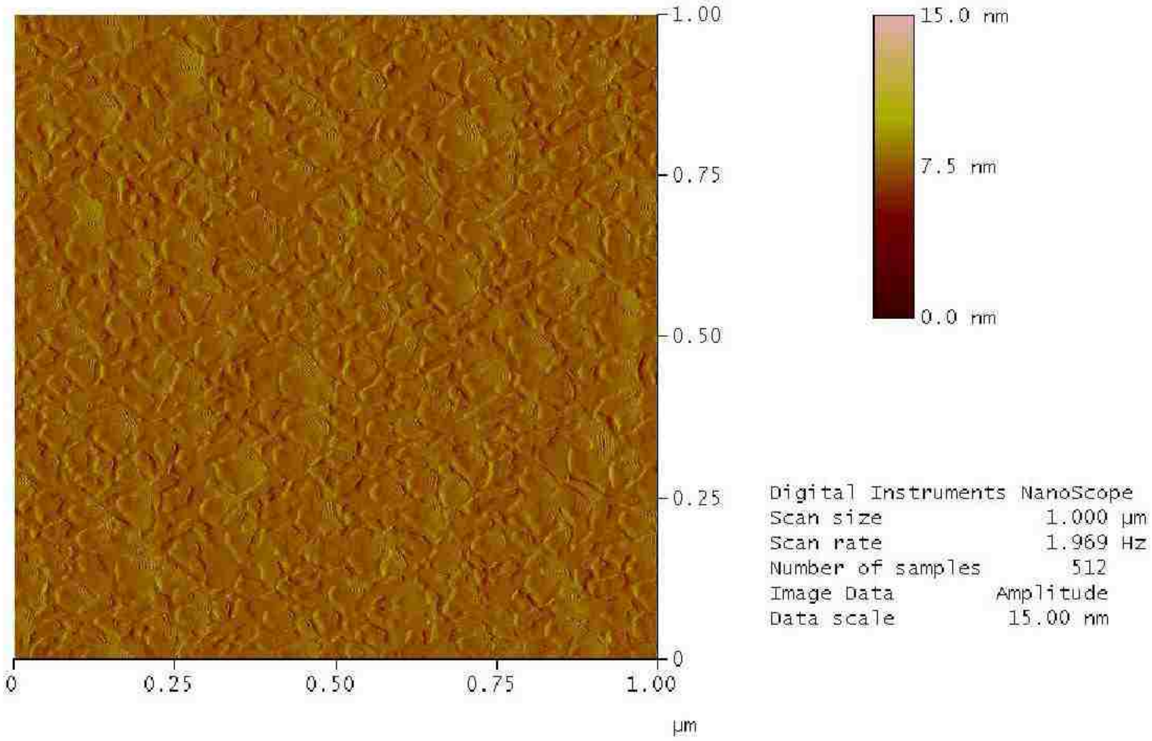

Figure 4.14. Silicon sample with thin film wear resistant coating when B/Q=0.1

We will examine the trace and retrace lines. These lines should be identical, but often times they are not because of noise and poor feedback tracking. If the Bi-harmonic AFM is improving measurement sensitivity, then we can expect that the feedback controller will receive a higher quality feedback signal. This should result in better control and thus better matching in trace and retrace. The scan lines are recorded and imported to Matlab as an ASCII file and scan lines are plotted for both trace and retrace. When the trace and retrace scan lines are plotted, it is observed that the Bi-harmonic AFM lines coincide well suggesting that the images are of better resolution when compared to the TAFM. Figure 4.15 and Figure 4.16 show some of the scan lines. The image has a total of 512 scan lines, only a few are shown here for comparison purposes.

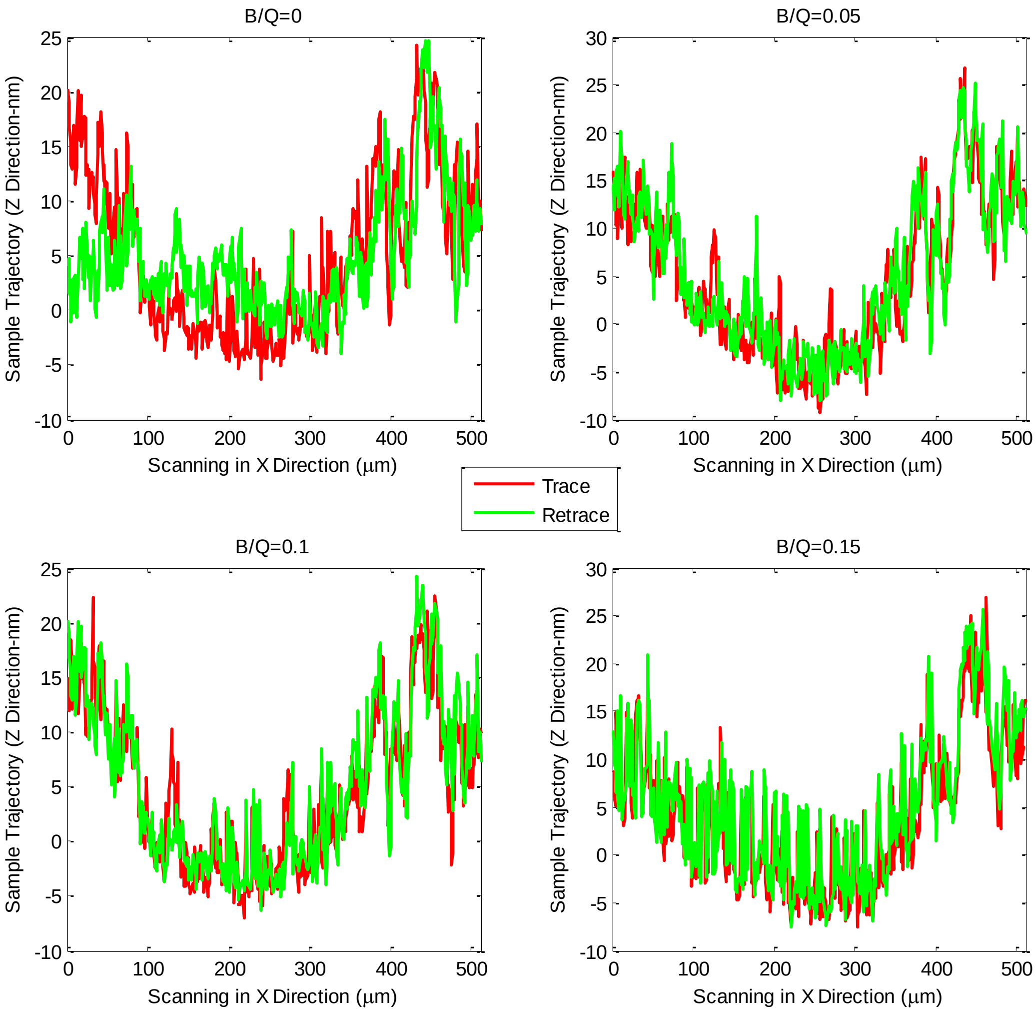

Figure 4.15. Scan Line 1

For higher B/Q values, some of the spikes are eliminated, and the sample is tracked better, identifying some minute irregularities in the sample. Quantification of sharpness and resolution of the image to bring out better comparison between the single harmonic and the bi-harmonic drive signal is a more ideal way to prove the measurement sensitivity results.

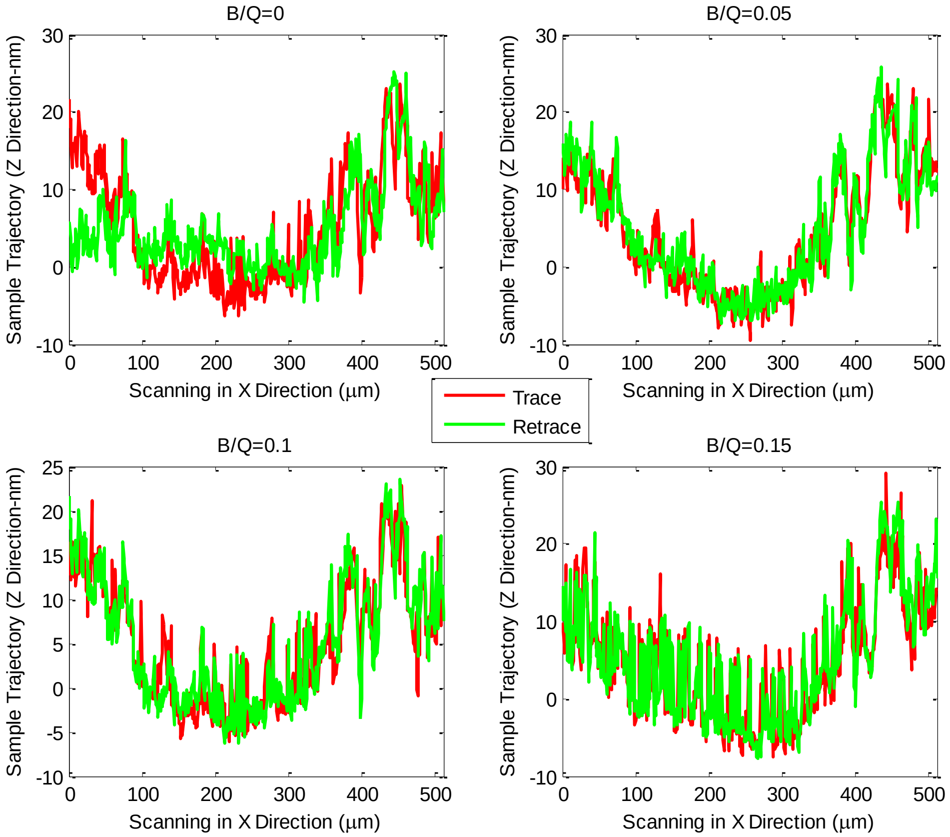

Figure 4.16. Scan Line 2

Analyzing the image is very important to determine the sharpness of these images. Initially, to determine the sharpness we relied upon that the fact that the human eye can be employed as an evaluation tool. But the differences being very subtle, a quantitative analysis of the sharpness of the image is required. Frequency and phase information is available for analysis. We consider only the frequency information in this thesis for the analysis. The image is imported in Matlab and a 2D Fourier transform is obtained. Turning this Fourier domain image into a binary distribution with a simple threshold operation at a suitable level or color coding as explained in [37], gives a difference in the frequency magnitude distribution which is related to the sharpness. A sharper image has more high frequency components than a blurry image. The intensity of the high frequency components is the measure to determine the sharpness of the image. The Fourier magnitude distributions as binary (threshold at 155) are shown in Figure 4.17, Figure 4.18 and Figure 4.19 for the images Figure 4.12, Figure 4.13 and Figure 4.14 respectively.

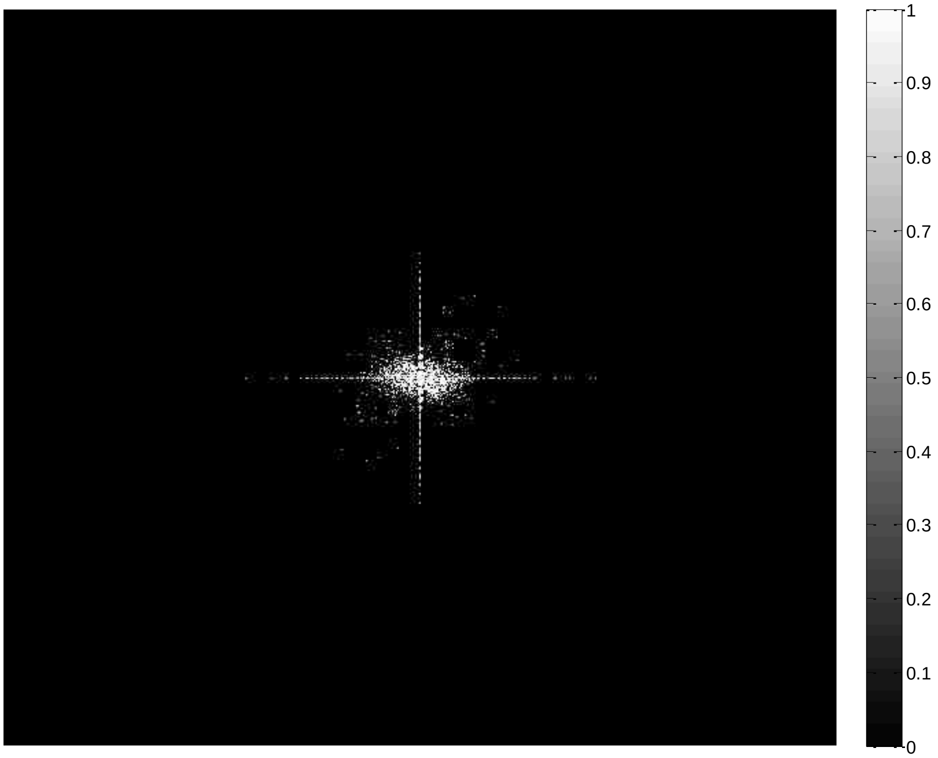

Figure 4.17. Fourier magnitude distribution for the image in Figure 4.12

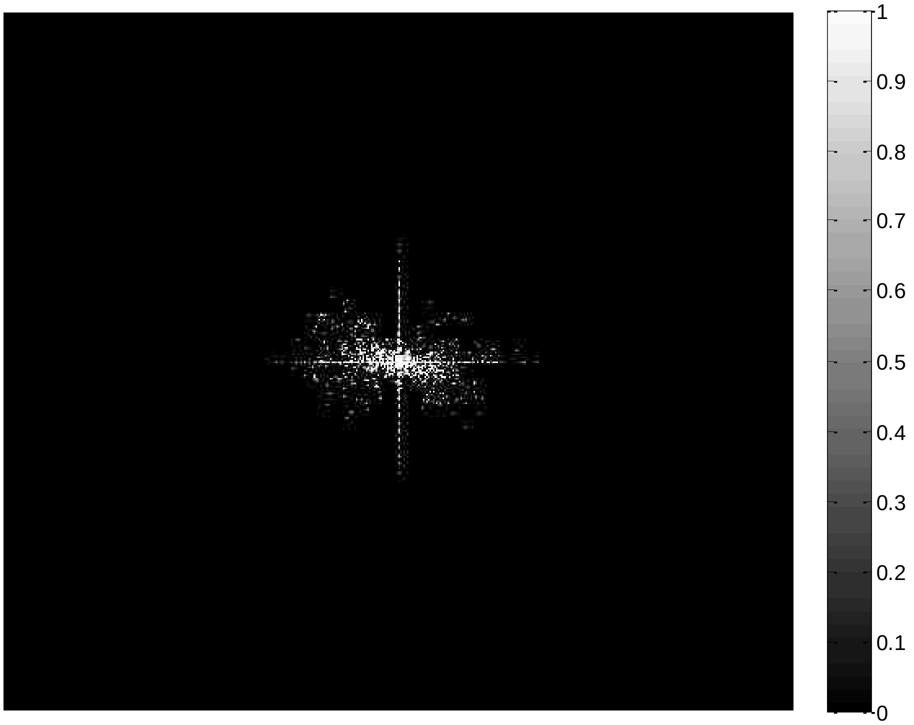

Figure 4.18. Fourier magnitude distribution for the image in Figure 4.13

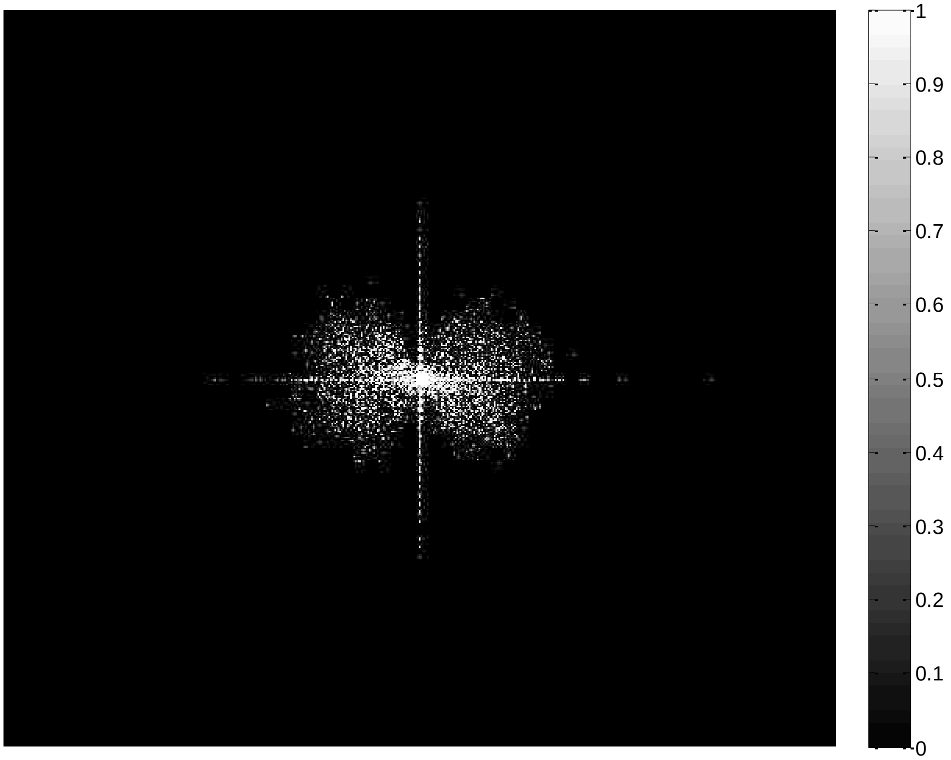

Figure 4.19. Fourier magnitude distribution for the image in Figure 4.14

In the fourier magnitude spectrum, the center value is called as the DC term and the frequency magnitudes surrounding it represents the high frequency components. We fit a circle using these components and as the radius of this circle increase, the image is sharper. The radius of the circles for the above used images is shown in the Table 4.5 and the Matlab code to obtain the same is attached in Appendix B.3.

Table 4.5. Radius of the circle enclosing the high frequency components in the spectrum

B/Q	**Radius**
0	0.03930
0.05	0.04780
0.1	0.07019

The quantitative analysis used here demonstrates the sharpness of the images and the bi-harmonic images are sharper when compared to the tapping mode AFM images thus proving that higher sensitivity gives better images.

5. CONCLUSION

A novel approach of using a bi-harmonic drive signal is developed for improving the measurement sensitivity when compared with the tapping mode AFM. The simulations results indicate that measurements sensitivity is increased whenever tapping frequency, β increases or tip-sample distance, x_s decreases. The ability to increase the β while maintaining a high amplitude state is limited by 'B' (the gain on the second harmonic of the drive signal). Therefore, for peak sensitivity, 'B' should be selected as large as possible and x_s as small as possible. 'B' is limited by the available power in the electrical drive system (before saturation occurs) and x_s is limited by the allowed impact forces (which increase with decreasing x_s).

This thesis presents a method for selecting bi-harmonic parameters based on the intuitive idea of generating a broad-valley sinusoidal trajectory. The broad valley of the trajectory places the cantilever probe near the surface for large portions of the trajectory. We have shown the stable region for the high amplitude state also increases using the bi-harmonic AFM. Placing the probe near the surface for a longer time effectively amplifies the attractive Van der waal's forces, which are necessary to stabilize the high amplitude mode. However, more fundamental dynamic analysis must be performed to fully explain this effect.

Through a numerical simulation it is shown that the stable frequency range for the high amplitude tapping state is extended by the bi-harmonic drive. A new measurement sensitivity metric which relates the change in tapping amplitude to the change in sample height is defined in this thesis.

In the single harmonic drive signal used in the tapping mode AFMs today, the sensitivity is approximately one. However, for bi-harmonic drive the sensitivity can be much larger than one - effectively amplifying measurement resolution without costly enhancements in sensor technology or filtering systems.

APPENDIX A

TECHNICAL DRAWINGS AND IMAGES FOR THE VEECO MULTIMODE SPM

A.1 VERTICAL DEFLECTION TEST POINTS

The optical tapping signal is hardware filtered on the AFM to remove low and high frequencies. In this thesis, the filtered signal could be used, however in future work it may be necessary to access the raw signal. Access to the raw signal is obtained as,

1) The vertical deflection is available at pin one of U1, which is marked in red.
2) The normalized vertical deflection is available at pins 7 and 12 of U5, which is shown in yellow.

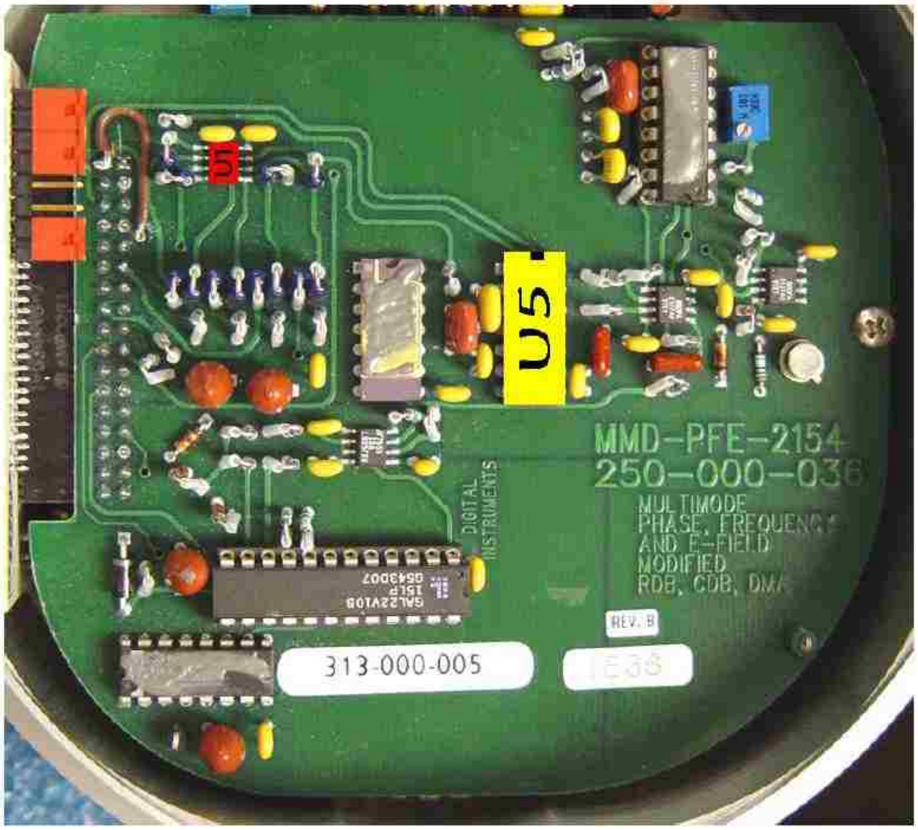

Figure A. 1. Photo of the underside of the microscope (access panel removed) [Photo provided by Veeco Instruments]

A.2 SIGNAL PATH IN A MULTIMODE SCANNING PROBE MICROSCOPE

The following figure shows the signal path in the SPM. This diagram is used to determine where to access various signals with the signal access modules.

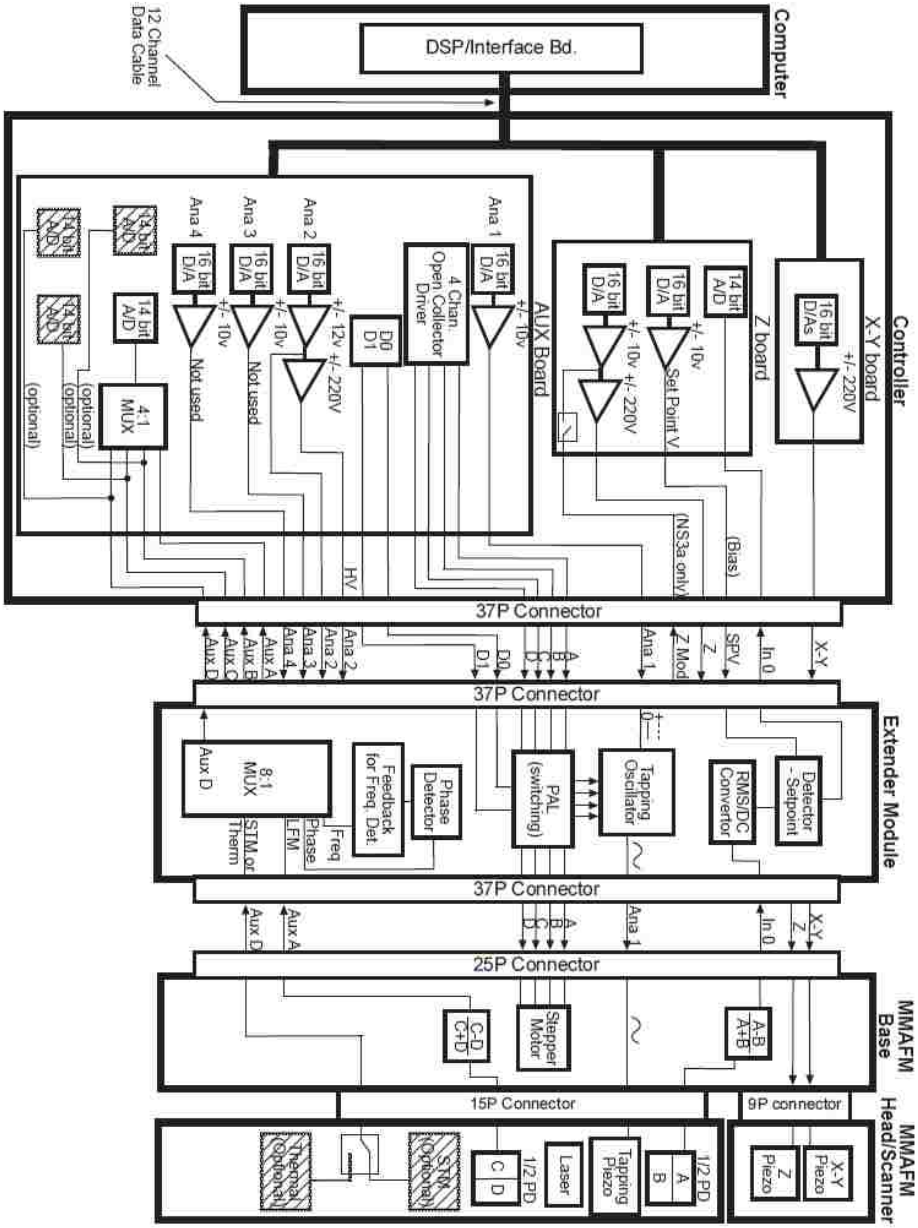

Figure A. 2 . Schematic of Veeco SPM signal routing (Veeco Instruments Phase MMAFM signal path manual, Pg. 1)

A.3 MULTIMODE SCANNING PROBE MICROSCOPE

Picture depicts the various parts in a Multimode scanning probe microscope.

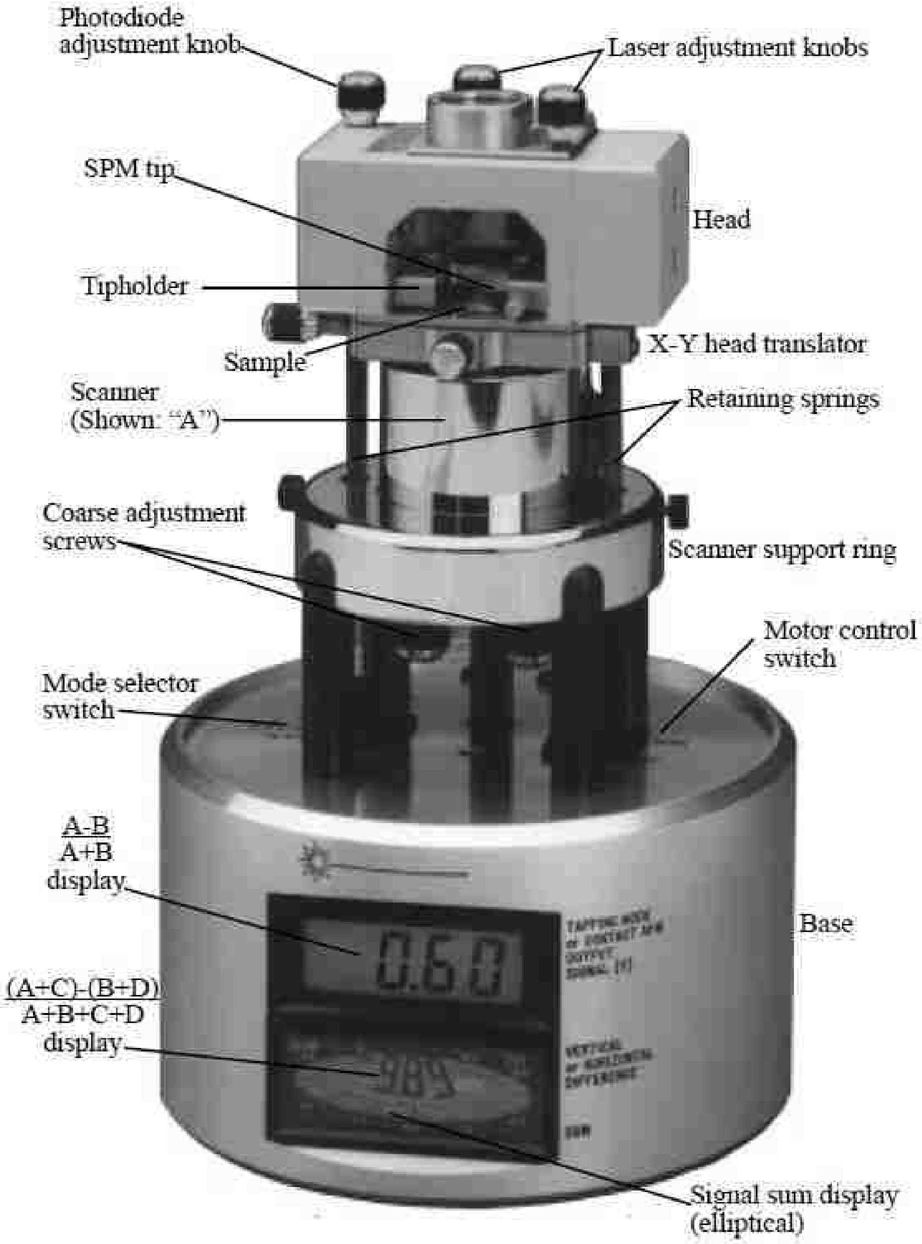

Figure A. 3. Multimode SPM [Digital Instruments Instruction Manual for SPMs, Version 4.12, Pg. 2-3]

A.4 SCANNING PROBE MICROSCOPE HEAD

The laser is reflected onto the photodiode from the shiny surface of the cantilever. Laser alignment is necessary any time a new cantilever is placed in the AFM. The mirror, photodiode and stage adjustment screws are shown in the figure below.

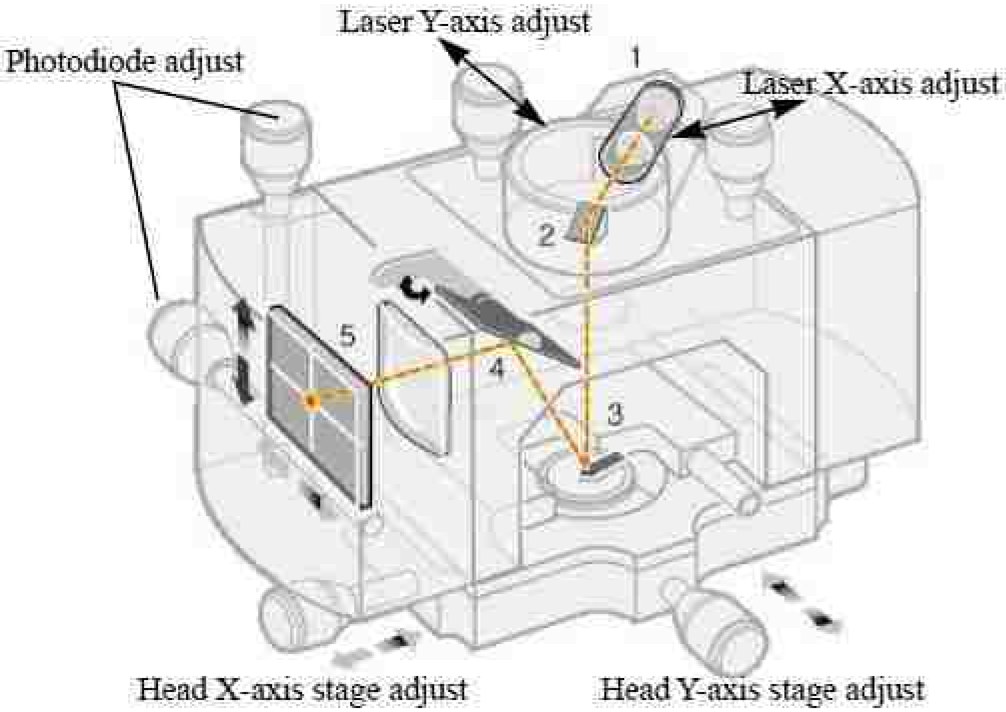

Figure A. 4. Multimode AFM head [Digital Instruments Training manual, Pg. 22]

APPENDIX B

MATLAB SOFTWARE USED TO ANALYSE THE EXPERIMENTAL DATA AND FOR THE NUMERICAL ANALYSIS

B.1 PROGRAM TO GET THE 95% CONFIDENCE INTERVAL AND AMPLITUDE BEFORE AND AFTER STEPPING

```
clear all;
close all;
clc;
format long;

load('Variables_Case8.mat');
Myfilt = Hd_FH_c;    %filter from fdatool
myx = x15;           % signal to filter

% Make ss filter

sampling_rate=25e6;

freq=317.7e3;

ts=1/sampling_rate;
[aaa,b,c,d]=ss(Myfilt);
Fss=ss(aaa,b,c,d,ts);
Fss_br = balreal(Fss);


t=0:ts:(length(myx)-1)*ts;

% filter signal
xf = lsim(Fss_br,myx);
myfilteredx = rot90(lsim(Fss_br,rot90(xf,2)),2);
figure; plot(myfilteredx)
vari=myfilteredx;

point=input('Enter the point to start counting 800 cycles: \n');

cycles=1000;
time=cycles/freq;
samples=sampling_rate*time;
samples_per_cycle=samples/cycles;
a=round(samples_per_cycle);

u=0;
l=0;

for i=1:a-1

   if mod(point,a)==0
      point=point;
      break
   else
      point=point+1;
   end

end

range1=point+(a*cycles);
```

```
range2=range1+(a*cycles);


r2=point-(a*cycles/2);
r1=r2-(a*cycles/2);

div =1000;
count=1;


for i=range1:a:range2-a

    u=max(vari(i:i+a));
    l=min(vari(i:i+a));

    aa(count)=u;
    bb(count)=l;

    if u<0
        cc(count)=abs(bb(count)-aa(count))/2;
    else
        cc(count)=(abs(bb(count))+aa(count))/2;
    end

    count=count+1;

 end

aa=aa';
bb=bb';
cc=cc';

amp=mean(cc);

% To get 95% Confidence Intervals

[h,bin]=hist(cc,100);
pdf=h./sum(h);
cdf= cumsum(pdf);

k=1;

while (k<=100)

   if cdf(k)> 0.025
       conf(1)=bin(k);
       break;
   end

   k=k+1;

end

k=1;
```

```
while (k<=100)

   if cdf(k)> 0.975
       conf(2)=bin(k);
       break;
   end

   k=k+1;

end

Ll=amp-conf(1);         % Upper and Lower Limits to plot using errobar
Uu=conf(2)-amp;

count1=1;

for i=r1:a:r2-a

    u1=max(vari(i:i+a));
    l1=min(vari(i:i+a));

    aa1(count1)=u1;
    bb1(count1)=l1;

    if u<0
        cc1(count1)=abs(bb1(count1)-aa1(count1))/2;
    else
        cc1(count1)=(abs(bb1(count1))+aa1(count1))/2;
    end
        count1=count1+1;

 end


aa1=aa1';
bb1=bb1';
cc1=cc1';

amp1=mean(cc1);

fprintf('%10.5f\t %10.5f\n',amp1,amp)
```

B.2 PROGRAM TO GET AN AMPLITUDE RESPONSE AT A PARTICULAR TIP SAMPLE DISTANCE

```
%% **** Simulate Nonlinear Response ****

% Set amplitude
clear all;
clc;

%Initial Conditions
K=7.5; %Spring Constant(nN/nm)
Q=100; %Q-Factor
a0=0.166; %Interatomic Distance(nm)
Et=129; %Elastic Moduli nN/(nm)^2
Es=70; %Elastic Moduli nN/(nm)^2
vt=0.28; %Poisson's Ratio
vs=0.17; %Poisson's Ratio
H=6.4e-2; %Hamaker Constant(nN-nm)
R=20; %Tip Radius(nm)

%Calculations
Estar=[((1-vt^2)/Et)+((1-vs^2)/Es)]^(-1); %Effective Tip Sample Stiffness

%For Input initial conditions
A1=1.5;
A0=0;
N=-0.5;


% initial conditions
convergence_epsilon = 1e-2;
x0=0; v0=0;

% offset
xs=4;

  % search range
  beta_v =1.5:-0.001:0.9;  % Sweep Up

  peak_to_peak = 0;
  Average_Force=0;

  for i=1:length(beta_v)

    xf=x0; vf=v0;
    beta = beta_v(i);


    display(sprintf('Calculating response for beta = %d',beta))

    flag_converged=0;
    max_history = 0;
    min_history = 0;
    run_number=0;
```

```
        while(~flag_converged)
            sim('pulse_input',2*pi/beta);

            run_number = run_number + 1;
            max_history(run_number) = max(x);
            min_history(run_number) = min(x);

        % check convergence
        if (run_number > 100)
            if (norm((max_history(run_number-99:run_number)-max_history(run_number)),2) <
convergence_epsilon)
                if (norm((min_history(run_number-99:run_number)-min_history(run_number)),2) <
convergence_epsilon)
                    flag_converged = 1;
                end
            end
        end
       if (mod(run_number,100)==0); display(sprintf('Running period #%i',run_number)); end;
        x0=xf; v0=vf;
    end

    % Get data
     peak_to_peak(i) = (max_history(run_number) - min_history(run_number))/2;
     display(sprintf(' Beta = %d completed',beta))
     Average_Force(i)=Favg/2/pi;

    end

plot(beta_v,peak_to_peak);

peak_to_peak'
display(sprintf('F'));
Average_Force'
```

B. 3 IMAGE PROCESSING TO GET THE FOURIER MAGNITUDE SPECTRUM

```
clear all;
clc;
close all;

format long;

x=imread('3_3.jpg');   % Enter the file name and the threshold value
thres=11.9793;

xx=double(rgb2gray(x))+1;

nor=size(xx);

llim=-0.5;
ulim=0.5;
XX=llim:1/nor(1):ulim-1/nor(1);
YY=llim:1/nor(2):ulim-1/nor(2);

variance=var(var(xx));

X=fft2(xx);
Y=fftshift(X);
Z=log(1+abs(Y));

count=0;

for i=1:nor(1)

   for j=1:nor(2)

      if Z(i,j)<=thres
         Z(i,j)=0;
      else
         Z(i,j)=1;
      end

      if Z(i,j)==1

         count=count+1;
         dist(count)=(sqrt((XX(i)^2)+(YY(j)^2)));

      else

         continue;

      end

   end

end
```

```
radius=mean(dist);
SN=sum(sum(abs(Y)));
figure;imshow(Z,[]);
colorbar;

fprintf('%10.5f \n %10.5f \n',variance,radius);
```

APPENDIX C

LABVIEW PROGRAMS USED IN THE EXPERIMENTS

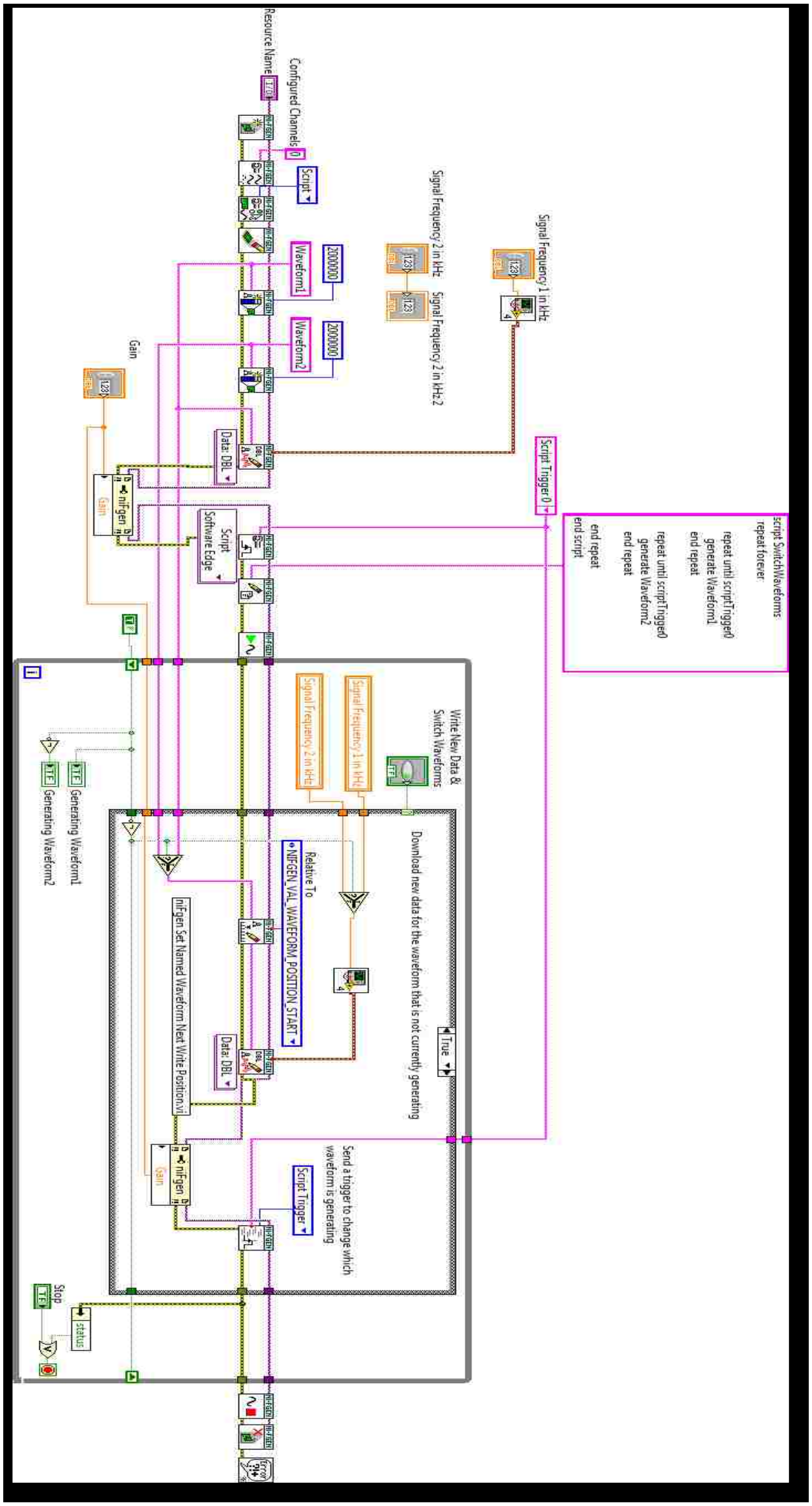

```
script SwitchWaveforms
  repeat forever

    repeat until scriptTrigger0
      generate Waveform1
    end repeat

    repeat until scriptTrigger0
      generate Waveform2
    end repeat

  end repeat
end script
```

Figure C. 1. Driving signal program

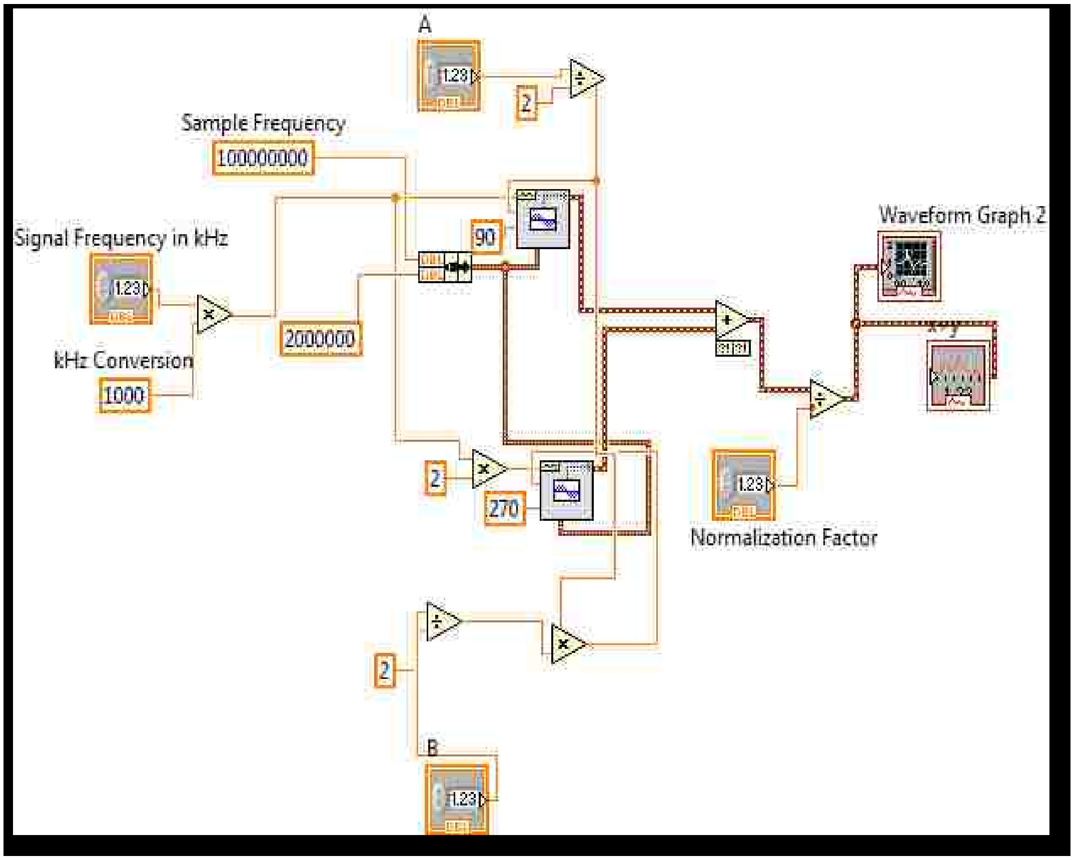

Figure C. 2. Sub VI from the driving signal program

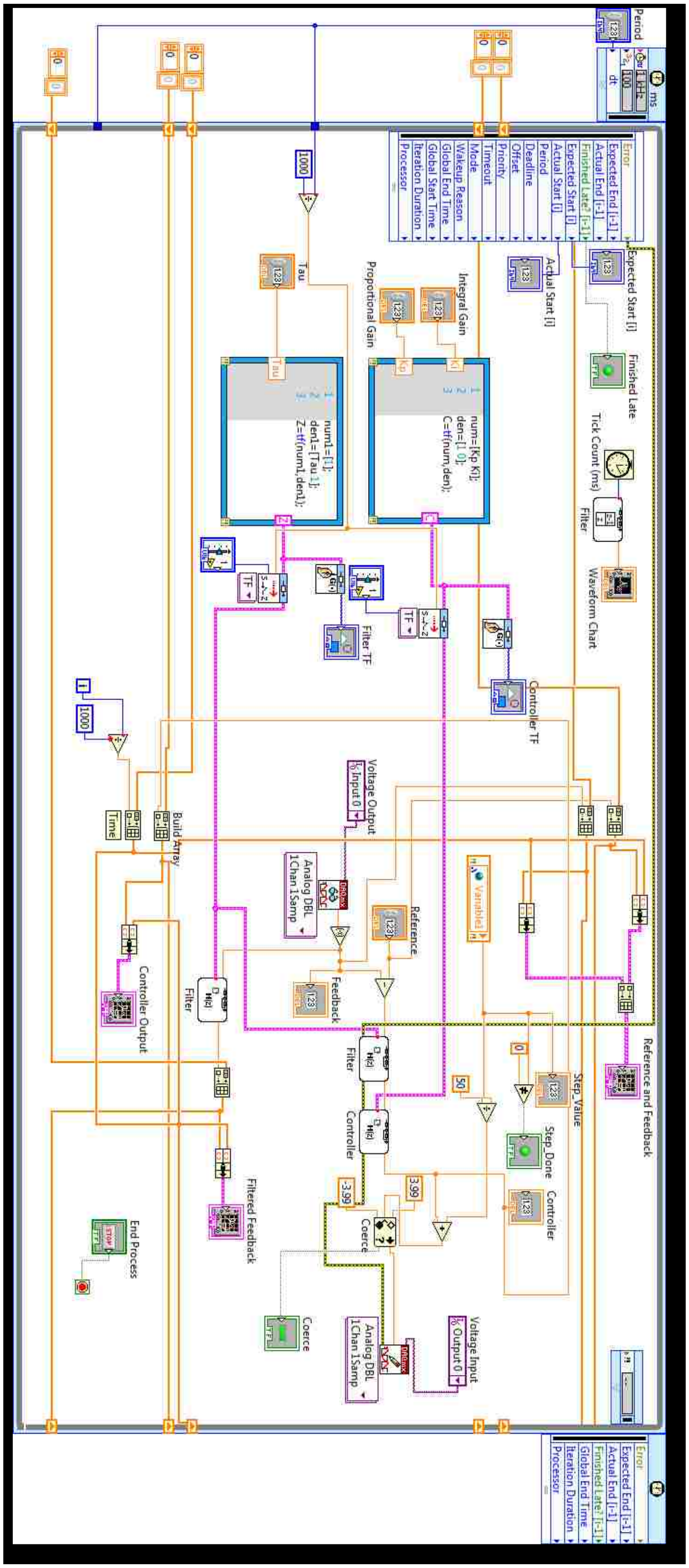

```
num=[Kp Ki];
den=[1 0];
C=tf(num,den);
```

```
num1=[1];
den1=[Tau 1];
Z=tf(num1,den1);
```

Figure C. 3. PI controller for Z piezo control

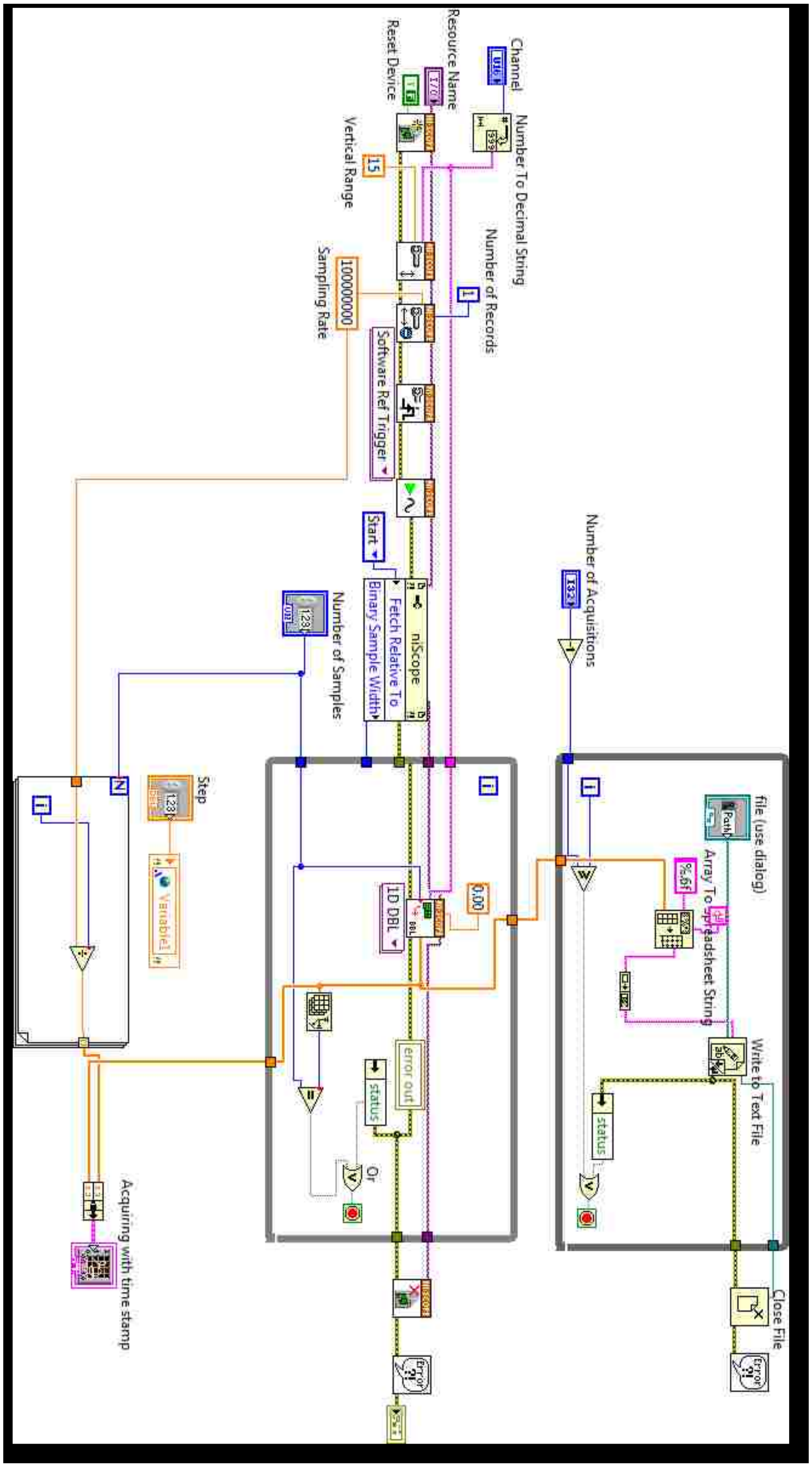

Figure C. 4. Acquisition from PXI 5122

APPENDIX D

AFM SAMPLES USED IN THE EXPERIMENTS

D.1 BUDGET SENSORS TIP CHECK CALIBRATION STANDARD

Tip check sample is an SPM sample for fast and easy determination of the tip condition. The following figure shows a comparison between different probe tips used to image this sample.

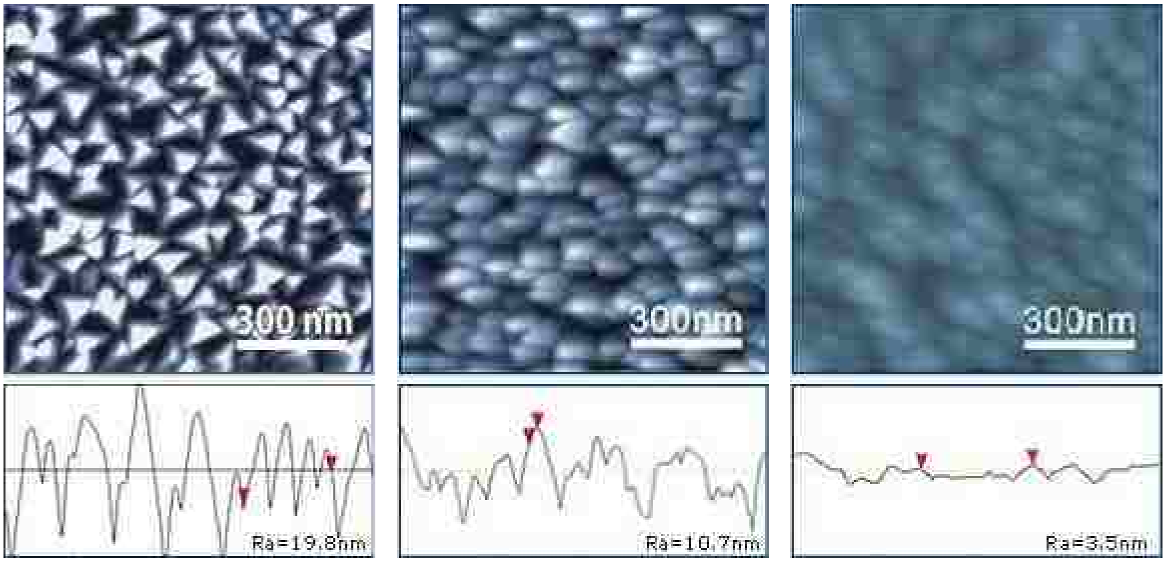

(a) (b) (c)

Figure D. 1. Imaging using different tips, (a) Good Tip, (b) worn out tip and (c) blunt or broken tip

D.2 BUDGET SENSORS HEIGHT STANDARD – 20 MG

This is a height standard sample which features silicon dioxide structure arrays on a 5x5 mm silicon chip. This is used to calibrate the Z-axis of the AFM system.

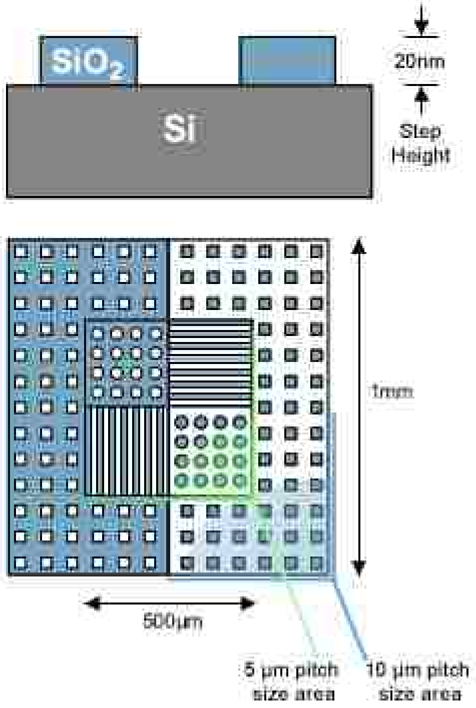

Figure D. 2. HS – 20MG sample with standard features for calibration.

D.3 GOLD SPUTTERED SILICON WAFER

This is a sample provided by the Materials Research centre, Missouri S&T (Dr. Matt O'Keefe).

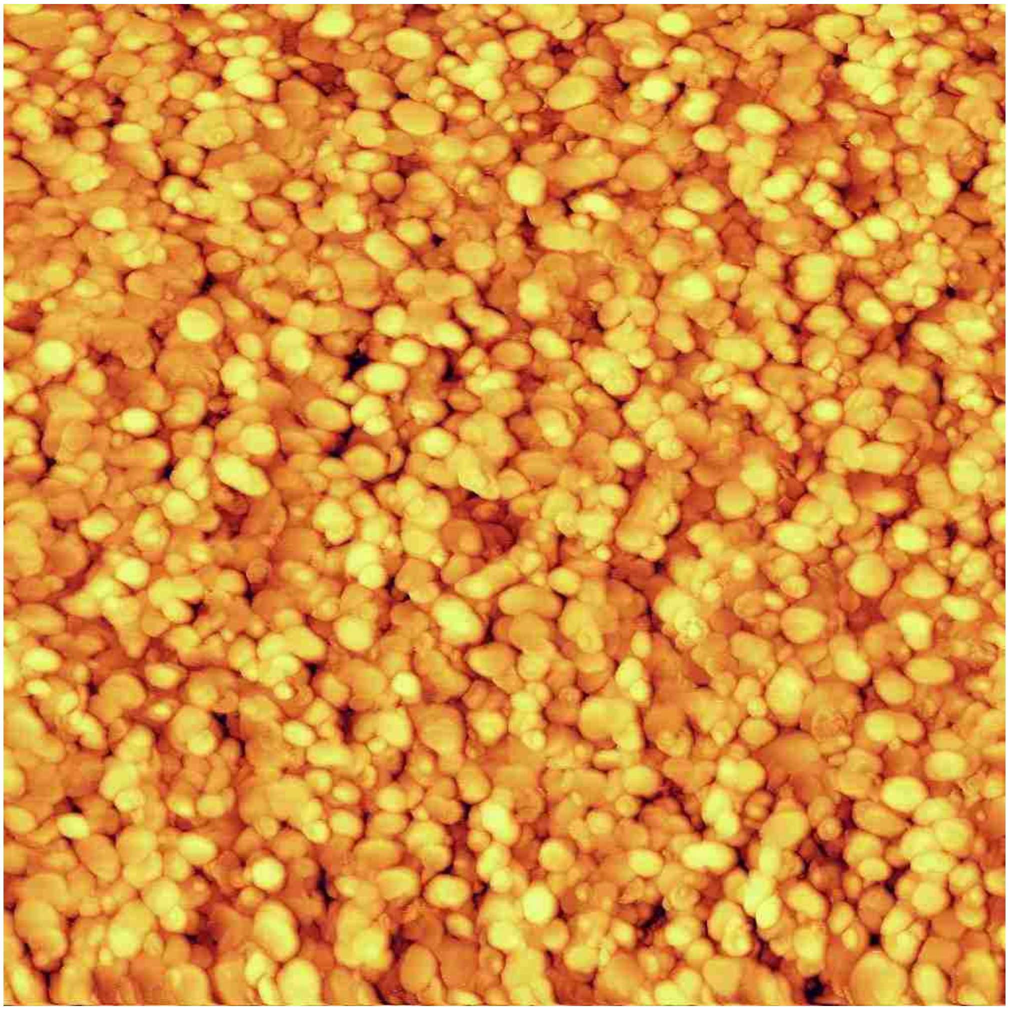

Figure D. 3. Sputtered gold layer on silicon, Image range: 200 nm and Height: 2.3 nm [Anfatec Instruments]

BIBLIOGRAPHY

1. Atomic Force Microscope. Binnig, G. and Quate, C.F. 9, 1986, Physical Review, Vol. 56, pp. 930-934.
2. Scanning Tunneling Microscope. Binnig, G. and Rohrer, H. 3, 1987, Review of Modern Physics, Vol. 59, pp. 615-625.
3. Optical Beam Deflection Atomic Force Microscopy: The Nacl (001) surface. Meyer, G. and Amer, N.M. 21, 1990, Applied Physical Letters, Vol. 56, pp. 2100-2101.
4. Acquisition of high precision images for non-contact atomic force microscopy. Pishkenari, H.N., Jalili, N. and Meghdari, A. 10, 2006, Mechatronics, Vol. 16, pp. 655-664.
5. Atomic force microscope lithography using amorphous silicon as a resist and advances in parallel operation. Minne, S.C., 3, 1995, Journal of Vacuum science and technology, Vol. 13, pp. 1380-1385.
6. Improving tapping mode atomic force microscope with piezoelectric cantilevers. Rogers, B., 2004, Ultramicroscopy, Vol. 100, pp. 267-676.
7. Tapping mode atomic force microscopy in liquid with an insulated piezoelectric microactuator. Rogers, B., 9, 2002, Review of Scientific Instruments, Vol. 73, pp. 3242-3244.
8. Atomic force microscope with magnetic force modulation. Florin, E., 3, 1994, Review of Scientific Instruments, Vol. 65, pp. 639-643.
9. Novel atomic force microscope probes with integrated electrostatic actuation and optical detection. Degertekin, F. L. 2007, IEEE, pp. 832-833.
10. Actuation of atomic force microscope cantilevers by acoustic radiation pressure. Onaran, A.G. and Degertekin, F. L. 2001, IEEE Ultrasonics Symposium, pp. 509-512.
11. Dynamic behavior of the tuning fork AFM probe. Bayat, D., 2008, Microelectronic Engineering, Vol. 85, pp. 1018-1021.
12. Atomic force microscopy for high speed imaging using cantilever with an integrated actuator and sensing. Manalis, S.R., Minne, S.C. and Quate, C.F. 6, 1995, Applied Physical Letters, Vol. 68, pp. 871-873.
13. Design and Modeling of a hihg speed AFM scanner. Schitter, G., 5, 2007, IEEE Transactions on control systems technology, Vol. 15, pp. 906-915.
14. Scanning Probe Microscopy: Training Notebook. s.l. : Digital Instruments, 2000.
15. A high speed force microscope for studying biological macromolecules. Ando, T., 22, 2001, Marine Biology, Vol. 98, pp. 12468-12472.
16. A review of atomic force microscopy imaging systems: Application to molecular metreology and biological sciences. Jalili, N. and Laxminarayana, K. 2004, Mechatronics, Vol. 14, pp. 907-945.

17. How does a tip tap. Burnham, N.A., Behrend, O.P. and Oulevey, F. 1997, Nanotechnology, Vol. 8, pp. 67-75.

18. Nonlineardynamics of atomic force microscope probes driven in Lennard Jones potential. Rutzel, S., Lee, S.I. and Raman, A. 2002, Proceedings of the Royal Society, Vol. 459, pp. 1925-1948.

19. How to measure energy dissipation in dynamic mode atomic force microscopy. Anczylowski, B., 1999, Applied Surface Science, Vol. 140, pp. 376-382.

20. Analysis of tip sample interaction in tapping mode atomic force microscope using an electrical circuit simulator. Sahin, O. and Atalar, A. 19, 2001, Applied Physical Letters, Vol. 78, pp. 2973-2975.

21. Nanoscience Instruments. [Online] Nanoscience, 2002. http://www.nanoscience.com/education/afm.html.

22. Integrated Solutions for nanotechnology. [Online] NT-MDT, 1998. http://www.ntmdt.com/spm-basics/view/dmt-model.

23. Elings, V.B. and Gurley, J.A. Method of driving a piezoelectric scanner linearly with time. 5051646 USA, November 29, 1990. [Patent]

24. Piezoelectric scanners for atomic force microscopes: Design of lateral sensors, identification and control. Daniele, A., 1999, American Control Conference, pp. 253-257.

25. A simple way to reduce hysteresis and creep when using piezoelectric actuators. Kaizuka, H. and Siu, B. 5, 1988, Japanese Journal of Applied Physics, Vol. 27, pp. 773-776.

26. Creep, hysteresis and vibration compensation for piezoactuators: Atomic force microscopy application. Croft, D., Shed, G. and Devasia, S. 2001, Journal of Dynamic Systems, Vol. 123, pp. 35-43.

27. Tuning interaction forces in tapping mode atomic force microscopy. Stark, R.W., Schitter, G. and Stemmer, A. 2003, Physical Review, Vol. 68.

28. How Much ADC Resolution Do You Really Need? [Online] Dataq Instruments, 2010. http://www.dataq.com/applicat/articles/adc-resolution.html.

29. Attractive and repulsive tip-sample regimes in tapping mode atomic force microscopy. Garcia, R. and Paulo, A.S. 7, 1999, Physical Review, Vol. 60, pp. 4961-4967.

30. Cantilever dynamics in amplitude modulation AFM: Continuous and discontinous transitions. Santos, S., 2010, Applied Physics, Vol. 43.

31. Role of attractive forces in tapping tip force microscopy. Kuhle, A., Sorensen, A.H. and Bohr, J. 10, 1997, Journal of Applied Physics, Vol. 81, pp. 6562-6569.

32. Cantilever dynamics and quality factor control in AC mode AFM height measurements. Chen, L., Yu, X. and Wang, D. 2007, Ultramicroscopy, Vol. 107, pp. 275-280.

33. A tutorial on the mechanisms, dynamics and control of atomic force microscopes. Abramovitch, D.Y., 2007, American Control Conference, pp. 3488-3502.

34. Melnikov-based dynamical analysis of microcantilevers in scanning probe microscopy. Ashhab, M., 1999, Nonlinear Dynamics, Vol. 20, pp. 197-220.

35. Nanoscope Command Reference Manual. s.l. : Digital Instruments, 2001.

36. A Novel method to method to correct the nonlinearity of piezoelectric scanner in STM by DNA evolution algorithm. Ziyuan, H. and Minrui, F. 2002, Proceedings of the IEEE TENCON, pp. 1471-1474.

37. Image sharpness measurement in scanning electron microscopy - Part I. Postel, M. and Vladar, A. 1998, Scanning, Vol. 20, pp. 1-9.

VITA

Santosh Ramaiah Kodandarama was born in Bangalore, India on April 11th, 1986. He obtained his Bachelor's degree in Mechanical Engineering on July 2008 from B. M. Sreenivasaiah College of Engineering which is affiliated to Visveswaraya Technological University, Belgaum, India.

He joined Missouri University of Science and Technology in the Fall 2008 semester to his pursue Masters in Mechanical Engineering with a specialization in Control Systems. He worked under Dr. Douglas A Bristow on a project partially funded by the Materials Research Center. The project was to develop a Bi-harmonic Atomic Force Microscope for better imaging at the atomic level. He received his Master of Science degree in May 2011.